7/5/95

Modeling The Impact of Nutrient Load Reduction on Water Quality and Seagrass in Roberts Bay and Little Sarasota Bay

A Final Report

Prepared for

Sarasota Bay National Estuary Program

and

Southwest Florida Water Management District

by

Y. Peter Sheng, Ph.D.
Professor and Principal Investigator

Eduardo A. Yassuda, Ph.D. Candidate

and

Changlu Yang, Graduate Assistant

Coastal & Oceanographic Engineering Department
P.O. Box 116590
University of Florida
Gainesville, Florida 32611-6590
June 1995

Executive Summary

This study aims to quantify the impact of reduced nutrient loading into Roberts Bay from Phillippi Creek on the water quality and light/seagrass in Roberts Bay and surrounding waters. The problem is complicated by the fact that there is little water quality data for calibrating water quality model, and the fact that epiphytic algae and seagrass may play important roles in the nutrient cycling and budget. Confronted with these problems and the short duration of this study, we developed a coupled hydrodynamics-water quality-light-seagrass model which is process-based and contains much less empiricism than existing water quality models. Using limited synoptic water quality data, we succeeded in calibrating the water quality model for the present land use condition. We then used the model to investigate the potential impact of reduced nutrient loading to Roberts Bay corresponding to future land use condition. With a 31% reduction in nutrient loading, noticeable impact is found in Roberts Bay only, although some slight changes are found in Little Sarasota Bay as well. The reduced nutrient loading is expected to lead to increased DO and light but reduced phytoplankton, CBOD, dissolved organic nitrogen and ammonia. There is not noticeable increase in seagrass biomass, since sediment nutrient concentration which controls the seagrass growth may still be saturated. With a 100% reduction in nutrient loading, the impact is more pronounced for such parameters as nitrogen and phytoplankton, but not significantly different for light and seagrass, due to the saturated nutrient concentration in the sediment column. There may be considerable uncertainty in the some of the model coefficients and processes, due to the severe lack of comprehensive field data. No sediment nutrient data was available at all. To improve the reliability of the coupled model so that it can be used for predictions, it is necessary to collect comprehensive field data in both the water column and sediment column.

Acknowledgement

The work reported herein has been conducted by the Coastal & Oceanographic Engineering Department of University of Florida with Dr. Sheng, Professor of Coastal & Oceanographic Engineering, as the Principal Investigator. Mr. Eduardo A. Yassuda, Ph.D. Candidate and Mr. Changlu Yang, Graduate Research Assistant, both in the Department of Coastal & Oceanographic Engineering, contributed to the modeling work. Dr. Peggy Fong generously provided her seagrass model (in Stella) to us. Dr. David Tomasko of SBNEP and SWFWMD provided valuable suggestion on the application of seagrass model. The work was supported by Sarasota Bay National Estuary Program through Southwest Florida Water Management District. Dr. David Tomasko served as the Projec Officer.

TABLE OF CONTENTS

List of Figures

List of Tables

1. INTRODUCTION

1.1. Description of the Problem

Established in 1989, the Sarasota Bay National Estuary Program (SBNEP) has been characterizing the environmental conditions in Sarasota Bay and formulating a comprehensive restoration and protection strategy for the Sarasota Bay estuarine system (Figure 1). The "State of the Bay" report (SBNEP, 1990) compiled available information on the Bay and the *Framework for Action* report (SBNEP, 1992) provided a synthesis on SBNEP's findings concerning the environmental health and status of the Bay. As outlined in the *Framework for Action* report, anthropogenic increases in nitrogen loads have compromised the environmental integrity of the Bay. In Roberts Bay and Upper Little Sarasota Bay (Segment 13 in Figure 2), elevated nitrogen loads appear to be related to increased phytoplankton populations, deteriorated water quality, increased epiphyte levels on seagrasses, decreased seagrass productivity, and increased hypoxia in bottom waters.

Based on the report produced by CDM (1992), however, significant reduction (25% below the existing level and 30% below the expected level in 2012 without management control) in nitrogen loading to Roberts Bay and Upper Little Sarasota Bay could be achieved by the year 2012, if a combination of management controls (cluster development with BMPs, restricted commercial/industrial imperviousness, and regional wastewater plan) are implemented. As shown in Table 7-6 of the CDM report, total N loading to Segment 13 is expected to be reduced from the present level of 468,530 lb/yr to 361,490 lb/yr. The reduced loading in total N would occur mainly in the watersheds for Phillippi Creek and Roberts Bay.

Tables I, II and III show the loadings to Sarasota Bay during average, wet and dry years, respectively for existing land use conditions. Tables IV and V show the loadings during wet and dry years, respectively, for 20-year future land use conditions. Based on these information, the SBNEP needs to quantify the response of the Bay to the expected nutrient reduction, in order to further develop the comprehensive restoration and enhancement plan for the Bay.

The objective of this project is to utilize a water quality model to determine the response of water column nutrient levels, water column chlorophyll concentrations, and, to the extent possible, light attenuation values to a 25-30% reduction in nutrient loading in Roberts Bay and Upper Little Sarasota Bay. The water quality model should incorporate such processes as advection, diffusion, settling, transformation, and benthic exchanges. Due to the significant flushing in Roberts Bay area, the advection process should be simulated with a hydrodynamics model. The problem, however, is made difficult because of the importance of epiphytes and seagrass in affecting the nutrient cycling and budget in Sarasota Bay (SBNEP 1992, Tomasko et al. 1995). Traditional water quality models were developed for deeper estuaries (e.g., Chesapeake Bay and James River) and lakes (e.g., Great Lakes) in temperate climate where seagrass and epiphytes do not have as significant effects on nutrient cycling and budget, and hence may not be applicable to Sarasota Bay.

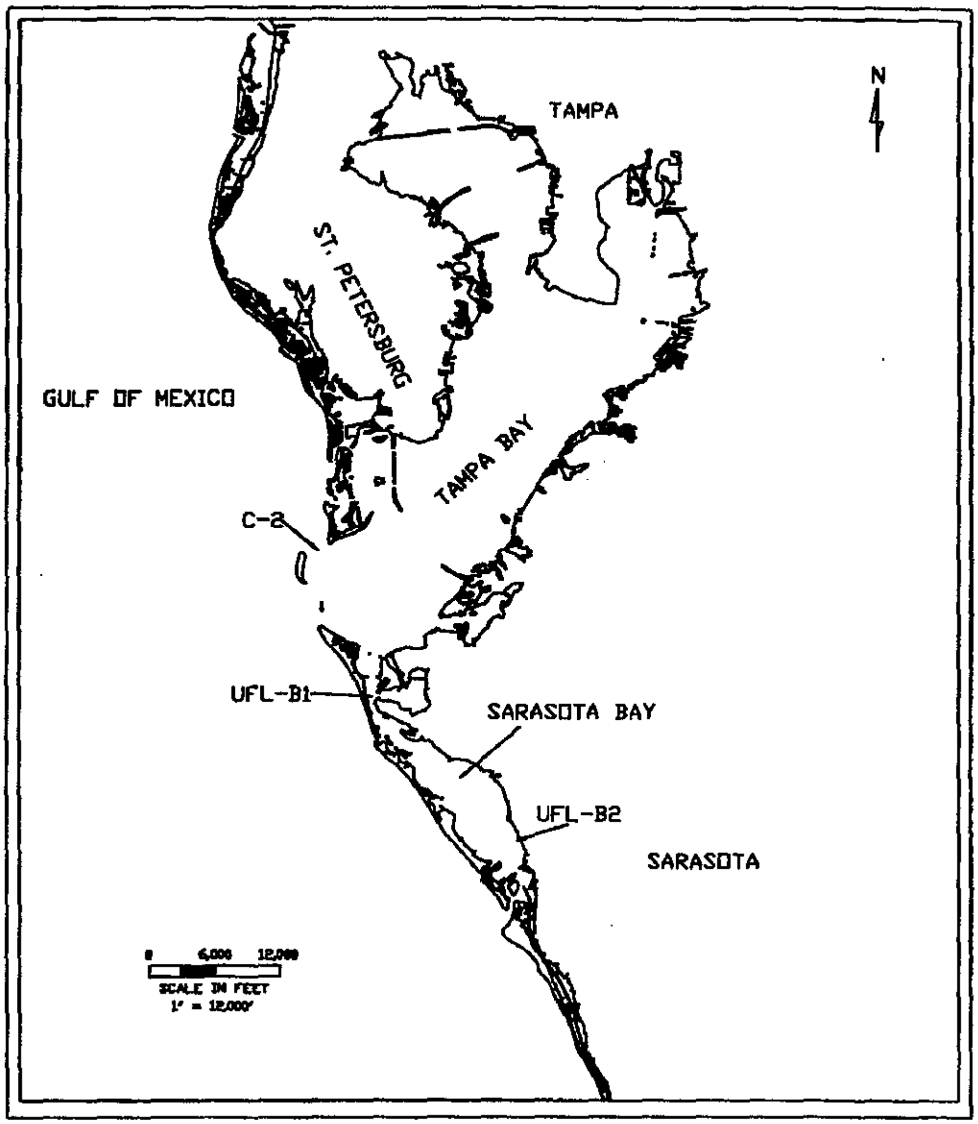

Figure 1. The Sarasota Bay Estuarine System.

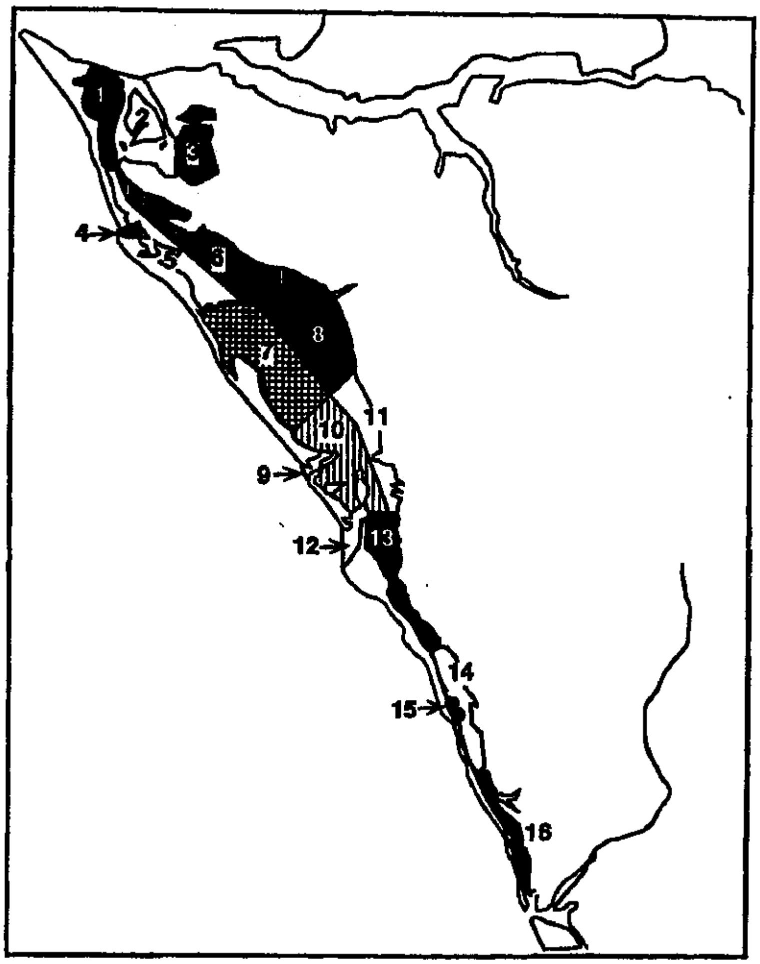

Figure 2. Segments of the Sarasota Bay system. (From SBNEP 1992)

Table I. Average year loadings to Sarasota Bay by watershed for existing land use conditions (from CDM 1992).

TABLE A-1

AVERAGE ANNUAL LOADINGS BY WATERSHED
FOR EXISTING LAND USE CONDITIONS

WATERSHED	AREA	TOTAL RUNOFF	TOTAL P			TOTAL N			LEAD			ZINC		
	(ac)	(in)	(lb)	(lb/ac)	(mg/l)	(lb)	(lb/ac)	(mg/l)	(lb)	(lb/ac)	(mg/l)	(lb)	(lb/ac)	(mg/l)
PHILLIPPI CREEK	36,417	25.24	66,860	1.84	0.32	362,950	9.97	1.74	7,410	0.20	0.036	9,450	0.26	0.045
PALMA SOLA 2	1,120	25.12	1,640	1.46	0.26	8,340	7.45	1.31	350	0.31	0.055	320	0.29	0.050
BOWLEES CREEK	6,489	33.61	11,100	1.71	0.22	64,320	9.91	1.30	6,970	1.07	0.141	4,270	0.66	0.086
WEST BRADENTON	4,395	28.94	7,250	1.65	0.25	35,910	8.17	1.25	1,490	0.34	0.052	1,410	0.32	0.049
CEDAR HAMMOCK	1,930	32.35	4,090	2.12	0.28	20,830	10.79	1.47	1,280	0.66	0.090	970	0.50	0.069
WEST BOWLEES	1,559	27.93	2,990	1.92	0.30	14,800	9.49	1.50	710	0.46	0.072	590	0.38	0.060
PALMA SOLA	900	23.47	1,710	1.90	0.36	7,490	8.32	1.56	230	0.26	0.048	220	0.24	0.046
SOUTH BRADENTON	4,635	27.87	12,550	2.71	0.43	56,260	12.14	1.92	590	0.13	0.020	1,120	0.24	0.038
WHITAKER BAYOU	5,015	40.74	20,270	4.04	0.44	89,870	17.92	1.94	3,630	0.72	0.078	3,630	0.72	0.078
MATHENY CREEK	3,800	35.96	11,390	3.00	0.37	57,290	15.08	1.85	2,040	0.54	0.066	2,100	0.55	0.068
CATFISH CREEK	3,360	21.73	3,590	1.07	0.22	18,640	5.55	1.13	240	0.07	0.015	560	0.17	0.034
NORTH CREEK	1,920	20.60	2,160	1.13	0.24	11,170	5.82	1.25	220	0.11	0.025	350	0.18	0.039
SOUTH CREEK	12,995	18.79	11,050	0.85	0.20	53,190	4.09	0.96	250	0.02	0.005	1,400	0.11	0.025
HUDSON BAYOU	1,595	32.58	3,070	1.92	0.26	16,570	10.39	1.41	1,440	0.90	0.122	930	0.58	0.079
SIESTA KEY	1,385	45.94	8,410	6.07	0.58	30,230	21.83	2.10	580	0.42	0.040	1,030	0.74	0.071
ANNA MARIA	919	28.32	1,740	1.89	0.29	8,660	9.42	1.47	450	0.49	0.076	360	0.39	0.061
PERICO	860	33.12	1,040	1.21	0.16	4,750	5.52	0.74	50	0.06	0.008	100	0.12	0.015
LONGBOAT KEY	1697	23.62	2,730	1.61	0.30	13,000	7.66	1.43	440	0.26	0.048	450	0.27	0.050
OTHER ISLANDS	900	27.94	1,640	1.82	0.29	8,360	9.29	1.47	310	0.34	0.054	290	0.32	0.051
DIRECT TO BAY	4,241	31.85	8,760	2.07	0.29	51,120	12.05	1.67	2,290	0.54	0.075	1,850	0.44	0.060
BAY SURFACE	33,280	54.60	61,730	1.85	0.15	337,460	10.14	0.82	2,470	0.07	0.006	60,080	1.81	0.146
TOTAL	129,412	34.26	245,770	2.09	0.30	1,271,210	10.05	1.44	33,440	0.38	0.054	91,480	0.44	0.058

Table II. Wet year loadings to Sarasota Bay by watershed for existing land use conditions (from CDM 1992).

TABLE A-8

WET YEAR LOADINGS BY WATERSHED
FOR EXISTING LAND USE CONDITIONS

WATERSHED	AREA	TOTAL RUNOFF	TOTAL P			TOTAL N			LEAD			ZINC		
	(ac)	(in)	(lb)	(lb/ac)	(mg/l)	(lb)	(lb/ac)	(mg/l)	(lb)	(lb/ac)	(mg/l)	(lb)	(lb/ac)	(mg/l)
PHILLIPPI CREEK	36,417	34.86	90,500	2.49	0.31	461,060	12.66	1.60	9,510	0.26	0.033	13,330	0.37	0.046
PALMA SOLA 2	1,120	34.98	2,310	2.06	0.26	11,380	10.16	1.28	460	0.41	0.052	440	0.39	0.050
BOWLEES CREEK	6,489	44.90	15,060	2.32	0.23	85,060	13.11	1.29	8,920	1.37	0.135	5,620	0.87	0.085
WEST BRADENTON	4,395	39.83	10,110	2.30	0.25	48,680	11.08	1.23	1,920	0.44	0.048	1,950	0.44	0.049
CEDAR HAMMOCK	1,930	43.45	5,500	2.85	0.29	27,550	14.27	1.45	1,640	0.85	0.086	1,290	0.67	0.068
WEST BOWLEES	1,559	38.24	4,090	2.62	0.30	19,830	12.72	1.47	910	0.58	0.067	810	0.52	0.060
PALMA SOLA	900	33.05	2,350	2.61	0.36	10,180	11.31	1.51	310	0.34	0.046	320	0.36	0.047
SOUTH BRADENTON	4,635	37.46	15,850	3.42	0.40	69,070	14.90	1.76	750	0.16	0.019	1,580	0.34	0.040
WHITAKER BAYOU	5,015	51.55	23,560	4.70	0.40	105,580	21.05	1.80	4,580	0.91	0.078	4,470	0.89	0.076
MATHENY CREEK	3,800	46.57	13,720	3.61	0.34	68,170	17.94	1.70	2,590	0.68	0.065	2,680	0.71	0.067
CATFISH CREEK	3,360	31.34	5,390	1.60	0.23	26,000	7.74	1.09	320	0.10	0.013	840	0.25	0.035
NORTH CREEK	1,920	29.87	3,210	1.67	0.25	15,450	8.05	1.19	290	0.15	0.022	530	0.28	0.041
SOUTH CREEK	12,995	27.85	17,510	1.35	0.21	79,060	6.08	0.96	360	0.03	0.004	2,360	0.18	0.029
HUDSON BAYOU	1,595	43.68	4,140	2.60	0.26	21,920	13.74	1.39	1,850	1.16	0.117	1,240	0.78	0.079
SIESTA KEY	1,385	56.49	9,460	6.83	0.53	34,830	25.15	1.96	720	0.52	0.041	1,200	0.87	0.068
ANNA MARIA	919	38.71	2,410	2.62	0.30	11,600	12.62	1.44	580	0.63	0.072	490	0.53	0.061
PERICO	860	46.02	1,570	1.83	0.18	6,800	7.91	0.76	80	0.09	0.009	160	0.19	0.018
LONGBOAT KEY	1,697	33.25	3,840	2.26	0.30	17,800	10.49	1.39	550	0.32	0.043	630	0.37	0.049
OTHER ISLANDS	900	38.53	2,260	2.51	0.29	11,090	12.32	1.41	400	0.44	0.051	400	0.44	0.051
DIRECT TO BAY	4,241	42.75	11,670	2.75	0.28	64,690	15.25	1.57	2,930	0.69	0.071	2,490	0.59	0.061
BAY SURFACE	33,280	69.70	78,800	2.37	0.15	430,790	12.94	0.82	3,150	0.09	0.006	76,700	2.30	0.146
TOTAL	129,412	45.57	323,310	2.73	0.29	1,626,590	12.93	1.38	42,920	0.49	0.051	119,530	0.59	0.058

TABLE A-9

DRY YEAR LOADINGS BY WATERSHED
FOR EXISTING LAND USE CONDITIONS

WATERSHED	AREA	TOTAL RUNOFF	TOTAL P			TOTAL N			LEAD			ZINC		
	(ac)	(in)	(lb)	(lb/ac)	(mg/l)	(lb)	(lb/ac)	(mg/l)	(lb)	(lb/ac)	(mg/l)	(lb)	(lb/ac)	(mg/l)
PHILLIPPI CREEK	36,417	16.79	46,410	1.27	0.33	277,180	7.61	2.00	5,610	0.15	0.040	6,050	0.17	0.044
PALMA SOLA 2	1,120	16.49	1,040	0.93	0.25	5,680	5.07	1.36	270	0.24	0.064	210	0.19	0.050
BOWLEES CREEK	6,489	23.81	7,660	1.18	0.22	46,400	7.15	1.33	5,320	0.82	0.152	3,130	0.48	0.089
WEST BRADENTON	4,395	19.43	4,710	1.07	0.24	24,740	5.63	1.28	1,130	0.26	0.058	950	0.22	0.049
CEDAR HAMMOCK	1,930	22.72	2,850	1.48	0.29	16,070	7.81	1.52	980	0.51	0.099	710	0.37	0.071
WEST BOWLEES	1,559	18.93	2,030	1.30	0.30	10,460	6.71	1.56	550	0.35	0.082	420	0.27	0.063
PALMA SOLA	900	15.06	1,100	1.22	0.38	5,140	5.71	1.67	180	0.20	0.059	140	0.16	0.046
SOUTH BRADENTON	4,635	19.43	9,680	2.09	0.47	45,050	9.72	2.21	440	0.09	0.022	710	0.15	0.035
WHITAKER BAYOU	5,015	31.33	17,380	3.47	0.49	76,200	15.20	2.14	2,810	0.56	0.079	2,870	0.57	0.081
MATHENY CREEK	3,800	26.71	9,360	2.46	0.41	47,800	12.58	2.08	1,570	0.41	0.068	1,600	0.42	0.070
CATFISH CREEK	3,360	13.25	2,000	0.60	0.20	12,130	3.61	1.20	170	0.05	0.017	290	0.09	0.029
NORTH CREEK	1,920	12.42	1,230	0.64	0.23	7,380	3.84	1.37	160	0.08	0.030	200	0.10	0.037
SOUTH CREEK	12,995	10.77	5,290	0.41	0.17	30,270	2.33	0.95	160	0.01	0.005	540	0.04	0.017
HUDSON BAYOU	1,595	22.95	2,140	1.34	0.26	11,950	7.49	1.44	1,100	0.69	0.133	680	0.43	0.082
SIESTA KEY	1,385	36.74	7,500	5.42	0.65	26,220	18.93	2.27	470	0.34	0.041	870	0.63	0.075
ANNA MARIA	919	19.27	1,180	1.28	0.29	6,130	6.67	1.53	350	0.38	0.087	250	0.27	0.062
PERICO	860	21.83	580	0.67	0.14	2,970	3.45	0.70	40	0.05	0.009	40	0.05	0.009
LONGBOAT KEY	1,697	15.18	1,750	1.03	0.30	8,850	5.22	1.52	320	0.19	0.055	280	0.16	0.048
OTHER ISLANDS	900	18.68	1,100	1.22	0.29	6,000	6.67	1.57	240	0.27	0.063	200	0.22	0.052
DIRECT TO BAY	4,241	22.35	6,210	1.46	0.29	39,410	9.29	1.83	1,740	0.41	0.081	1,290	0.30	0.060
BAY SURFACE	33,280	41.70	47,150	1.42	0.15	257,730	7.74	0.82	1,890	0.06	0.006	45,890	1.38	0.146
TOTAL	129,412	24.44	178,050	1.52	0.30	962,760	7.54	1.64	25,500	0.29	0.060	67,320	0.32	0.058

Table III. Dry year loadings to Sarasota Bay by watershed for existing land use condition (from CDM 1992).

Table IV. Wet year loadings to Sarasota Bay by watershed for 20-year future land use conditions (from CDM 1992).

WET YEAR LOADINGS BY WATERSHED
FOR 20-YEAR FUTURE LAND USE CONDITIONS
WITH SELECTED MANAGEMENT STRATEGY (ALTERNATIVES 5A, 7 AND 8)

WATERSHED	AREA	TOTAL RUNOFF	TOTAL P			TOTAL N			LEAD			ZINC		
	(ac)	(in)	(lb)	(lb/ac)	(mg/l)	(lb)	(lb/ac)	(mg/l)	(lb)	(lb/ac)	(mg/l)	(lb)	(lb/ac)	(mg/l)
PHILLIPPI CREEK	36,417	34.42	80,000	2.20	0.28	378,890	10.40	1.33	9,840	0.27	0.035	13,570	0.37	0.048
PALMA SOLA 2	1,120	36.20	2,350	2.10	0.26	11,800	10.54	1.28	470	0.42	0.051	460	0.41	0.050
BOWLEES CREEK	6,489	46.02	14,990	2.31	0.22	86,350	13.31	1.28	9,040	1.39	0.134	5,750	0.89	0.085
WEST BRADENTON	4,395	40.37	9,980	2.27	0.25	48,820	11.11	1.21	1,940	0.44	0.048	1,980	0.45	0.049
CEDAR HAMMOCK	1,930	43.45	5,500	2.85	0.29	27,550	14.27	1.45	1,640	0.85	0.086	1,290	0.67	0.068
WEST BOWLEES	1,559	38.40	4,090	2.62	0.30	19,910	12.77	1.47	910	0.58	0.067	810	0.52	0.060
PALMA SOLA	900	34.05	2,060	2.29	0.30	9,580	10.64	1.38	320	0.36	0.046	320	0.36	0.046
SOUTH BRADENTON	4,635	45.75	19,210	4.14	0.40	91,520	19.75	1.90	850	0.18	0.018	1,800	0.39	0.037
WHITAKER BAYOU	5,015	47.25	18,770	3.74	0.35	84,030	16.76	1.56	4,510	0.90	0.084	4,070	0.81	0.076
MATHENY CREEK	3,800	41.53	8,320	2.19	0.23	45,270	11.91	1.27	2,600	0.68	0.073	2,350	0.62	0.066
CATFISH CREEK	3,360	33.90	5,530	1.65	0.21	26,280	7.82	1.02	380	0.11	0.015	950	0.28	0.037
NORTH CREEK	1,920	32.13	3,300	1.72	0.24	15,310	7.97	1.09	300	0.16	0.021	560	0.29	0.040
SOUTH CREEK	12,995	29.03	18,030	1.39	0.21	81,740	6.29	0.96	410	0.03	0.005	2,470	0.19	0.029
HUDSON BAYOU	1,595	43.68	4,140	2.60	0.26	21,920	13.74	1.39	1,850	1.16	0.117	1,240	0.78	0.079
SIESTA KEY	1,385	60.24	10,630	7.68	0.56	38,330	27.68	2.03	740	0.53	0.039	1,320	0.95	0.070
ANNA MARIA	919	39.13	2,430	2.64	0.30	11,750	12.79	1.44	580	0.63	0.071	490	0.53	0.060
PERICO	860	46.18	1,550	1.80	0.17	6,790	7.90	0.75	80	0.09	0.009	160	0.19	0.018
LONGBOAT KEY	1697	34.09	3,880	2.29	0.30	18,310	10.79	1.40	560	0.33	0.043	640	0.38	0.049
OTHER ISLANDS	900	39.00	2,280	2.53	0.29	11,240	12.49	1.41	400	0.44	0.050	410	0.46	0.052
DIRECT TO BAY	4,241	41.53	10,970	2.59	0.27	55,670	13.13	1.39	2,940	0.69	0.074	2,500	0.59	0.063
BAY SURFACE	33,280	69.70	78,800	2.37	0.15	430,790	12.94	0.82	3,150	0.09	0.008	76,700	2.30	0.146
TOTAL	129,412	45.76	306,810	2.66	0.28	1,521,850	12.62	1.33	43,510	0.49	0.052	119,840	0.59	0.058

Note: Loading totals do not include pollutant settling in tidal tributaries. See text for discussion of settling in tributaries.

Table V. Dry year loadings to Sarasota Bay by watershed for 20-year future land use conditions (from CDM 1992).

TABLE C-9

DRY YEAR LOADINGS BY WATERSHED
FOR 20-YEAR FUTURE LAND USE CONDITIONS
WITH SELECTED MANAGEMENT STRATEGY (ALTERNATIVES 5A, 7 AND 8)

WATERSHED	AREA	TOTAL RUNOFF	TOTAL P			TOTAL N			LEAD			ZINC		
	(ac)	(in)	(lb)	(lb/ac)	(mg/l)	(lb)	(lb/ac)	(mg/l)	(lb)	(lb/ac)	(mg/l)	(lb)	(lb/ac)	(mg/l)
PHILLIPPI CREEK	36,417	16.11	36,610	1.01	0.28	194,560	5.34	1.46	5,790	0.16	0.044	6,140	0.17	0.046
PALMA SOLA 2	1,120	17.40	1,090	0.97	0.25	5,970	5.33	1.35	280	0.25	0.063	230	0.21	0.052
BOWLEES CREEK	6,489	24.64	7,660	1.18	0.21	47,410	7.31	1.31	5,390	0.83	0.149	3,230	0.50	0.089
WEST BRADENTON	4,395	19.83	4,650	1.06	0.24	24,910	5.67	1.28	1,150	0.26	0.058	970	0.22	0.049
CEDAR HAMMOCK	1,930	22.72	2,850	1.48	0.29	15,070	7.81	1.52	980	0.51	0.099	710	0.37	0.071
WEST BOWLEES	1,559	19.05	2,040	1.31	0.30	10,530	6.75	1.56	550	0.35	0.082	420	0.27	0.062
PALMA SOLA	900	15.81	940	1.04	0.29	4,800	5.33	1.49	180	0.20	0.056	150	0.17	0.047
SOUTH BRADENTON	4,635	27.27	13,820	2.98	0.48	68,960	14.88	2.41	510	0.11	0.018	910	0.20	0.032
WHITAKER BAYOU	5,015	26.96	12,550	2.50	0.41	54,530	10.87	1.78	2,740	0.55	0.089	2,470	0.49	0.081
MATHENY CREEK	3,800	21.25	4,050	1.07	0.22	24,630	6.48	1.35	1,540	0.41	0.084	1,240	0.33	0.068
CATFISH CREEK	3,360	15.36	2,170	0.65	0.19	11,950	3.56	1.02	210	0.06	0.018	370	0.11	0.032
NORTH CREEK	1,920	14.38	1,310	0.69	0.21	7,050	3.67	1.19	170	0.09	0.027	230	0.12	0.037
SOUTH CREEK	12,995	11.81	5,810	0.45	0.17	32,230	2.48	0.93	190	0.01	0.005	630	0.05	0.018
HUDSON BAYOU	1,595	22.95	2,140	1.34	0.26	11,950	7.49	1.44	1,100	0.69	0.133	680	0.43	0.082
SIESTA KEY	1,385	40.48	8,660	6.25	0.68	29,710	21.45	2.34	490	0.35	0.039	990	0.71	0.078
ANNA MARIA	919	19.58	1,190	1.29	0.29	6,230	6.78	1.53	350	0.38	0.086	260	0.28	0.064
PERICO	860	21.95	570	0.66	0.13	2,970	3.45	0.69	40	0.05	0.009	40	0.05	0.009
LONGBOAT KEY	1697	15.80	1,790	1.05	0.29	9,200	5.42	1.51	330	0.19	0.054	300	0.18	0.049
OTHER ISLANDS	900	19.03	1,130	1.26	0.29	6,100	6.78	1.57	240	0.27	0.062	200	0.22	0.052
DIRECT TO BAY	4,241	21.07	5,530	1.30	0.27	30,370	7.16	1.50	1,740	0.41	0.086	1,290	0.30	0.064
BAY SURFACE	33,280	41.70	47,150	1.42	0.15	257,730	7.74	0.82	1,890	0.06	0.006	45,890	1.38	0.146
TOTAL	129,412	24.47	163,730	1.47	0.28	856,860	7.23	1.43	25,880	0.29	0.060	67,350	0.32	0.058

1.2. Previous Study

The study area is very shallow, generally ranging from 30 cm to 3 meters deep. Geometry of the study area is very complex. Phillippi Creek provides an annual average discharge of about 1.63 mgd with a concentration of 3.78 mg/l for TN (CDN, 1992). The study area (Segment 13) has only 1,438 ac. surface area (vs. 33, 280 ac. surface area for the entire Bay), but has 42,805 ac. drainage area (vs. 96,132 ac. for the entire Bay). The Florida Trophic State Index for this area is fair. As shown in Table VI, the circulation and flushing study conducted by Sheng and Peene (1992) and Sheng et al. (1995) indicated that the study area is well flushed compared to the segment behind the Midnight Pass (Segment 14). Thus, for this study, a hydrodynamics model should be used to quantify the flow in the Roberts Bay area. Sheng et al. (1995) recently detailed a comprehensive field and modeling study on the circulation and transport in the entire Sarasota Bay estuarine system. A multi-dimensional curvilinear-grid circulation model was sufficiently calibrated and validated with field data collected in Sarasota Bay and Tampa Bay during 1990, 1991, and 1992.

Synoptic water quality data were collected at 101 sampling stations in the Sarasota Bay estuarine system during 1991 (Mote Marine Laboratory 1993). Stations 51 to 94 are within the region of interest of this study. The field investigation was carried out every three months on the following days: 08/08/90, 11/14/90, 02/12/91, and 05/14/91. The water quality parameters measured include the following: Dissolved Oxygen near the surface and near the bottom, Total Phosphorus, Ortho-Phosphorus, Ammonia-N, Nitrate-N & Nitrite-N, Total Kjeldahl-N, and Chlorophyll-a. These data provide four snapshots of the DO and nutrients concentrations of the estuarine system, but provide no information on the temporal DO and nutrients dynamics. These data will be described in detail in Chapter 2.

As shown in Figure 3, diurnal DO concentration measured with HydroLab DataSonde Model IIH/III in the Midnight Pass area during 1991 (Sheng et al. 1995) fluctuated between high values of 7-8 ppm during the morning to low values of 0-1 ppm during the evening and predawn hours due to oxygen demand of epiphytes in bottom water. Based on these preliminary continuous DO measurements, the quarterly synoptic sampling in Sarasota Bay was modified to include more continuous DO measurement at selected stations. Marshall and Leverone (1994) reported on the continuous DO measurements in sarasota Bay during July through October 1993. They found that hypoxia probably occurs in most Sarasota Bay segments due to either nutrient enrichment (Heyl 1992) or poor flushing (Sheng and Peene 1992), except near the passes.

Table VI. Calculated relative flushing rates (% total mass flushed after 8 days of model simulation) in various sections of the Sarasota Bay system.

Section	Segments	Includes	Relative Flushing Quality	% of Mass Flushed After 8 days
1	1,2	Anna Maria Sound Cortez Bridge	Good	81
2	3	Palma Sola Bay	Poor	31
3	4,5,6	Longboat Pass Tidy Island	Good	64
4	7,8	Middle Sarasota Bay	Poor	32
5	9,10,11,12	New Pass, Big Pass, Southern Sarasota Bay	Good	81
6	13	Roberts Bay	Good	76
7	14,15	Little Sarasota Bay Midnight Pass	Poor	27
8	16	Blackburn Bay	Good	72

Epiphytic algae can be found on the leaves of seagrass at the bottom of an estuary, while macroalgae can be found on the sandy bottom. Seagrass in Roberts Bay covers 16.8% of the segment area, compared to 32% in City Island area, 50.6% in West Palma Sola Bay, and 40.9% in Blackburn Bay (Culter, 1992). <u>*Halodule wrightii*</u> and <u>*Thalassia testudinum*</u> are present in the study area. Seagrass slows down the flow and traps suspended sediments and nutrients. Hence silt and clay particles are often found near the seagrass. Because of the smaller seagrass area in the study area, the effect of epiphytic algae is expected to be less important than in other areas of Sarasota Bay. Nevertheless, to quantify the effect of 25-30% reduction in nutrient loading on the nutrient concentration in the study area, it is useful to include epiphytic algae and seagrass in the water quality model.

Seagrass data were collected at four meadows of turtle grass (Thalassia testudinum) on a bimonthly basis from June 1992 to July 1993 (Tomasko et al. 1995). Data indicated substantial spatial and temporal differences in turtle grass parameters, but smaller variation in water quality parameters. Turtle grass productivity and biomass were negatively correlated with watershed nitrogen loads, while water quality parameters did not show clear responses to differences in watershed nutrient inputs. The results suggest that traditional water quality monitoring programs can fail to detect the onset or continuance of nutrient-induced declines or growths in seagrass biomass and productivity. The results also suggest that traditional water quality models, which do not consider the nutrient-induced seagrass declines or growths, may not be useful for computing Pollutant load Reduction Goal (PLRG) in an estuary like Sarasota Bay.

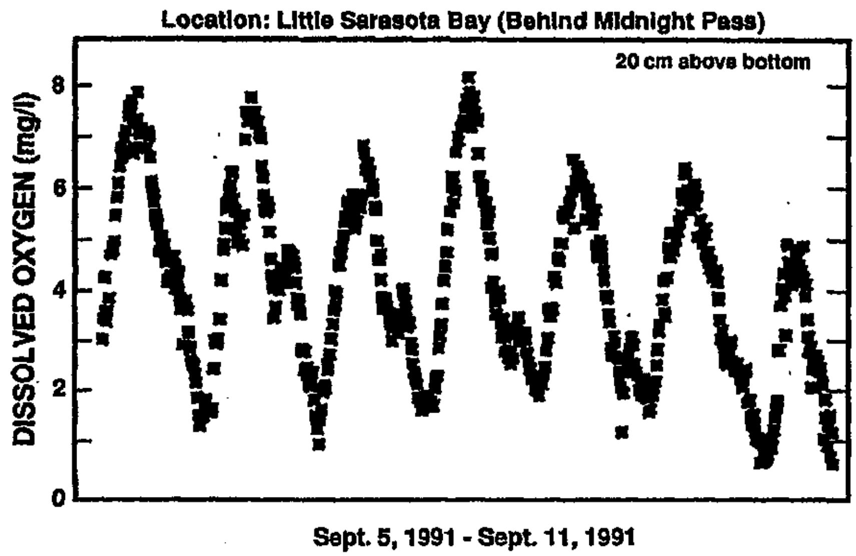

Figure 3. Continuous DO concentrations measured in Little Sarasota Bay behind Midnight Pass during September 5-11, 1991. High DO is usually measured during early morning hours. Low DO is usually found in late afternoon and evening.

1.3. Scope of This Study

In order to accomplish the objectives described in the previous section, we decided to conduct a modeling study on the circulation and water quality dynamics of the Roberts Bay area under present and future land use conditions described in Tables I to V. Due to the short duration of the study and the lack of comprehensive data, we decided to use the vertically-integrated version of the curvilinear-grid 3-D hydrodynamics model of Sarasota Bay (Sheng and Peene 1991, 1992; Sheng et al. 1995) to compute the circulation in the study area.

To compute the water quality dynamics in Roberts Bay, we decided to develop a curvilinear-grid vertically-integrated water quality model. The water quality model includes the processes of advection, diffusion, and transformations for DO, Nitrogen species, Phosphorus species, phytoplankton, CBOD, and suspended sediment concentration. The transformation processes in the water quality model are based on those used in the WASP model (Ambrose et al. 1994) with some modifications. However, unlike the WASP model which often uses crudely calculated or calibrated advective and diffusive fluxes, our water quality model uses the flow filed (i.e., advection and diffusion) computed by the curvilinear-grid hydrodynamics model. When the WASP model is coupled to a hydrodynamics model, it often uses a large time step and coarse spatial grid for the water quality model but a smaller time step and fine spatial grid for the hydrodynamics model. To eliminate errors associated with the coupling of fine-grid hydrodynamics model and coarse-grid water quality model, we use the same time step and spatial grid for a dynamically coupled hydrodynamics and water quality model.

To assess the effects of nutrient load reduction on the seagrass in Sarasota Bay, we also decided to include a seagrass dynamics model in the overall modeling system. The seagrass model is based on the model developed by Fong and Harwell (1994) with some modifications.

1.4. Organization of This Report

In the following Chapter 2, water quality data used for this modeling study are described. Chapter 3 describes the hydrodynamics model, the water quality model and the seagrass model. Chapter 4 presents model results of water quality and seagrass simulations for present and future land use conditions. Conclusions and recommendations are given in Chapter 5.

2. WATER QUALITY DATA FOR MODEL SIMULATIONS

2.1. Existing Condition

As described in Chapter 1, water quality data from 101 monitoring stations in Sarasota Bay were collected by Sarasota Bay National Estuary Program (Mote Marine Laboratory 1993). Theses data were taken from Anna Maria Sound, Big Sarasota Bay, Roberts Bay, and Little Sarasota Bay. Only stations 51 to 94 are within the region of interest of the present study (Figure 4). These synoptic data were collected on four days: 08/08/90, 11/14/90, 02/12/91, and 05/14/91. These data are shown in Tables VII, VIII, IX, and X. Negative values in the original data provided to us by SBNEP have been set to zeros. (I,J) in the tables represent the grid indices of the sampling stations in the curvilinear grid of the numerical model shown in Figure 5. The grid is finer than the Sarasota Bay grid used by Sheng et al. (1995) as shown in Figure 6. As shown in Figure 5, additional grid points have been added in the Phillippi Creek area and the Midnight Pass area.

Figure 7 shows the locations of the water quality sampling stations in the numerical grid. Due to the sparse sampling stations in a fine grid, we decided to divide the numerical grid into five zones so that it is easier to specify the initial conditions for water quality model simulations and to compare the model results with data. Model simulations are conducted by solving the equations inside each and every fine grid cell, but initial conditions and final conditions of model runs are given in terms of the zone-averaged values. As shown in Figure 8, the five zones are:

- Zone 1: Offshore Water
- Zone 2: Big Sarasota Bay

• Zone 3: Roberts Bay

• Zone 4: Little Sarasota Bay

• Zone 5: Blackburn Bay

We processed the raw data provided to us by SBNEP to produce the averaged concentrations inside the five zones. Data in Zone 5 (Blackburn Bay) are assumed to be the same as those in Zone 2 (Big Sarasota Bay). The measured DO at two vertical levels are averaged to produce a vertically averaged DO concentration. In addition, we assume that the Inorganic Phosphorus concentration is equal to the difference between Total Phosphorus and Ortho-Phosphorus, while Organic Nitrogen concentration is obtained by subtracting Ammonia-N, Nitrate-N and Nitrite-N from Total Kjeldahl-N. Phytoplankton concentration is assumed to be the same as the Chlorophyll-a concentration. If at a certain station the data is negative, that number is simply discarded in computing the zone-averaged values. For the species not measured, i.e. CBOD, the values are given to be around 1.5 inside the Bay and 0.5 in the offshore zones.

The zone-averaged water quality data during the four synoptic surveys are shown in Figures 9, 10, 11, and 12 for Zones 1, 2, 3, and 4, respectively. These data are used to provide initial conditions for the water quality model simulation and to compare with the zone-averaged model results.

9

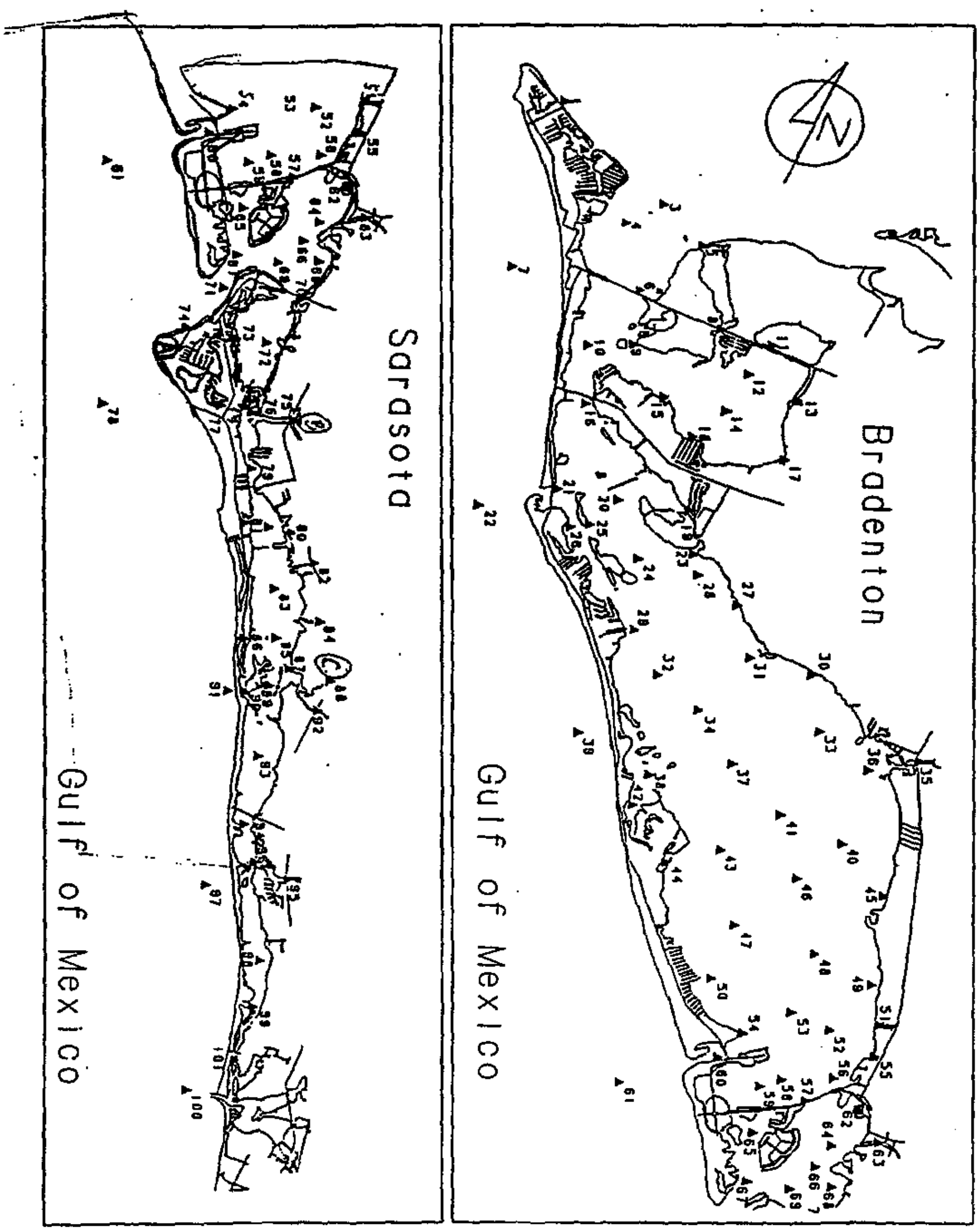

Figure 4. Locations of the quarterly water quality sampling stations in Sarasota Bay during 1990-1991. Negative values have been set to zeros.

TABLE VII. Measured water quality data at Stations 51 to 94 in Sarasota Bay on August 8, 1990.

#	I	J	DO	SED	OP	IP	AN	NN	ON	Chl-a
51	5	19	7.00	16.40	0.75	0.00	1.33	0.31	0.00	13.61
52	6	18	5.45	7.60	10.11	0.00	0.00	0.03	0.61	0.00
53	6	16	6.45	8.20	0.04	0.03	0.00	0.06	0.19	0.00
54	5	12	7.65	8.40	0.09	0.00	0.00	0.07	0.16	11.28
55	7	19	6.30	24.80	9.69	0.00	0.00	0.04	0.45	0.00
56	8	18	5.80	14.40	0.07	0.05	0.00	0.04	0.27	11.64
57	9	16	5.75	10.00	0.06	0.03	0.00	0.07	0.75	5.22
58	9	15	6.25	11.20	1.10	0.01	0.00	0.18	0.17	2.90
59	9	14	7.25	21.60	0.14	0.00	0.00	0.02	0.80	0.92
60	8	10	6.40	2.80	0.33	0.00	0.00	0.09	0.13	1.86
61	6	4	6.20	7.40	0.03	0.02	0.00	0.09	0.01	0.68
62	14	21	6.75	11.20	0.11	0.00	0.00	0.00	0.70	10.48
64	16	20	6.60	15.20	3.61	0.00	0.00	0.00	0.48	10.28
65	17	13	6.30	7.20	0.05	0.00	0.00	0.05	0.34	3.46
66	19	19	6.20	12.40	0.12	0.00	0.00	0.04	0.41	2.31
67	21	13	6.15	12.40	0.02	0.00	0.00	0.03	0.58	0.00
68	19	22	7.00	10.80	0.10	0.04	0.00	0.04	0.34	6.41
69	20	19	7.65	4.00	0.07	0.07	0.00	0.13	0.60	4.38
70	22	22	6.05	10.40	0.17	0.06	0.00	0.09	0.32	4.58
71	21	10	6.15	4.40	0.53	0.04	0.00	0.22	0.07	3.70
72	28	22	6.45	14.80	0.30	0.05	0.00	0.02	0.67	30.14
73	20	17	5.85	16.40	0.77	0.04	0.00	0.05	0.53	11.43
74	22	5	6.30	4.00	0.03	0.02	0.00	0.04	0.23	2.30
75	38	28	5.35	6.00	0.22	0.19	0.11	0.10	0.85	15.00
76	22	17	6.35	19.20	0.10	0.06	0.00	0.04	0.56	12.55
78	28	1	5.55	11.20	0.08	0.05	0.00	0.09	0.18	2.30
79	43	20	6.00	16.80	0.05	0.15	0.00	0.07	0.58	0.00
80	54	22	4.50	9.20	0.30	0.00	0.00	0.31	0.43	13.20
81	53	22	4.40	18.60	0.17	0.03	0.00	0.10	0.52	14.38
82	57	22	3.70	7.60	0.21	0.10	0.04	0.11	0.87	16.48
83	63	23	4.90	8.80	0.18	0.00	0.00	0.09	0.91	0.71
85	69	23	5.15	12.80	0.16	0.05	0.00	0.88	0.00	10.71
86	69	13	5.30	7.60	0.14	0.02	0.00	0.08	0.36	4.51
87	72	24	6.75	12.00	0.20	0.05	0.00	0.11	0.48	5.23
88	70	31	4.90	6.80	0.17	0.14	0.00	0.09	0.93	19.82
89	79	17	7.10	12.00	0.00	0.04	0.00	0.05	0.73	5.70
90	85	12	5.55	13.20	0.11	0.06	0.00	0.00	0.57	14.62
91	79	7	5.95	13.20	3.11	0.04	0.00	0.10	0.00	5.54
93	92	20	5.45	4.80	0.09	0.07	0.00	0.05	0.34	12.39
94	96	15	5.85	6.82	0.90	0.00	0.01	0.04	0.24	7.30

TABLE VIII. Measured water quality data at Stations 51 to 94 in Sarasota Bay on November 14 1990.

#	I	J	DO	SED	OP	IP	AN	NN	ON	Chl-a
51	5	19	6.95	4.00	0.08	0.07	0.00	0.14	0.42	6.27
52	6	18	6.60	8.80	0.10	0.04	0.00	0.07	0.16	5.46
53	6	16	7.20	10.40	0.02	0.10	0.00	0.10	0.58	3.43
54	5	12	8.60	10.40	0.09	0.04	0.00	0.08	0.60	4.21
55	7	19	5.90	8.00	0.13	0.04	0.00	0.04	0.92	10.08
56	8	18	6.65	9.20	0.16	0.01	0.00	0.03	0.93	5.29
57	9	16	6.70	7.60	0.16	0.01	0.06	0.03	0.74	6.11
58	9	15	6.65	8.40	0.18	0.01	0.00	0.01	0.85	3.66
59	9	14	6.90	6.40	0.11	0.03	0.00	0.02	1.31	6.17
60	8	10	6.70	10.40	0.04	0.07	0.00	0.03	0.82	3.76
61	6	4	6.40	6.00	0.00	0.00	0.00	0.09	1.01	8.16
62	14	21	6.65	7.20	0.11	0.01	0.00	0.05	1.01	7.22
64	16	20	7.35	6.40	0.10	0.02	0.00	0.13	0.93	3.36
65	17	13	6.60	8.00	0.12	0.03	0.00	0.04	0.78	9.15
66	19	19	7.00	7.20	0.18	0.01	0.00	0.05	0.72	6.07
67	21	13	6.85	7.20	0.18	0.01	0.00	0.05	0.72	6.07
68	19	22	9.10	5.60	0.22	0.14	0.00	0.10	0.73	4.14
69	20	19	9.95	10.80	0.13	0.00	0.00	0.03	0.90	6.62
70	22	22	9.00	5.20	0.16	0.01	0.00	0.02	1.38	5.94
71	21	10	7.60	5.60	0.17	0.02	0.00	0.05	0.34	3.22
72	28	22	9.20	6.80	0.10	0.02	0.00	0.02	0.86	7.46
73	20	17	8.60	12.40	0.09	0.05	0.00	0.12	0.18	6.75
74	22	5	6.85	13.20	0.15	0.00	0.11	0.26	0.41	4.04
75	38	28	7.25	9.60	0.04	0.12	0.02	0.26	0.85	6.55
76	22	17	8.55	8.00	0.06	0.08	0.00	0.15	0.00	8.65
78	28	1	8.00	11.20	0.13	0.00	0.00	0.06	0.01	3.60
79	43	20	7.90	11.20	0.21	0.00	0.00	0.03	1.06	6.99
80	54	22	8.05	7.20	0.05	0.26	0.34	0.09	1.33	11.43
81	53	22	7.65	12.00	0.04	0.08	0.00	0.11	0.01	6.88
82	57	22	6.60	4.00	0.00	0.23	0.00	0.20	0.80	6.08
83	63	23	7.80	9.20	0.08	0.09	0.01	0.11	0.86	9.60
85	69	23	8.15	13.60	0.13	0.02	0.00	0.06	1.41	9.23
86	69	13	7.50	16.40	0.28	0.02	0.00	0.05	1.05	10.44
87	72	24	10.10	6.40	0.13	0.01	0.00	0.03	1.26	20.75
88	70	31	4.60	2.40	0.05	0.05	0.00	0.18	0.64	0.00
89	79	17	7.90	19.20	0.24	0.03	0.00	0.05	0.52	11.61
90	85	12	7.80	15.60	0.13	0.01	0.00	0.05	1.18	8.21
91	79	7	7.40	8.00	0.14	0.02	0.00	0.06	0.72	2.98
93	92	20	7.30	20.00	0.13	0.01	0.00	0.02	1.22	7.95
94	96	15	7.60	14.40	0.02	0.02	0.00	0.02	0.63	8.92

TABLE IX. Measured water quality data at Stations 51 to 94 in Sarasota Bay on February 12, 1991.

#	I	J	DO	SED	OP	IP	AN	NN	ON	Chl-a
51	5	19	6.70	74.00	0.51	0.56	0.00	0.69	0.00	4.91
52	6	18	7.20	22.40	0.19	0.04	0.00	0.10	0.20	20.50
53	6	16	7.30	14.00	0.08	0.06	0.00	0.03	0.18	3.19
54	5	12	7.65	8.00	0.01	0.05	0.00	0.02	0.15	8.03
55	7	19	5.20	43.60	0.19	0.04	0.00	0.00	0.65	18.73
56	8	18	6.90	30.00	0.10	0.03	0.00	0.04	0.38	8.48
57	9	16	7.00	16.00	0.57	0.04	0.00	0.04	0.34	4.68
58	9	15	7.45	21.00	0.04	0.03	0.00	0.00	0.45	4.65
59	9	14	7.50	6.80	0.17	0.02	0.00	0.02	0.22	3.22
60	8	10	8.00	13.20	0.28	0.02	0.00	0.02	0.31	2.27
61	6	4	7.60	20.80	0.07	0.03	0.00	0.01	0.17	3.80
62	14	21	7.30	15.20	0.06	0.02	0.00	0.01	0.56	1.63
64	16	20	7.30	8.40	0.01	0.04	0.00	0.03	0.29	4.07
65	17	13	6.85	14.00	0.07	0.03	0.00	0.06	0.15	4.35
66	19	19	7.10	10.00	0.11	0.04	0.00	0.05	0.20	4.55
67	21	13	7.05	13.20	0.08	0.03	0.00	0.05	0.30	7.11
68	19	22	9.50	17.60	0.15	0.02	0.00	0.05	0.36	4.28
69	20	19	10.95	13.60	0.08	0.03	0.00	0.06	0.21	3.90
70	22	22	9.35	10.80	0.00	0.06	0.00	0.06	0.33	4.06
71	21	10	8.60	6.80	0.23	0.02	0.00	0.04	0.19	3.54
72	28	22	9.15	22.30	0.42	0.04	0.00	0.02	0.31	7.64
73	20	17	9.40	9.20	0.06	0.08	0.01	0.01	0.31	3.43
74	22	5	8.40	13.20	0.00	1.79	0.00	0.16	0.39	1.08
75	38	28	6.15	6.00	0.03	0.18	0.00	0.20	0.49	10.48
76	22	17	8.60	17.20	0.06	0.05	0.00	0.03	0.34	3.63
78	28	1	8.50	10.00	0.09	0.09	0.00	0.04	0.15	1.24
79	43	20	8.40	19.00	0.17	0.05	0.00	0.06	0.35	3.87
80	54	22	10.35	8.80	0.01	0.22	0.00	0.11	0.63	16.22
81	53	22	8.10	17.70	0.01	0.07	0.00	0.04	0.29	4.48
82	57	22	6.50	7.60	0.03	0.25	0.00	0.25	0.97	10.28
83	63	23	8.60	6.80	0.00	0.07	0.00	0.03	0.23	0.59
85	69	23	8.05	7.60	0.06	0.06	0.00	0.00	0.40	5.84
86	69	13	9.30	7.60	0.11	0.03	0.00	0.03	0.56	5.50
87	72	24	9.30	14.40	0.10	0.06	0.00	0.07	0.33	4.96
88	70	31	3.50	0.80	0.00	0.09	0.00	0.15	0.78	4.45
89	79	17	7.80	20.00	0.11	0.06	0.00	0.08	0.53	7.74
90	85	12	8.60	11.60	0.12	0.06	0.00	0.05	0.27	4.01
91	79	7	8.00	17.20	0.00	0.11	0.00	0.05	3.22	2.07
93	92	20	6.90	12.80	0.08	0.06	0.00	0.00	0.51	6.18
94	96	15	6.80	10.60	0.05	0.05	0.00	0.04	0.42	6.99

TABLE X. Measured water quality data at Stations 51 to 94 in Sarasota Bay on May 14, 1991.

#	I	J	DO	SED	OP	IP	AN	NN	ON	Chl-a
51	5	19	5.90	17.60	0.14	0.01	0.00	0.16	0.89	0.68
52	6	18	6.85	8.40	0.03	0.02	0.00	0.08	0.37	0.26
53	6	16	6.65	3.60	0.00	0.02	0.00	0.09	0.38	0.06
54	5	12	7.65	4.80	0.01	0.02	0.00	0.06	0.57	0.33
55	7	19	5.75	8.80	0.03	0.02	0.00	0.01	0.70	0.79
56	8	18	6.40	16.40	0.03	0.02	0.00	0.00	0.73	0.58
57	9	16	7.65	6.00	0.04	0.01	0.00	0.02	0.62	0.17
58	9	15	7.05	6.00	0.01	0.01	0.00	0.05	0.45	0.09
59	9	14	9.25	11.20	0.01	0.01	0.00	0.03	0.62	0.07
60	8	10	7.65	17.20	0.00	0.01	0.00	0.04	0.30	0.08
61	6	4	7.60	6.40	0.00	0.01	0.00	0.04	0.38	0.08
62	14	21	7.95	18.80	0.03	0.01	0.00	0.04	0.68	0.59
64	16	20	8.75	12.80	0.00	0.01	0.00	0.04	0.31	0.24
65	17	13	8.20	9.20	0.01	0.01	0.00	0.03	0.50	0.05
66	19	19	8.50	11.60	0.00	0.01	0.00	0.02	0.43	0.16
67	21	13	8.45	8.40	0.00	0.02	0.00	0.01	0.34	0.13
68	19	22	9.55	10.40	0.00	0.01	0.00	0.01	0.42	0.20
69	20	19	9.55	11.60	0.00	0.01	0.00	0.02	0.42	0.21
70	22	22	8.50	4.00	0.00	0.03	0.00	0.04	0.53	0.14
71	21	10	8.05	5.60	0.00	0.08	0.00	0.02	0.30	0.07
72	28	22	8.25	12.80	0.00	0.04	0.00	0.04	0.37	0.28
73	20	17	6.95	11.20	0.03	0.02	0.00	0.03	0.29	0.41
74	22	5	7.55	2.60	0.00	0.01	0.00	0.03	0.60	0.19
75	38	28	4.90	9.20	0.00	0.10	0.00	0.04	1.06	0.47
76	22	17	7.20	11.20	0.05	0.02	0.00	0.02	0.61	0.00
78	28	1	7.65	4.80	0.00	0.01	0.00	0.05	0.40	0.12
79	43	20	6.60	28.40	0.01	0.06	0.00	0.06	0.62	0.46
80	54	22	4.30	6.80	0.14	0.09	0.00	0.19	0.68	0.81
81	53	22	5.40	8.40	0.02	0.07	0.00	0.06	0.60	0.28
82	57	22	3.35	10.00	0.14	0.21	0.00	0.28	0.75	0.36
83	63	23	6.40	14.00	0.06	0.06	0.00	0.03	0.76	0.36
85	69	23	7.10	6.40	0.05	0.05	0.00	0.04	0.72	0.43
86	69	13	6.45	4.40	0.03	0.03	0.00	0.05	0.76	0.36
87	72	24	7.85	8.00	0.03	0.05	0.00	0.07	0.77	0.39
88	70	31	3.30	12.00	0.23	0.23	0.11	0.10	1.09	1.73
89	79	17	7.35	6.40	0.06	0.02	0.01	0.09	1.24	0.49
90	85	12	7.40	4.40	0.02	0.04	0.00	0.03	0.84	0.40
91	79	7	8.10	4.00	0.00	0.01	0.00	0.03	0.33	0.13
93	92	20	6.60	23.00	0.40	0.19	0.00	0.05	1.68	0.92
94	96	15	7.50	9.20	3.58	0.02	0.00	0.03	0.50	0.25

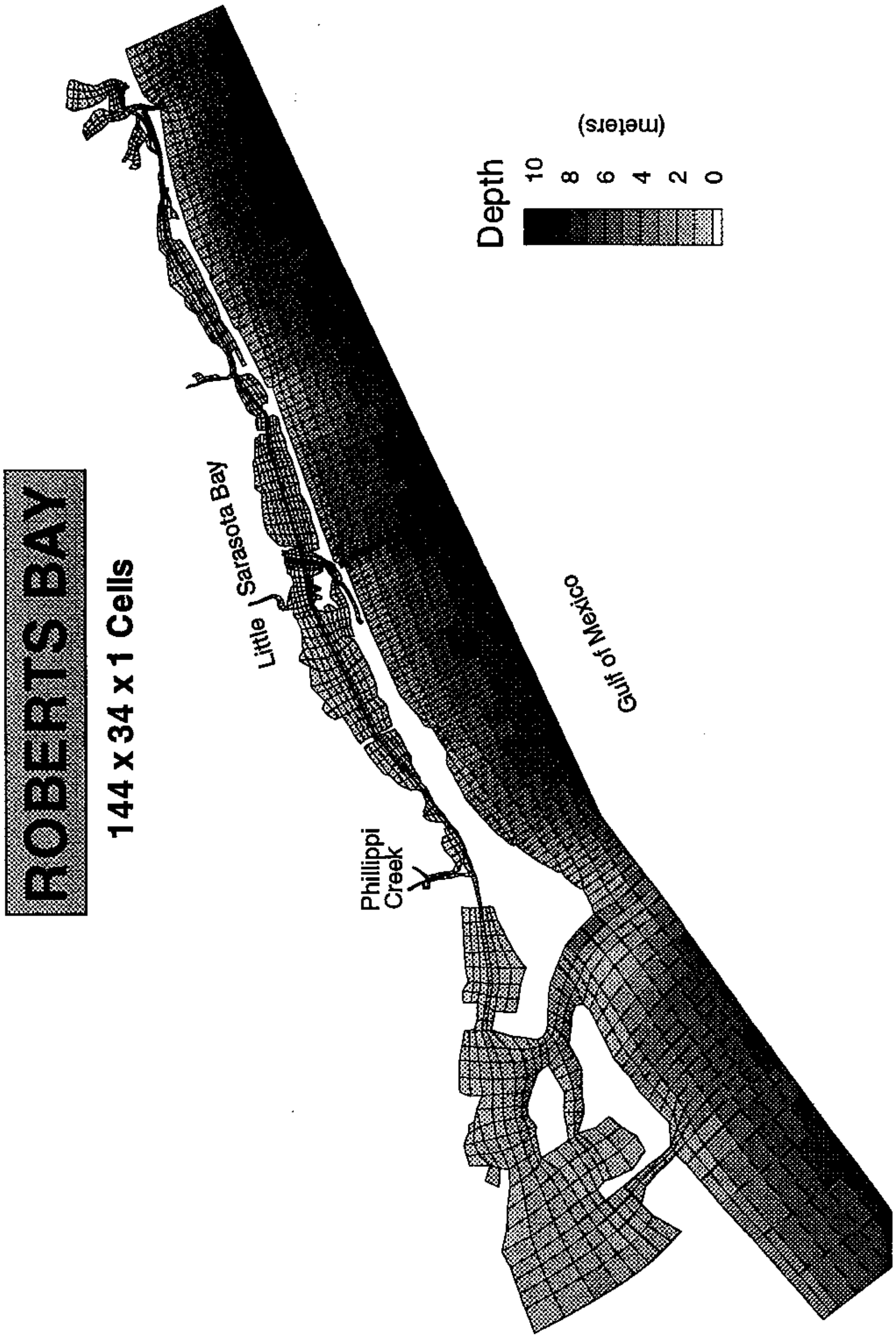

Figure 5. A curvilinear grid for the study area.

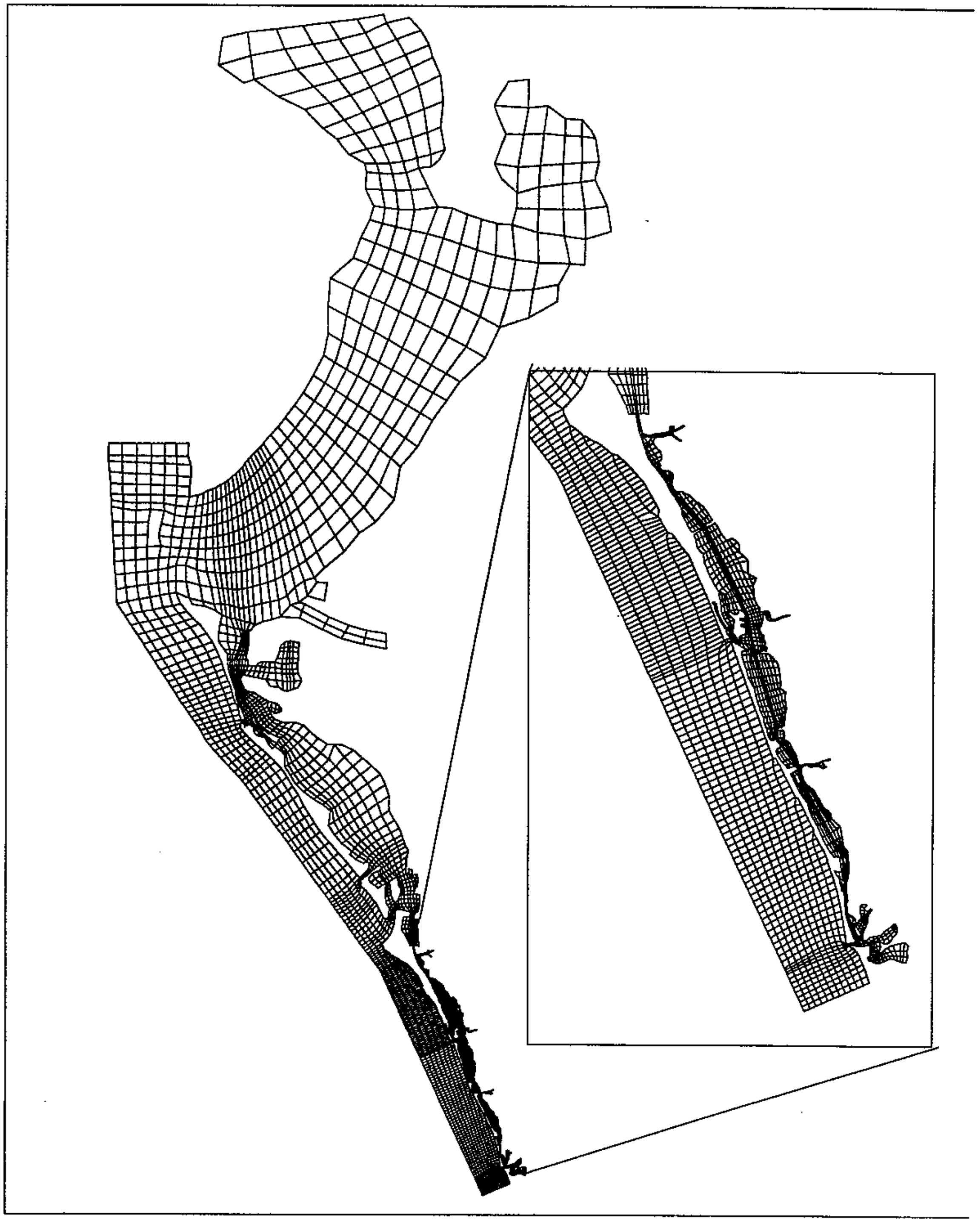

Figure 6. A refined boundary-fitted grid used for model simulation of Sarasota Bay circulation.

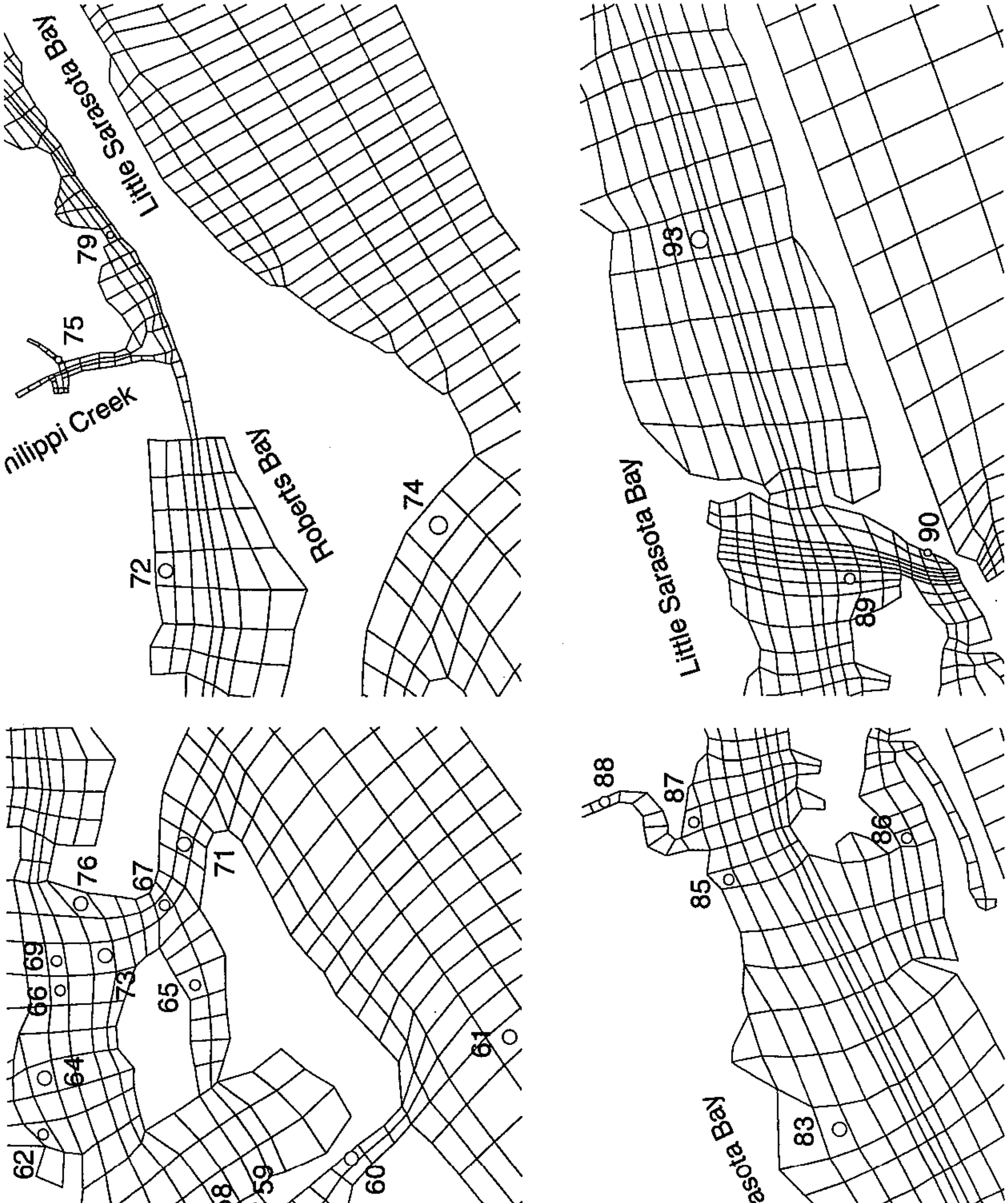

Figure 7. Locations of the quarterly water quality sampling stations inside the curvilinear numerical grid.

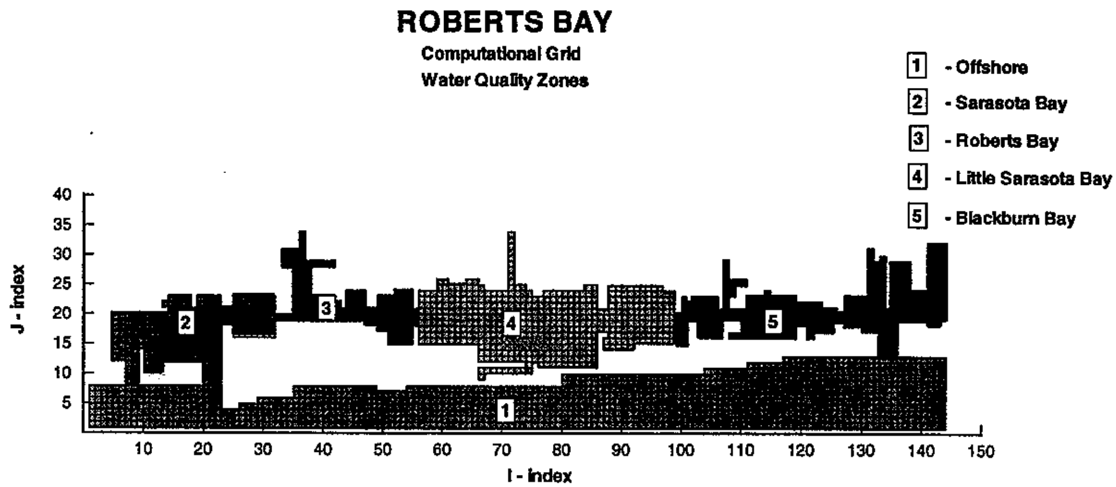

Figure 8. The five zones with similar water quality characteristics, shown in the computational grid.

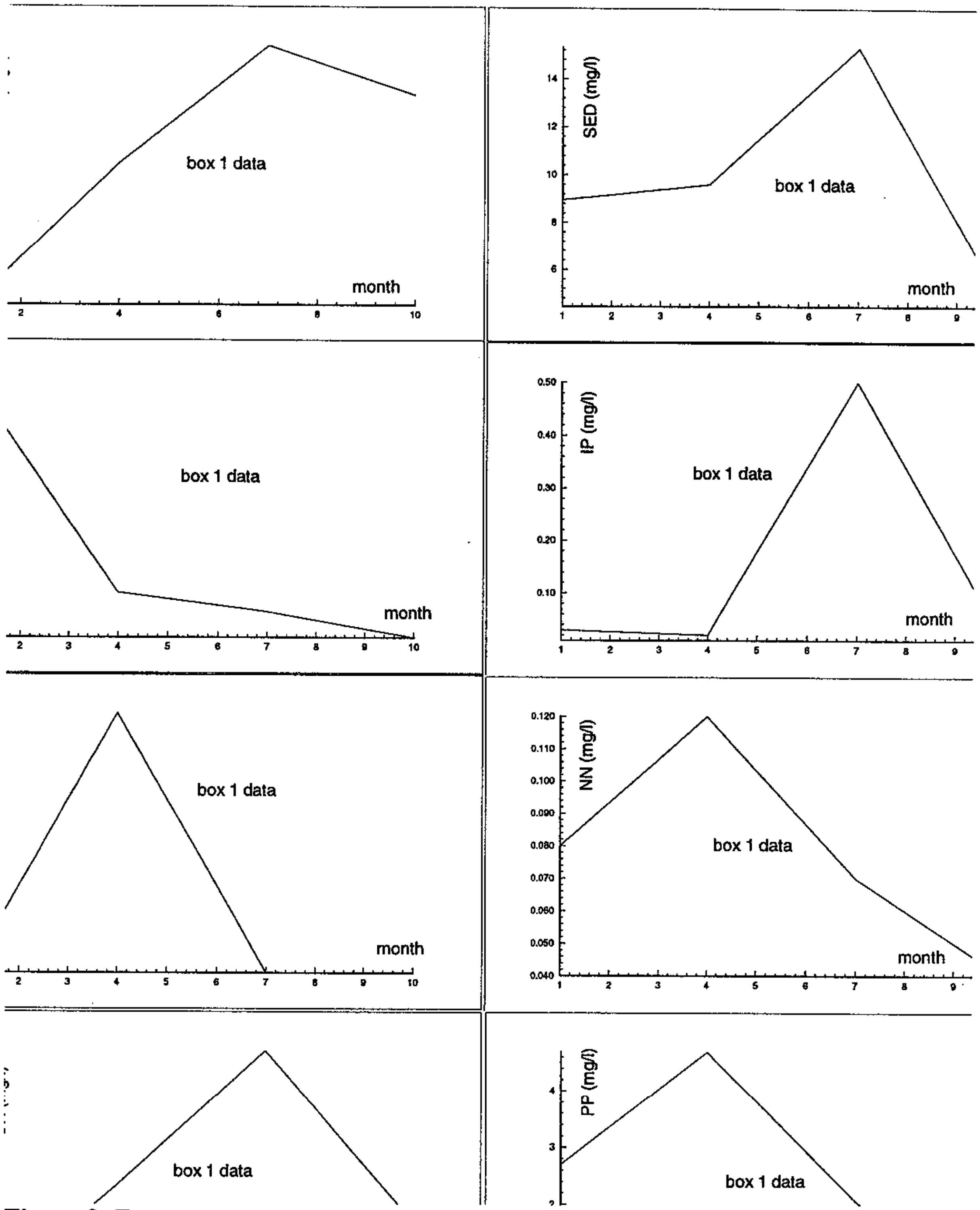

Figure 9. Zone-averaged water quality data inside Zone 1 (Offshore Water) during August 1990 and May 1991.

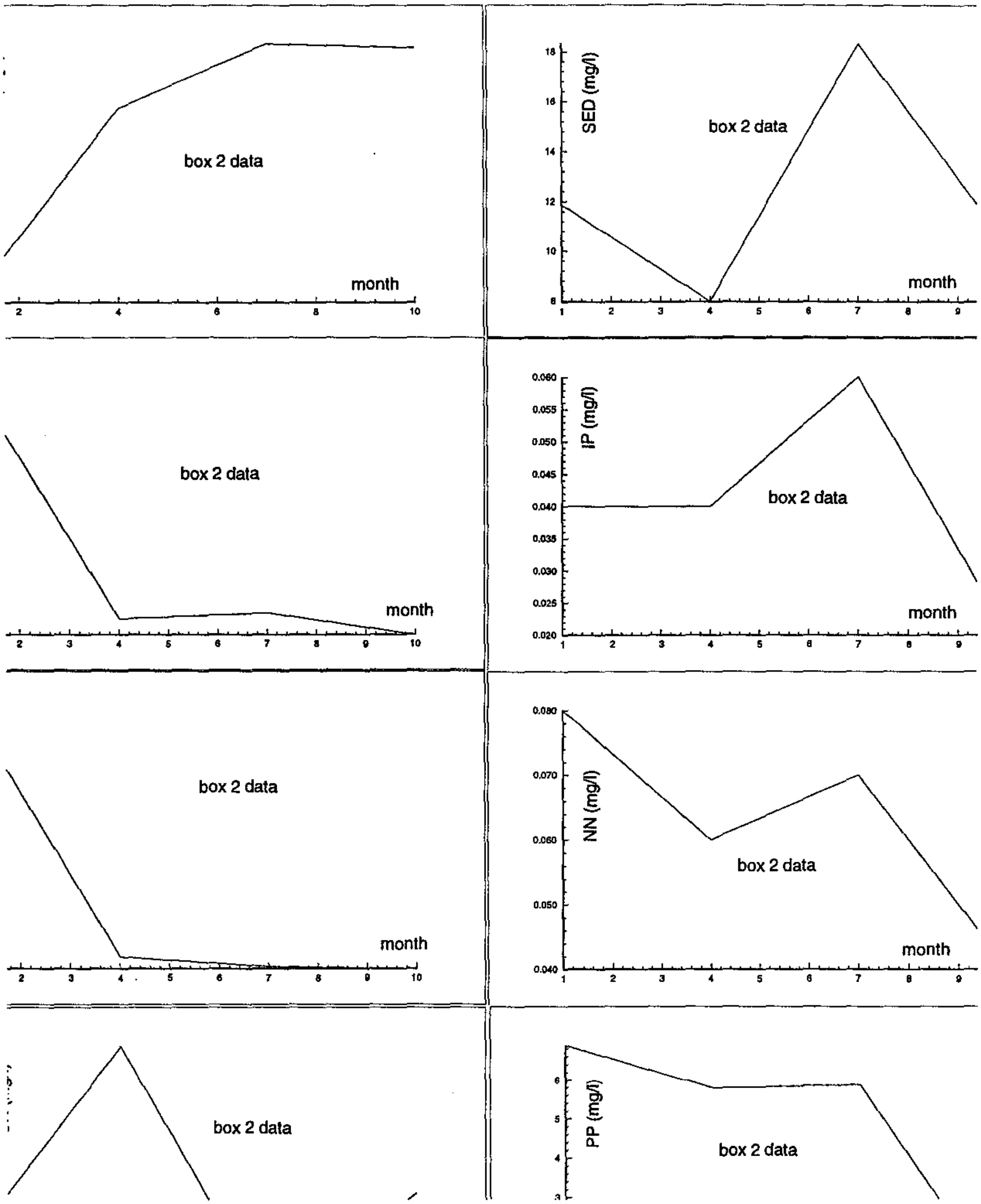

Figure 10. Zone-averaged water quality data inside Zone 2 (Big Sarasota Bay) and Zone 5 (Blackburn Bay) during August 1990 and May 1991.

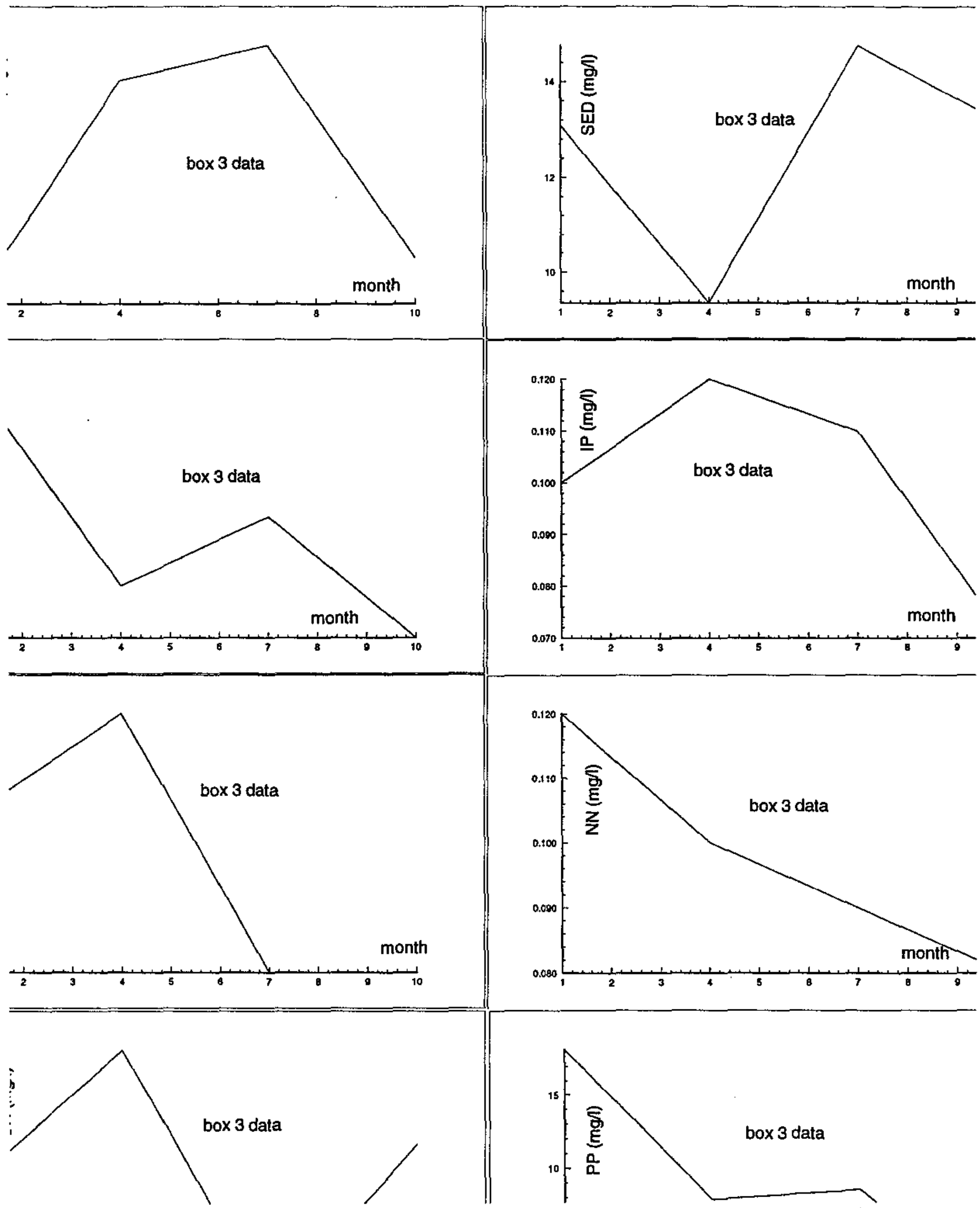

Figure 11. Zone-averaged water quality data inside Zone 3 (Roberts Bay) during August 1990 and May 1991.

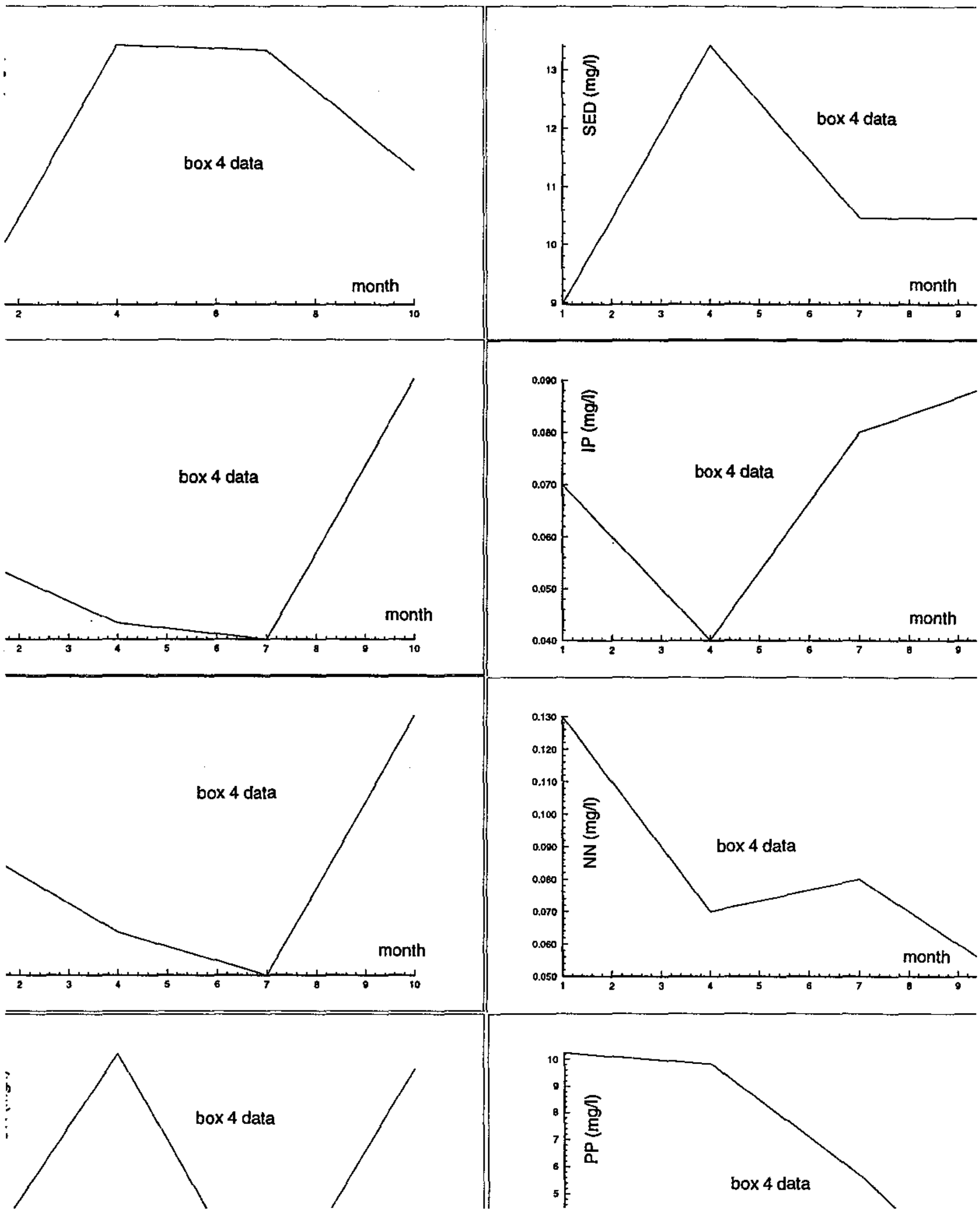

Figure 12. Zone-averaged water quality data inside Zone 4 (Little Sarasota Bay) during August 1990 and May 1991.

2.2. Future Condition

Tables I, II, III, IV, and V show the nutrient loadings into the Sarasota Bay system for present and future land use conditions. Data presented in Section 2.1 are used to calibrate the water quality model for present land use condition. Once the model has been calibrated, it will be used to simulate the response of the Bay to reduced nutrient loading corresponding to the future land use conditions.

As shown in Tables I, II, III, IV and V, there are several freshwater sources for Roberts Bay and Little Sarasota Bay. Since Phillippi Creek is definitely the dominant source of freshwater and there is insufficient data to allow us to specify the detailed freshwater flow from the watershed, model simulations for this study will assume that all the nutrient loading enter into Roberts Bay from Phillippi Creek.

Based on the loadings shown in the tables and mass balance considerations, we obtained the following loadings for present and future land use conditions:

<u>Wet Year Present Condition</u>

River Discharge Rate (Q_0) =	1 m^3/sec
Total Phosphorus (P_0) =	0.31 mg/l
Total Nitrogen (N_0) =	1.6 mg/l
Ammonia Nitrogen (C_1) =	0.01 mg/l
Nitrate Nitrogen (C_2) =	1.0 mg/l
Dissolved Organic Nitrogen (C_7) =	0.5 mg/l
Phytoplankton (C_4) =	0.36 mg/l

Inorganic Phosphorus (C_3) =	0.2 mg/l
Organic Phosphorus (C_8) =	0.1 mg/l
CBOD (C_5) =	0.36 mg/l
DO (C_6) =	6.0 mg/l

where the variable names shown inside the parentheses are those used in the WASP model and our present water quality model.

Dry Year Present Condition

River Discharge Rate (Q_0) =	1 m^3/sec
Total Phosphorus (P_0) =	0.33 mg/l
Total Nitrogen (N_0) =	2.0 mg/l
Ammonia Nitrogen (C_1) =	0.01 mg/l
Nitrate Nitrogen (C_2) =	1.2 mg/l
Dissolved Organic Nitrogen (C_7) =	0.6 mg/l
Phytoplankton (C_4) =	0.76 mg/l
Inorganic Phosphorus (C_3) =	0.21 mg/l
Organic Phosphorus (C_8) =	0.1 mg/l
CBOD (C_5) =	0.76 mg/l
DO (C_6) =	6.0 mg/l

Wet Year Future Condition

With 31% reduction in nutrient loading, the discharge is assumed to be unchanged while the nutrient concentrations are reduced to:

River Discharge Rate (Q_0) =	1 m^3/sec
Total Phosphorus (P_0) =	0.214mg/l
Total Nitrogen (N_0) =	1.12 mg/l
Ammonia Nitrogen (C_1) =	0.01 mg/l
Nitrate Nitrogen (C_2) =	0.7 mg/l
Dissolved Organic Nitrogen (C_7) =	0.35 mg/l
Phytoplankton (C_4) =	0.24 mg/l
Inorganic Phosphorus (C_3) =	0.14 mg/l
Organic Phosphorus (C_8) =	0.07 mg/l
CBOD (C_5) =	0.24 mg/l
DO (C_6) =	6.0 mg/l

<u>Dry Year Future Condition</u>

River Discharge Rate (Q_0) =	1 m^3/sec
Total Phosphorus (P_0) =	0.23 mg/l
Total Nitrogen (N_0) =	1.39 mg/l
Ammonia Nitrogen (C_1) =	0.01 mg/l
Nitrate Nitrogen (C_2) =	0.83 mg/l
Dissolved Organic Nitrogen (C_7) =	0.41 mg/l
Phytoplankton (C_4) =	0.52 mg/l

Inorganic Phosphorus (C_3) =	0.14 mg/l
Organic Phosphorus (C_8) =	0.077mg/l
CBOD (C_5) =	0.52 mg/l
DO (C_6) =	6.0 mg/l

The impact of reduced nutrient loadings to the Bay is expected to be greater during wet years. Hence, in the actual model simulations, we will focus on the wet year simulations of present and future land use conditions. As it can be shown later, in order to show significant impact, we had to reduce the loadings by 100%, which is achieved by setting all concentrations at Phillippi Creek to zero.

3. MODELS

3.1. THE CIRCULATION MODEL

Dimensional Equations in Cartesian Grids

The basic assumptions of the vertically-integrated version of CH3D model are: (1) hydrostatic pressure distribution, (2) Boussinesque approximation, and (3) eddy-viscosity concept is employed. The basic equations for an incompressible fluid in a right-handed Cartesian coordinate system (x, y, z) are:

$$\frac{\partial u}{\partial x} + \frac{\partial v}{\partial y} + \frac{\partial w}{\partial z} = 0 \tag{1}$$

$$\begin{aligned}\frac{\partial u}{\partial t} + \frac{\partial u^2}{\partial x} + \frac{\partial uv}{\partial y} + \frac{\partial uw}{\partial z} &= fv - \frac{1}{\rho_o}\frac{\partial p}{\partial x} + \frac{\partial}{\partial x}\left(A_H \frac{\partial u}{\partial x}\right) \\ &+ \frac{\partial}{\partial y}\left(A_H \frac{\partial u}{\partial y}\right) + \frac{\partial}{\partial z}\left(A_v \frac{\partial u}{\partial z}\right)\end{aligned} \tag{2}$$

$$\begin{aligned}\frac{\partial v}{\partial t} + \frac{\partial uv}{\partial x} + \frac{\partial v^2}{\partial y} + \frac{\partial vw}{\partial z} &= -fu - \frac{1}{\rho_o}\frac{\partial p}{\partial y} + \frac{\partial}{\partial x}\left(A_H \frac{\partial v}{\partial x}\right) \\ &+ \frac{\partial}{\partial y}\left(A_H \frac{\partial v}{\partial y}\right) + \frac{\partial}{\partial z}\left(A_v \frac{\partial v}{\partial z}\right)\end{aligned} \tag{3}$$

$$\frac{\partial p}{\partial z} = -\rho g \tag{4}$$

$$\frac{\partial T}{\partial t} + \frac{\partial uT}{\partial x} \frac{\partial vT}{\partial y} + \frac{\partial wT}{\partial z} = \frac{\partial}{\partial x}\left(K_H \frac{\partial T}{\partial x}\right) + \frac{\partial}{\partial y}\left(K_H \frac{\partial T}{\partial y}\right) + \frac{\partial}{\partial z}\left(K_v \frac{\partial T}{\partial z}\right) \tag{5}$$

$$\frac{\partial S}{\partial t} + \frac{\partial uS}{\partial x} + \frac{\partial vS}{\partial y} + \frac{\partial wS}{\partial z} = \frac{\partial}{\partial x}\left(D_H \frac{\partial S}{\partial x}\right) + \frac{\partial}{\partial y}\left(D_H \frac{\partial S}{\partial y}\right) + \frac{\partial}{\partial y} + \left(D_v \frac{\partial S}{\partial z}\right) \tag{6}$$

$$\rho = \rho\,(T,S) \tag{7}$$

where (u, v, w) are velocities in (x, y, z) directions, f is the Coriolis parameter defined as $2\Omega \sin\phi$, where Ω is the rotational speed of the earth, and ϕ is the latitude, ρ is density, p is pressure, T is temperature, S is salinity, (A_H, K_H, D_H) are horizontal turbulent eddy coefficients, and (A_v, K_v, D_v) are vertical turbulent eddy viscosities.

Various forms of the equation of state can be used. In the present model, the equation given by Eckert (1958) is used:

$$\begin{aligned} \rho &= P/(\alpha + 0.698P) \\ P &= 5890 + 38T - 0.375T^2 + 3S \\ \alpha &= 1779.5 + 11.25T - 0.0745T^2 - (3.8 + 0.10T)\,S \end{aligned} \tag{8}$$

where T is in °C, S is in ppt and ρ is in gm/cm^3.

Equations (1) through (4) can be integrated in the vertical direction from the bottom $(z = -h)$ to the free surface $(z = \zeta)$ to obtain:

$$\frac{\partial \zeta}{\partial t} + \underset{\sim}{\nabla} \cdot \bar{U} = 0 \tag{9}$$

$$\begin{aligned} \frac{\partial \bar{U}}{\partial t} + \underset{\sim}{\nabla} \cdot \left(\frac{\bar{U}}{H} \right) &= -f\hat{z} x \bar{U} + \frac{\bar{\tau}_s}{\rho_o} - \frac{\bar{\tau}_b}{\rho_o} \\ &+ \underset{\sim}{\nabla} \cdot \left(A_H \underset{\sim}{\nabla} \bar{U} \right) \underset{\sim}{\nabla} P_a - gH \underset{\sim}{\nabla} \zeta - \frac{gH^2}{2\rho_o} \underset{\sim}{\nabla} \tilde{\rho} \end{aligned} \tag{10}$$

$$\frac{\partial \tilde{T}}{\partial t} + \underset{\sim}{\nabla} \cdot \left(\bar{U} \tilde{T} \right) = \frac{q_s}{\rho_o} - \frac{q_b}{\rho_o} + \underset{\sim}{\nabla} \cdot \left(K_H \underset{\sim}{\nabla} \tilde{T} \right) \tag{11}$$

$$\frac{\partial \tilde{S}}{\partial t} + \underset{\sim}{\nabla} \cdot \left(\bar{U} \tilde{S} \right) = \frac{e_s}{\rho_o} - \frac{e_b}{\rho_o} + \underset{\sim}{\nabla} \cdot \left(D_H \underset{\sim}{\nabla} \tilde{S} \right) \tag{12}$$

where $\bar{U}$ is the vertically-integrated velocity vector (U, V), U is defined as $\int_{-h}^{\zeta} u\, dz$, V is defined as $\int_{-h}^{\zeta} v\, dz$, $H = \zeta + h$ and is the total depth, (τ_s, q_s, e_s) represent the surface fluxes of (momentum, heat, salinity), (τ_b, q_b, e_b) represent the bottom fluxes, and ρ, T, and S are vertically-averaged quantities. The vector equations can be further expanded into the following equations:

$$\frac{\partial \zeta}{\partial t} + \frac{\partial U}{\partial x} + \frac{\partial V}{\partial y} = 0 \tag{13}$$

$$\begin{aligned} \frac{\partial U}{\partial t} &+ \frac{\partial}{\partial x}\left(\frac{UU}{H}\right) + \frac{\partial}{\partial y}\left(\frac{UV}{H}\right) = fV + \frac{\tau_{sx}}{\rho_o} - \frac{\tau_{bx}}{\rho_o} \\ &+ \frac{\partial}{\partial x}\left(A_H \frac{\partial U}{\partial x}\right) + \frac{\partial}{\partial y}\left(A_H \frac{\partial U}{\partial y}\right) \\ &- \frac{H}{\rho_o}\frac{\partial P_a}{\partial x} - gH\frac{\partial \zeta}{\partial x} - \frac{gH^2}{2\rho_o}\frac{\partial \rho}{\partial x} \end{aligned} \tag{14}$$

$$\begin{aligned} \frac{\partial V}{\partial t} &+ \frac{\partial}{\partial x}\left(\frac{UV}{H}\right) + \frac{\partial}{\partial y}\left(\frac{VV}{H}\right) = -fU + \frac{\tau_{sy}}{\rho_o} - \frac{\tau_{by}}{\rho_o} \\ &+ \frac{\partial}{\partial x}\left(A_H \frac{\partial V}{\partial x}\right) + \frac{\partial}{\partial y}\left(A_H \frac{\partial V}{\partial y}\right) \\ &- \frac{H}{\rho_o}\frac{\partial P_a}{\partial y} - gH\frac{\partial \zeta}{\partial y} - \frac{gH^2}{2\rho_o}\frac{\partial \rho}{\partial y} \end{aligned} \tag{15}$$

$$\frac{\partial T}{\partial t} + \frac{\partial}{\partial x}(UT) + \frac{\partial}{\partial y}(VT) = \frac{q_s}{\rho_o} - \frac{q_b}{\rho_s} + \frac{\partial}{\partial x}\left(K_H \frac{\partial T}{\partial x}\right) + \frac{\partial}{\partial y}\left(K_H \frac{\partial T}{\partial y}\right) \tag{16}$$

$$\frac{\partial S}{\partial t} + \frac{\partial}{\partial x}(US) + \frac{\partial}{\partial y}(VS) = \frac{e_s}{\rho_o} - \frac{e_b}{\rho_s} + \frac{\partial}{\partial x}\left(K_H \frac{\partial S}{\partial x}\right) + \frac{\partial}{\partial y}\left(K_H \frac{\partial S}{\partial y}\right) \tag{17}$$

Boundary-Fitted Curvilinear Grid

To better resolve complex geometries in the horizontal directions, CH2D allows the use of a generalized curvilinear (boundary-fitted) grid. The boundary-fitted grid is actually a more natural grid to use than the Cartesian grid in a more complex domain. For example, it is natural to use a cylindrical grid in the horizontal directions to resolve the flow in a circular arc, while it is natural to use spherical grid to resolve the flow between two concentric spheres. Thompson (1983) developed a method to generate a 2-D boundary-fitted grid in complex domain by solving the elliptic equations, which relate the generally non-orthogonal curvilinear coordinates in the physical plane, x and y, with the uniformly-spaced coordinates in the transformed plane, ε and η. As shown in Figure 13, the basic problem is to solve:

$$\xi_{xx} + \xi_{yy} = P \tag{18}$$

$$\eta_{xx} + \eta_{yy} = Q \tag{19}$$

with the following boundary conditions:

$$\begin{aligned} \xi &= \xi(x,y) \qquad \text{on 1 and 3} \\ \eta &= \text{constant} \end{aligned} \tag{20}$$

$$\begin{aligned} \xi &= \text{constant} \qquad \text{on 2 and 4} \\ \eta &= \eta(x,y) \end{aligned} \tag{21}$$

where the functions P and Q may be chosen to obtain the desired grid resolution and alignment. In practice, one actually solves the following equations, which are readily obtained by interchanging the dependent and independent variables in Equations 18 and 19:

$$\alpha x_{\xi\xi} - 2\beta x_{\xi\eta} + \gamma x_{\eta\eta} + \alpha \bar{P} x_{\xi} + \gamma \bar{Q} x_{\eta} = 0 \tag{22}$$

$$\alpha y_{\xi\xi} - 2\beta y_{\xi\eta} + \gamma y_{\eta\eta} + \alpha \bar{P} y_{\xi} + \gamma \bar{Q} y_{\eta} = 0 \tag{23}$$

where

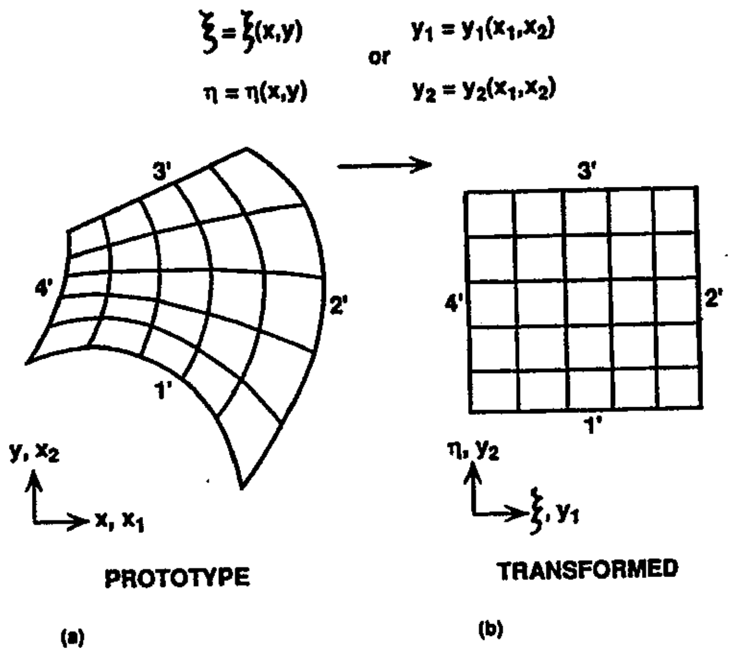

Figure 13 Numerical Grids in Prototype System and Transformed System.

$$
\begin{aligned}
\alpha &= x_{\eta^2} + y_{\eta^2} \\
\beta &= x_\xi x_\eta + y_\xi y_\eta \\
\gamma &= x_{\xi^2} + y_{\xi^2} \\
P &= \frac{1}{J^2}\left(x_{\eta^2} + y_{\eta^2}\right)\bar{P} \\
Q &= \frac{1}{J^2}\left(x_{\xi^2} + y_{\xi^2}\right)\bar{Q} \\
J &= x_\xi y_\eta - x_\eta y_\xi
\end{aligned}
\tag{24}
$$

with the transformed boundary conditions:

$$
\begin{aligned}
x &= f_i(\xi, \eta_i) \qquad \text{on i = 1 and 3} \\
y &= g_i(\xi, \eta_i)
\end{aligned}
\tag{25}
$$

$$
\begin{aligned}
x &= f_i(\xi_i, \eta) \qquad \text{on i = 2 and 4} \\
y &= g_i(\xi_i, \eta)
\end{aligned}
\tag{26}
$$

Equations of Motion in Curvilinear Grid System

In the boundary-fitted grid system, it is customary to work with the contravariant velocity components U^1 and U^2 which are perpendicular to the coordinate axes ξ and η . The equations for ζ, U^1, U^2 and T are listed in the following:

$$\frac{\partial \zeta}{\partial t} + \frac{1}{\sqrt{g_o}} \left\{ \frac{\partial}{\partial \xi}\left(\sqrt{g_o}\, U^1\right) + \frac{\partial}{\partial \eta}\left(\sqrt{g_o}\, U^2\right) \right\} = 0 \tag{27}$$

$$\begin{aligned}
\frac{\partial U^1}{\partial t} &+ \frac{\partial}{\partial \xi}\left(\frac{U^1 U^1}{H}\right) + \frac{\partial}{\partial \eta}\left(\frac{U^1 U^2}{H}\right) + \left(2D^1_{11} + D^2_{12}\right)\frac{U^1 U^1}{H} \\
&+ \left(3D^1_{12} + D^2_{22}\right)\frac{U^1 U^2}{H} + D^1_{22}\frac{U^2 U^2}{H} = \frac{g_{12}}{\sqrt{g_o}} f U^1 + \frac{g_{22}}{\sqrt{g_o}} f U^2 \\
&+ \tau^1_s - c_d\left[g_{11}(U^1)^2 + 2 g_{12} U^1 U^2 + g_{22}(U^2)^2\right]^{1/2} U^1 \\
&- \frac{H}{\rho_o}\left(g^{11}\frac{\partial P_a}{\partial \xi} + g^{12}\frac{\partial P_a}{\partial \eta}\right) - gH\left(g^{11}\frac{\partial \zeta}{\partial \xi} + g^{12}\frac{\partial \zeta}{\partial \eta}\right) \\
&- \frac{gH^2}{2\rho_o}\left(g^{11}\frac{\partial \rho}{\partial \xi} + g^{12}\frac{\partial \rho}{\partial \eta}\right) + \text{Horizontal Diffusion}
\end{aligned} \tag{28}$$

$$\begin{aligned}
\frac{\partial U^2}{\partial t} &+ \frac{\partial}{\partial \xi}\left(\frac{U^1 U^2}{H}\right) + \frac{\partial}{\partial \eta}\left(\frac{U^2 U^2}{H}\right) + \left(2D^2_{22} + D^1_{12}\right)\frac{U^2 U^2}{H} \\
&+ \left(3D^2_{12} + D^2_{22}\right)\frac{U^1 U^2}{H} + D^2_{11}\frac{U^1 U^1}{H} = -\frac{g_{12}}{\sqrt{g_o}} f U^2 - \frac{g_{11}}{\sqrt{g_o}} f U^1 \\
&+ \tau^2_s - c_d\left[g_{11}(U^1)^2 + 2 g_{12} U^1 U^2 + g_{22}(U^2)^2\right]^{1/2} U^2 \\
&- \frac{H}{\rho_o}\left(g^{12}\frac{\partial P_a}{\partial \xi} + g^{22}\frac{\partial P_a}{\partial \eta}\right) - gH\left(g^{12}\frac{\partial \zeta}{\partial \xi} + g^{22}\frac{\partial \zeta}{\partial \eta}\right) \\
&- \frac{gH^2}{2\rho_o}\left(g^{12}\frac{\partial \rho}{\partial \xi} + g^{22}\frac{\partial \rho}{\partial \eta}\right) + \text{Horizontal Diffusion}
\end{aligned} \tag{29}$$

$$\begin{aligned}
\frac{\partial HT}{\partial t} &+ \frac{1}{\sqrt{g_0}}\left[\frac{\partial}{\partial \xi}\left(\sqrt{g_0}\, U^1 HT\right) + \frac{\partial}{\partial \eta}\left(\sqrt{g_0}\, U^2 HT\right)\right] = q_s - q_b \\
&+ K_H\left[g^{11}\left(HT_{,1}\right)_{,1} + g^{12}\left(HT_{,1}\right)_{,2} + g^{21}\left(HT_{,2}\right)_{,1} + g^{22}\left(HT_{,2}\right)_{,2}\right]
\end{aligned} \tag{30}$$

$$\frac{\partial HS}{\partial t} + \frac{1}{\sqrt{g_0}} \left[\frac{\partial}{\partial \xi} \left(\sqrt{g_0}\, U^1 HS \right) + \frac{\partial}{\partial \eta} \left(\sqrt{g_0}\, U^2 HS \right) \right] = e_s - e_b$$
$$+ K_H \left[g^{11} \left(HS_{,1} \right)_{,1} + g^{12} \left(HS_{,1} \right)_{,2} + g^{21} \left(HS_{,2} \right)_{,1} + g^{22} \left(HS_{,2} \right)_{,2} \right] \qquad \textbf{(31)}$$

where g^{ij} is the inverse of g_{ij} and D^i_{jk} is the Christopher symbol. An equation for U^2 similar to Equation (27) can be derived. The above equations contain the smallest possible number of terms. Although some extra terms are introduced due to the transformation, the equations become significantly simplified if an orthogonal or conformal grid can be used. Boundary conditions are simple because the local grid lines are always parallel to the contravariant velocity components. In addition, staggered grid used in the Cartesian-grid model of Sheng (1983) can still be used here.

The above model equations are valid within any boundary-fitted grid. Once a specific grid transformation is defined, model results can be obtained by using the same basic numerical model.

Non-Dimensionalization of Equations

The dimensionless equations make it easy for a user to compare the relative importance of various terms in the equations. When properly non-dimensionalized, the part of each term contained within a parenthesis or bracket should be of unity order, hence the dimensionless number(s) will indicate the order of that term. The added insight justifies the slightly more complicated form of the dimensionless equations.

Dimensionless Variables

$$
\begin{aligned}
(u^*, v^*, w^*) &= (u, v, wX_r/Z_r)/U_r \\
(x^*, y^*, z^*) &= (x, y, z\,X_r/Z_r)/X_r \\
(\tau_x^*, \tau_y^*) &= (\tau_x^w)/\rho_o f Z_r U_r \\
t^* &= tf \\
q_s^* &= T_o/(T_r - T_o)^* \, q/\rho_o \, c_p \, f Z_r T_o \\
\zeta^* &= g\zeta / f U_r X_r = \zeta / S_r \\
\rho^* &= (\rho - \rho_o)/(\rho_r - \rho_o) \\
T^* &= (T - T_o)/(T_r - T_o) \qquad (32) \\
A_H^* &= A_H / A_{Hr} \\
A_v^* &= A_v / A_{vr} \\
K_H^* &= K_H / K_{Hr} \\
K_v^* &= K_v / K_{vr} \\
D_H^* &= D_H / D_{Hr} \\
D_v^* &= D_v / D_{vr} \\
\omega^* &= \omega X_r / U_r
\end{aligned}
$$

Dimensionless Numbers

Vertical Ekman Number: $E_v = A_{vr} / f Z_r^2 = t_i / t_{vdm}$

Lateral Ekman Number: $E_H = A_{Hr} / f x_r^2 = t_i / t_{ldm}$

Vertical Prandtl Number: $Pr_v = A_{vr} / K_{vr} = t_{vdh} / t_{vdm}$

Lateral Prandtl Number: $Pr_H = A_{Hr} / K_{Hr} = t_{ldh} / t_{ldm}$

Vertical Schmidt Number: $Sc_v = A_{vr} / D_{vr} = t_{vds} / t_{vdm}$

Lateral Schmidt Number: $Sc_H = A_{Hr} / D_{Hr} = t_{lds} / t_{ldm}$

Froude Number: $Fr = U_r / (g Z_r)^{1/2} = t_{ge} / t_c$

Rossby Number:

$$Ro = U_r / f X_r = t_i / t_c$$

$$\beta = g Z_r / f^2 X_r^2 \equiv (Ro/Fr)^2 = (t_i / t_{ge})^2$$

$$S_z = S_r / Z_r$$

$$\varepsilon = (\rho_r - \rho_o)/\rho_o$$

Densimetric Froude Number: $$Fr_D = Fr \Big/ \sqrt{\varepsilon} = t_{gi} / t_c$$

Transformation Rules for Variables in Boundary-Fitted Grids

Generation of a boundary-fitted grid is an essential step in the development of a boundary-fitted hydrodynamic model. It is, however, only the first step. A more important step is the transformation of governing equations into the boundary-fitted coordinates. A straightforward method is to only transform the dependent variables, i.e., the coordinates, while retaining the Cartesian components of velocities. Johnson (1982) developed such a 2-D vertically-integrated model of estuarine hydrodynamics. The advantage of such a method is its simplicity in generating the transformed equations via the chain rule. Additional disadvantages are: (1) the boundary conditions are quite complicated because the Cartesian velocity components are generally not aligned with the grid lines, (2) the staggered grid cannot be readily used, and (3) numerical instability may develop unless additional variables (e.g., surface elevation or pressure) are solved at additional grid points (Bernard, 1984).

The following relationships are valid for the three components in a non-Cartesian system is:

$$u^i = (g_{ii})^{-1/2} \quad u(i) \qquad (\text{no sum on } i) \tag{33}$$

$$u_i = (g_{ii})^{-1/2} \; g_{ij} \, u(j) \qquad (\text{no sum on } i) \tag{34}$$

$$u(i) \equiv \bar{u}_i \tag{35}$$

where g is the diagonal element of the metric tensor g_{ij}:

$$g_{ij} = \frac{\partial x^{\ell}}{\partial \xi^i} \frac{\partial x^n}{\partial \xi^j} \delta_{\ell n} \tag{36}$$

which for the two-dimensional case of interest is:

$$g_{ij} = \begin{pmatrix} x_{\xi^2} + y_{\xi^2} & x_{\xi} x_{\eta} + y_{\xi} y_{\eta} \\ x_{\eta} x_{\xi} + y_{\eta} y_{\xi} & x_{\eta^2} + y_{\eta^2} \end{pmatrix} = \begin{pmatrix} g_{11} & g_{12} \\ g_{21} & g_{22} \end{pmatrix} \tag{37}$$

The three components follow different rules for transformation between the prototype and the transformed plane:

$$\bar{u}^i = \frac{\partial \xi^i}{\partial x^j} u^j \tag{38}$$

$$\bar{u}^i = \frac{\partial \xi^j}{\partial x^i} u_j \tag{39}$$

$$\bar{u}(i) = (\bar{g}_{jj})^{1/2} \frac{\partial \xi^i}{\partial x^j} u(j) \tag{40}$$

where the unbarred quantities represent the components in the prototype system while the barred quantities represent the components in the transformed system.

Dimensionless Equations in Boundary-Fitted Coordinates

It is clear that if a proper transformation is given, one can compute the metric tensor and Christoffel symbols accordingly, and then expand the tensor invariant equations in terms of the two contravariant velocity components and sum up all the terms over the range of indices. This process is rather tedious and highly prone to human error. To alleviate these problems, we used a symbolic manipulator to expand the tensor-invariant equations. After rearranging the resulting terms of expansion, we obtain the following vertically-integrated equations:

The vertically-integrated equations are:

$$\zeta_t + \frac{\beta}{\sqrt{g_o}} \left[\frac{\partial}{\partial \xi} \left(\sqrt{g_o}\, U \right) + \frac{\partial}{\partial \eta} \left(\sqrt{g_o}\, V \right) \right] = 0 \tag{41}$$

$$\begin{aligned} \frac{\partial U}{\partial t} = & - H \left(g^{11} \frac{\partial \zeta}{\partial \xi} + g^{12} \frac{\partial \zeta}{\partial \eta} \right) + \frac{g_{12}}{\sqrt{g_o}} U + \frac{g_{22}}{\sqrt{g_o}} V \\ & - Ro \,[\, \text{Nonlinear}\mathit{InertiaTerms} \,] + \tau_s^1 - \tau_b^1 \\ & - \frac{HRo}{Fr^2} [\, \text{Baroclinic}\mathit{Terms} \,] \\ & + HE_H A_H [\, \text{Horizontal}\mathit{DiffusionTerms} \,]_\xi \end{aligned} \tag{42}$$

$$\frac{\partial V}{\partial t} = - H\left(g^{21}\frac{\partial \zeta}{\partial \xi} + g^{22}\frac{\partial \zeta}{\partial \eta}\right) - \left(\frac{g_{11}}{\sqrt{g_o}}U + \frac{g_{21}}{\sqrt{g_o}}V\right)$$

$$- Ro\ [\,\mathrm{Nonlinear}\mathit{InertiaTerms}\,] + \tau_s^2 - \tau_b^2 \qquad (43)$$

$$- \frac{HRo}{Fr^2}[\,\mathrm{Baroclinic}\mathit{Terms}\,]$$

$$+ HE_H A_H [\,\mathrm{Horizontal}\mathit{DiffusionTerms}\,]_\eta$$

$$\frac{1}{H}\frac{\partial HT}{\partial t} = -\frac{Ro}{H}\frac{1}{\sqrt{g_o}}\left[\frac{\partial}{\partial \zeta}\left(\sqrt{g_o}\,UT\right) + \frac{\partial}{\partial \eta}\left(\sqrt{g_o}\,VT\right)\right]$$
$$+ \frac{E_H}{Pr_H}\left[g^{11}T_{,1,1} + g^{12}T_{,1,2} + g^{21}T_{,2,1} + g^{22}T_{,2,2}\right] \qquad (44)$$

$$\frac{1}{H}\frac{\partial HS}{\partial t} = -\frac{Ro}{H}\frac{1}{\sqrt{g_o}}\left[\frac{\partial}{\partial \zeta}\left(\sqrt{g_o}\,US\right) + \frac{\partial}{\partial \eta}\left(\sqrt{g_o}\,VS\right)\right]$$
$$+ \frac{E_H}{Pr_H}\left[g^{11}S_{,1,1} + g^{12}S_{,1,2} + g^{21}S_{,2,1} + g^{22}S_{,2,2}\right] \qquad (45)$$

where the variables U and V now represent the contravariant velocity components.

Boundary and Initial Conditions

Along the shoreline where river inflow or outflow may occur, the conditions are generally:

$$\begin{aligned} U &= U(x,y,t) \\ V &= V(x,y,t) \\ T &= T(x,y,t) \\ S &= S(x,y,t) \end{aligned} \qquad (46)$$

Along a solid boundary, both the normal and tangential velocity components are zero. In addition, the normal derivatives of temperature and salinity are zero.

Along an open boundary, either ζ or the velocity can be specified. For the elevation ζ, there are currently several options:

$$\begin{aligned} \zeta &= \zeta(x,y,t) = \sum_{n=1}^{n_{max}} A_n \cos\left(\frac{\partial \pi t}{T_n + \phi_n}\right) \\ \frac{\partial \zeta}{\partial x} &= 0 \quad \text{or} \quad \frac{\partial \zeta}{\partial y} = 0 \end{aligned} \tag{47}$$

where A_n, T_n, and ϕ_n are the amplitude, period, and phase angle of the tabular tidal constituents.

When open boundary conditions are given in terms of ζ, the normal velocity component is assumed to be of zero slope while the tangential velocity component may be either (1) zero, or (2) zero slope, or (3) computed from the momentum equations.

The salinity along an open boundary or river entrance is computed from a 1-D advection equation during the outflow. During the inflow, however, the salinity value at the open boundary can either take on a prescribed value or be determined from the 1-D advection equation while using the boundary salinity value and the prescribed salinity value to evaluate the spatial flux term.

Due to the use of contravariant velocity components, the lateral boundary conditions in the (ξ, η) grid are similar to those in the (x, y) system. Along the solid boundary, no-slip condition dictates that the tangential velocity is zero while the slip condition requires that the normal velocity is zero. When flow is specified at the open boundary or river boundary, the normal velocity component is prescribed.

To initiate a run, the initial spatial distributions of $\zeta, U, V, T,$ and S need to be specified. When initial data are unknown, one could start with zero initial fields. When initial data are known at a limited number of locations, an initial field can be generated by some interpolation scheme. It is desirable if the interpolated field satisfies the conservation law governing that field variable. For practical simulations, the model usually assumes zero initial flow if little initial data is known. This is reasonable because the spin-up time of the flow field is relatively short due to the use of a variable time-stepping scheme. In case of salinity simulation, the spin-up time is longer and sufficient spin-up time should be allowed in model simulations.

Initial conditions on vectors, if given in the Cartesian or prototype system, such as the velocity and the surface stress, must be first transformed before being used in the transformed equations. Thus, the surface stress in the transformed coordinate system is given by:

$$\bar{\tau}^1 = \frac{\partial \xi}{\partial x}\tau^1 + \frac{\partial \xi}{\partial y}\tau^2 \tag{48}$$

$$\bar{\tau}^2 = \frac{\partial \eta}{\partial x}\tau^1 + \frac{\partial \eta}{\partial y}\tau^2 \tag{49}$$

where $\bar{\tau}^1, \bar{\tau}^2$ are the contravariant components of the stress in the transformed system and τ^1, τ^2 are the contravariant components in the Cartesian system. Note that in the Cartesian system, the contravariant, covariant and physical components of a vector are identical. The contravariant components of the initial velocity vectors can be transformed in the same manner to obtain the proper initial conditions for the transformed momentum equations.

3.2. THE WATER QUALITY MODEL

Water quality models (e.g., Imbodin, 1974; Chen and Orlob, 1978; Ambrose et al., 1988; Sheng et al., 1991; Cerco and Dortch, 1992; Sheng and Chen, 1993) can be used to provide computation of water quality parameters (temperature, salinity, sediment, nutrients, oxygen, phytoplankton, zooplankton, etc.) in water bodies. Basically, a water quality model solves conservation equations of various water quality parameters related to the phosphorus cycle, nitrogen cycle, and oxygen cycle. For typical estuaries, the nitrogen cycle is more important than the phosphorus cycle since nitrogen is usually the limiting nutrient for algal growth. For each water quality parameter, the conservation equation includes the following types of terms: (i)evolution term (rate of change of concentration in a control volume), (ii)advection terms (fluxes into/out of the control volume due to the advection of flow field), (iii)diffusion/dispersion terms (fluxes into/out of the control volume due to turbulent diffusion of the flow field), and (iv)tranformation terms (fluxes due to such processes as adsorption/desorption, oxidation, excretion, decay, growth, biodegradation, and photodegradation etc.). In addition to the above terms in the conservation equations, water quality models require accurate specification of external loadings. A successful water quality modeling effort requires the following: accurate prescription of the external loading, accurate computation of the flow field and advective and diffusive fluxes, and accurate description of the transformation processes.

The various water quality models differ in terms of the following aspects: (i)calculation of the advection terms, (ii)calculation of the diffusion/dispersion terms, and (iii)details of the trasnsformation processes. These aspects are discusssed in the following paragraphs.

Advection Terms - Coupling between Hydrodynamic and Water Quality Models

Ideally, water quality model should use the same grid and time step as the hydrodynamic model. In such case, results of the hydrodynamic model can be directly used in the water quality model without any averaging which may distort the flow results. However, traditional water quality models (e.g., the WASP model) typically use very coarse grids and do not use a hydrodynamic model to compute the flow field. Instead, such model determines the flow field by matching simulated and measured time-averaged salinity or conservative species field while solving the "mass balance" equation (instead of the hydrodynamic equations). The computed flow field may contain large error. Recently, the WASP model allows one to compute the flow field by using a simple link-node model DYNHYD. However, because the DYNHYD model is basically a one-dimensional model, it fails to compute the accurate flow field complex water body such as the Roberts Bay and Upper Little Sarasota Bay (Sheng and Peene, 1992). Thus, the advection terms in the water quality model may contain large uncertainty. More recently, Cerco and Dortch (1992) modified the WASP model to simulate the water quality dynamics in Chesapeake Bay by coupling the WASP model with a 3-D hydrodynamic model. The hydrodynamic model used a relatively fine (about 1 km minimum) grid and a small time step, while the water quality model used a spatial grid of 5-10 km and a time step of 3 hours. The 3-D water quality model developed by Sheng et al. (1991) and Sheng and Chen (1992) used the same fine grid and small time step for the hydrodynamic and water quality models.

For this study, we use the basic hydrodynamics model of Sarasota Bay to simulate the flow field in ths study area and use the same time step and spatial grid for the water quality model which is based on the WASP transformation processes. As it can be seen later, this procedure compleltely eliminates the tedious procedure for producing "calibrated" advective fluxes and "dispersion coefficients" required by the

WASP models. Sheng and Yassuda (1995) used a curvilinear-grid 3-D model for Tampa Bay to calculate the advective fluxes along the boundaries of 14 WASP boxes covering the entire Tampa Bay. A more direct procedure is to use the 3-D model to compute the water quality equations as well as the hydrodynamics equations with the same time step and spatial grid.

Diffusion/Dispersion Fluxes

The diffusion/dispersion terms in the conservation equation for water quality parameters represent the effect turbulent mixing on the transport of water quality parameters. The horizontal diffusion represents the effect of sub-grid scale mixing, while the vertical diffusion represents the mixing induced by wind and tide and affected by vertical stratification. Thus, horizontal diffusion/dispersion coefficients should be proportional to the characteristic velocity and length scale of the sub-grid turbulent eddies. Thus, the characteristic velocity is a fraction of the horizontal velocity, while the length scale is a fraction of the horizontal grid. However, traditional water quality models (e.g., WASP) treat the diffusion/dispersion coefficients as ad-hoc "adjustable" coefficients. The diffusion/dispersion coefficients are adjusted in order to achieve a fit between simulated and measured water quality parameter. When little data exist, the uncertainty contained in the diffusion/dispersion coefficients is high.

For this study, since the water quality model and hydrodynamic model are coupled with the same grid and time step, the diffusion coefficients in the water quality model are determined from the hydrodynamic model without any ad-hoc adjustment afterwards. In the case of many water quality modeling studies, WASP model is either not or only loosely coupled to a hydrodynamic model, there exists large uncertainty in the estimated diffusion/dispersion coefficients.

Transformation Processes

In the WASP model, water quality models are generally concerned with the modeling of nitrogen cycle, phosphorus cycle, and DO balance. The transformation processes include adsorption/desorption, oxidation, excretion, decay, growth, biodegradation, and photodegradation etc., and are hence very complicated. Due to the lack of field data, most of these processes are modeled with relatively simple reactions such as first-order reaction or saturation reaction with numerous empirical coefficients determined from idealized laboratory experiments. The transformation processes are influenced by numerous physical, chemical, and biological parameters. Insufficient field data exist to fully establish the definitive relationships for the transformation processes. As such, there is uncertainty in the transformation processes. Guidance on the selection of important model coefficients for water quality models have been provided by U.S. Environmental Protection Agency (see e.g., USEPA, 1990) in recently released "Technical Guidance Manual for Performing Waste Load Allocations". Typically, to achieve model results which compare well with data, it is often necessary to carry out hundreds of simulations using the model and hundreds of possible combinations of model coefficients (see e.g., Simons and Lam, 1980). Existing water quality models have not addresses the uncertainty/error issue adequately (Beck, 1987). As more data for specific water bodies become available, water quality model can be better calibrated and validated and hence become more reliable.

Because WASP model was developed with data from the deeper and temperate estuary of Potomac/Putaxent and the Great Lakes, the model does not include many processes that are potentially important in Sarasota Bay. These processes include the following: (i)benthic fluxes due to diffusion and possibly resuspension, (ii)existence of epiphytic algae and macroalgae and their responses to nutrient load reduction, and (iii)effects of epiphytic algae and macroalgae, as well as chlorophyll-a and suspended sediments on light attenuation in water column. Sheng and Chen (1993) developed a water quality model which contains a circulation model, a sediment transport model, and numerous transformation processes and benthic fluxes of nutrients. The WASP model assumes equilibrium partitioning between the adsorbed and dissolved nutrients. Thus, resuspended sediments lead to immediate increase in dissolved nutrient concentration. The model of Sheng and Chen (1993), on the other hand, includes a rate constant for the adsorption/desorption kinetics, thus producing more realistic model results.

Stretagy of Water Quality Modeling for This Study

Based on the above review of water quality models and consideration of the particular water body of interest, the water quality model used for the present study has the following features:

- It contains the processes of advection, diffusion and transformations in a vertically-integrated curvilinear grid system.
- The advective and fissusive fluxes are computed by the vertically-integraed version of the Sarasota Bay circulation model (Sheng et al. 1995).
- The circulation model and water quality model use the same time step and spatial grid for model simulations.
- The water quality model contains a dynamic sediment transport model which includes such processes as advection, diffusion, settling, deposition and resuspesion.
- The transformation processes contained in the water quality model are based on those used in the WASP model (Ambrose et al. 1994) shown in Appendix A, but with some modifications.
- To simulate the response of Roberts Bay to nutrient load reduction, we include a seagrass

dynamics model and a light attenuation model.

3.2.1. Water Quality Equations

In the following, equations for the oxygen cycle, phosphorus cycle and nitrogen cycle in both the water column and the sediment column are listed. Each of the conservation equations for the water quality species consists of three parts: advection due to the flow field, diffusion due to the flow field, and transformation processes. For simplicity, the advection and diffusion terms, which are similar to the corresponding terms shown in the equations for salinity and temperature, are not given. Only the transformation terms are listed in these equations.

Water-Column Oxygen Balance Equations

CBOD:

$$\frac{\partial C_5}{\partial t} = \underbrace{+ a_{oc} K_{1D} C_4}_{\text{death}} \quad \underbrace{- K_D \theta_D^{T-20} \frac{C_6}{K_{BOD} + C_6} C_5}_{\text{oxidation}} \quad \underbrace{- \frac{V_{s3}(1 - f_{D5})}{H} C_5}_{\text{settling}}$$

$$\underbrace{- \frac{5}{4} \frac{32}{14} K_{2D} \theta_{2D}^{T-20} \frac{K_{NO_3}}{K_{NO_3} + C_6} C_2}_{\text{denitrification}} \quad \underbrace{+ \frac{V_{R3}}{H} (1 - f_{D5j}) C_{5j}}_{\text{resuspension}} \tag{50}$$

$$\underbrace{- \frac{E_{dif}}{HH_j} (C_5 f_{D5} - C_{5j} f_{D5j})}_{\text{diffusion}}$$

DO:

$$\frac{\partial C_6}{\partial t} = \underbrace{+ K_2 (C_S - C_6)}_{\text{reaeration}} \quad \underbrace{- K_D \theta_D^{T-20} \frac{C_6}{K_{BOD} + C_6} C_5}_{\text{oxidation}} \quad \underbrace{- \frac{64}{14} K_{12} \theta_{12}^{T-20} \frac{C_6}{K_{NIT} + C_6} C_1}_{\text{nitrification}}$$

$$\underbrace{+ G_{p1} \left[\frac{32}{12} + \frac{48}{14} \frac{14}{12} \left(1 - P_{NH_3}\right) \right] C_4}_{\text{growth}} \quad \underbrace{- \frac{32}{12} K_{1R} \theta_{1R}^{T-20} C_4}_{\text{respiration}} \tag{51}$$

$$\underbrace{- \frac{E_{dif}}{HH_j} \theta_S^{T-20} (C_6 - C_{6j})}_{\text{diffusion}}$$

Sediment-Column Oxygen Balance Equations

CBOD:

$$\frac{\partial C_{5j}}{\partial t} = \underbrace{+ a_{oc} K_{PZD} \theta_{PZD}^{T-20} C_{4j}}_{\text{decomposition}} \quad \underbrace{- K_{DS} \theta_{DS}^{T-20} C_{5j}}_{\text{oxidation}} \quad \underbrace{- \frac{5}{4} \frac{32}{14} K_{2D} \theta_{2D}^{T-20} C_{2j}}_{\text{denitrification}}$$

$$\underbrace{+ \frac{V_{s3}}{H_j}(1 - f_{D5}) C_5}_{\text{settling}} \quad \underbrace{- \frac{V_{r3}}{Hj}(1 - f_{D5j}) C_{5j}}_{\text{resuspension}} \quad \underbrace{+ \frac{E_{dif}}{Hj^2}(C_5 f_{D5} - C_{5j} f_{D5j})}_{\text{diffusion}} \tag{52}$$

DO:

$$\frac{\partial C_{6j}}{\partial t} = \underbrace{- K_{DS} \theta_{DS}^{T-20} C_{5j}}_{\text{oxidation}} \quad \underbrace{+ \frac{E_{dif}}{Hj^2}(C_6 - C_{6j})}_{\text{diffusion}} \tag{53}$$

Water-Column Nitrogen Cycle Equations

Phytoplankton - (PP):

$$\frac{\partial}{\partial t}(a_{nc}C_4) = \underset{\text{growth}}{G_{p1}a_{nc}C_4} \quad \underset{\text{death}}{-D_{p1}a_{nc}C_4} \quad \underset{\text{settling}}{-\frac{V_{s4}}{H}a_{nc}C_4} \tag{54}$$

Dissolved Organic Nitrogen - (DON):

$$\frac{\partial C_7}{\partial t} = \underset{\text{death}}{D_{p1}a_{nc}f_{on}C_4} \quad \underset{\text{mineralization}}{-K_{71}\theta_{71}^{T-20}\frac{C_4}{C_4+K_{mpc}}C_7} \quad \underset{\text{settling}}{-\frac{V_{s3}(1-f_{D7})}{H}C_7} \quad \underset{\text{resuspension}}{+\frac{E_{sed}}{HH_j}\left(\frac{C_{7j}}{C_{sed}}\right)} \tag{55}$$

Ammonium - (AN):

$$\begin{aligned}\frac{\partial C_1}{\partial t} = \; & \underset{\text{death}}{D_{p1}a_{nc}(1-f_{on})C_4} \quad \underset{\text{mineralization}}{+K_{71}\theta_{71}^{T-20}\frac{C_4}{C_4+K_{mpc}}C_7} \quad \underset{\text{growth}}{-G_{p1}a_{nc}P_{NH3}C_4} \\ & \underset{\text{nitrification}}{-K_{12}\theta_{12}^{T-20}\frac{C_6}{C_6+K_{NIT}}C_1} \quad \underset{\text{diffusion}}{-\frac{E_{dif}}{HH_j}(C_1f_1-C_{1j}f_{1j})} \quad \underset{\text{volatilization}}{-(0)}\end{aligned} \tag{56}$$

Nitrate - (NN):

$$\frac{\partial C_2}{\partial t} = \underbrace{K_{12}\theta_{12}^{T-20}\frac{C_6}{c_6+K_{NIT}}C_1}_{\text{nitrification}} \quad \underbrace{-G_{p1}a_{nc}(1-P_{NH3})C_4}_{\text{growth}} \quad \underbrace{-K_{2D}\theta_{2D}^{T-20}\frac{K_{NO_3}}{K_{NO_3}+C_6}C_2}_{\text{denitrification}}$$
$$\underbrace{-\frac{E_{dif}}{HH_j}(C_2f_2-C_{2j}f_{2j})}_{\text{diffusion}} \tag{57}$$

Sediment Column Nitrogen Cycle Equations

Particulate Organic Nitrogen - (PON):

$$\frac{\partial}{\partial t}(a_{nc}C_{4j}) = \underbrace{\frac{V_{s4}}{H_j}a_{nc}C_{4j}}_{\text{settling}} \quad \underbrace{-a_{nc}K_{PZD}\theta_{PZD}^{T-20}C_{4j}}_{\text{decomposition}} \tag{58}$$

Dissolved Organic Nitrogen - (DONj):

$$\frac{\partial C_{7j}}{\partial t} = \underbrace{K_{PZD}\theta_{PZD}^{T-20}a_{nc}f_{on}C_{4j}}_{\text{decomposition}} \quad \underbrace{-K_{OND}\theta_{OND}^{T-20}C_{7j}}_{\text{mineralization}} \quad \underbrace{-\frac{E_{sed}}{H_j^2}\left(\frac{C_{7j}}{C_{sed}}\right)}_{\text{resuspension}}$$
$$\underbrace{+\frac{V_{s3}(1-f_{D7})}{H_j}C_7}_{\text{settling}} \quad \underbrace{+\frac{E_{dif}}{H_j^2}(C_7f_7-C_{7j}f_{7j})}_{\text{diffusion}} \tag{59}$$

Ammonium - (ANj):

$$\frac{\partial C_{1j}}{\partial t} = \underbrace{K_{PZD}\theta_{PZD}^{T-20}a_{nc}\left(1-f_{on}\right)C_{4j}}_{\text{decomposition}} \quad \underbrace{+K_{OND}\theta_{OND}^{T-20}C_{7j}}_{\text{mineralization}}$$

$$\underbrace{+\frac{E_{dif}}{H_j^2}\left(C_1f_1 - C_{1j}f_{1j}\right)}_{\text{diffusion}} \quad \underbrace{-K_{12j}\theta_{12}^{T-20}\frac{C_6}{C_6+K_{NIT}}C_{1j}}_{\text{nitrification}} \qquad (60)$$

Nitrate - (NNj):

$$\frac{\partial C_{2j}}{\partial t} = \underbrace{K_{12j}\theta_{12}^{T-20}\frac{C_6}{c_6+K_{NIT}}C_{1j}}_{\text{nitrification}} \quad \underbrace{-K_{2D}\theta_{2D}^{T-20}\frac{K_{NO_3}}{K_{NO_3}+C_4}C_{2j}}_{\text{denitrification}} \quad \underbrace{+\frac{E_{dif}}{HH_j}\left(C_2f_2 - C_{2j}f_{2j}\right)}_{\text{diffusion}} \qquad (61)$$

Water Column Phosphorus Cycle Equations

WATER COLUMN

PP-P:

$$\frac{\partial}{\partial t}\left(a_{pc}C_4\right) = \underbrace{G_{p1}a_{pc}C_4}_{\text{growth}} \quad \underbrace{-D_{p1}a_{pc}C_4}_{\text{death}} \quad \underbrace{-\frac{V_{s4}}{H}a_{pc}C_4}_{\text{settling}} \qquad (62)$$

Organic Phosphorus - (OP):

$$\frac{\partial C_8}{\partial t} = \underbrace{D_{p1} a_{pc} f_{op} C_4}_{\text{death}} \underbrace{- K_{83} \theta_{83}^{T-20} \frac{C_4}{C_4 + K_{mpc}} C_8}_{\text{mineralization}} \underbrace{- \frac{V_{s3}(1 - f_{D8})}{H} C_8}_{\text{settling}} \underbrace{+ \frac{E_{sed}}{HH_j}\left(\frac{C_{8j}}{C_{sed}}\right)}_{\text{resuspension}} \quad (63)$$

Inorganic Phosphorus - (IP):

$$\frac{\partial C_3}{\partial t} = \underbrace{D_{p1} a_{pc}(1 - f_{op}) C_4}_{\text{death}} \underbrace{+ K_{83} \theta_{83}^{T-20} \frac{C_4}{C_4 + K_{mpc}} C_8}_{\text{mineralization}} \underbrace{- G_{p1} a_{pc} C_4}_{\text{growth}} \underbrace{+ \frac{E_{sed}}{HH_j}\left(\frac{C_{3j}}{C_{sed}}\right)}_{\text{resuspension}} \quad (64)$$

Sediment Column Phosphorus Cycle Equations

PP-P:

$$\frac{\partial}{\partial t}(a_{pc} C_{4j}) = \underbrace{\frac{V_{s4}}{H_j} a_{pc} C_{4j}}_{\text{settling}} \underbrace{- a_{pc} K_{PZD} \theta_{PZD}^{T-20} C_{4j}}_{\text{decomposition}} \quad (65)$$

OP:

$$\frac{\partial C_{8j}}{\partial t} = \underbrace{K_{PZD} \theta_{PZD}^{T-20} a_{pc} f_{op} C_{4j}}_{\text{decomposition}} \underbrace{- K_{OPD} \theta_{OPD}^{T-20} f_{D8j} C_{8j}}_{\text{mineralization}} \underbrace{- \frac{E_{sed}}{H_j^2}\left(\frac{C_{8j}}{C_{sed}}\right)}_{\text{resuspension}} \underbrace{+ \frac{V_{s3}(1 - f_{D8})}{H_j} C_8}_{\text{settling}} \underbrace{+ \frac{E_{dif}}{H_j^2}(C_8 f_8 - C_{8j} f_{8j})}_{\text{diffusion}} \quad (66)$$

IP

$$\frac{\partial C_{3j}}{\partial t} = \underset{\text{decomposition}}{K_{PZD}\theta_{PZD}^{T-20}a_{pc}\left(1-f_{op}\right)C_{4j}} + \underset{\text{mineralization}}{K_{OPD}\theta_{OPD}^{T-20}f_{D8j}C_{8j}} - \underset{\text{resuspension}}{\frac{E_{sed}}{H_j^2}\left(\frac{C_{3j}}{C_{sed}}\right)} \quad (67)$$

Water Quality Model Coefficients

Model coefficients used in the water quality model are explained in Table XI. The values of the coefficients used by the standard WASP model and those in our model simulations are shown in Table XII.

Table XI. Coefficients Used in the Water Quality Model

AHJ	-	Thickness of sediment active layer (cm)
ANC	-	Phytoplankton nitrogen-carbon ratio (mg N / mg C)
AOC	-	Oxygen-carbon ratio (mg O_2 / mg C)
APC	-	Phosphorus-carbon ratio (mg P / mg C)
C3JCS	-	Fraction of inorganic phosphorus in the sediment layer
C7JCS	-	Fraction of organic nitrogen in the sediment layer
C8JCS	-	Fraction of organic phosphorus in the sediment layer
DP1	-	Phytoplankton death rate (day^{-1})
EDIF	-	Diffusive exchange coefficient (m^2/day)
F1	-	Fraction of dissolved ammonium nitrogen in the water column
F1J	-	Fraction of dissolved ammonium nitrogen in the sediment layer
F2	-	Fraction of dissolved (nitrate+nitrite) nitrogen in the water column
F2J	-	Fraction of dissolved (nitrate+nitrite) nitrogen in the sediment layer
FD5	-	Fraction of dissolved CBOD in the water column
FD5J	-	Fraction of dissolved CBOD in the sediment layer
FD7	-	Fraction of dissolved organic nitrogen in the water column
FD7J	-	Fraction of dissolved organic nitrogen in the sediment layer
FD8	-	Fraction of dissolved organic phosphorus in the water column
FD8J	-	Fraction of dissolved organic phosphorus in the sediment layer
FDAY	-	Fraction of day that is daylight
FIMAX	-	Maximum photosynthetic quantum yield (mg C / E)
FON	-	Fraction of dead and respired phytoplankton recycled to the nitrogen pool
FOP	-	Fraction of dead and respired phytoplankton recycled to the phosphorus pool
K12	-	Nitrification rate in the water column (day^{-1})
K12j	-	Nitrification rate in the sediment layer (day^{-1})
K1C	-	Phytoplankton maximum growth rate (day^{-1})
K1D	-	Phytoplankton death rate (day^{-1})

K1R	-	Phytoplankton endogenous respiration (day^{-1})
K2	-	Re-aeration rate at 20 °C (day^{-1})
K2D	-	Denitrification rate (day^{-1})
K71	-	Organic nitrogen mineralization rate at 20 °C (day^{-1})
K83	-	Dissolved organic phosphorus mineralization rate at 20 °C (day^{-1})
KBOD	-	Half-saturation constant for oxidation of CBOD (mg O_2 / L)
KC	-	Light attenuation coefficient due to phytoplankton (m^2 / mg Chl-a)
KD	-	De-oxygenation rate at 20 °C (day^{-1})
KDS	-	Organic carbon (as CBOD) decomposition rate (day^{-1})
KE	-	Light attenuation coefficient (m^{-1})
KMN	-	Half-saturation const. for inorganic nitrogen uptake by phytoplankton (μg N/L)
KMP	-	Half-saturation const. for inorg. phosphorus uptake by phytoplankton (μg P/L)
KMPC	-	Half-saturation constant for mineralization of phytoplankton (mg C/L)
KNIT	-	Half-saturation constant for DO limitation in the nitrification process (mg O_2/L)
KNO3	-	Half-saturation const. for DO limitation in the denitrification process (mg N/L)
KOND	-	Organic nitrogen decomposition rate (day^{-1})
KOPD	-	Organic phosphorus decomposition rate (day^{-1})
KPZD	-	Phytoplankton decomposition rate (day^{-1})
S1C	-	Temperature coefficient for phytoplankton maximum growth
SOLARI	-	Maximum daily light intensity (lg/day)
SOND	-	Temperature coefficient for organic nitrogen decomposition
SOPD	-	Temperature coefficient for organic phosphorus decomposition
SPZD	-	Temperature coefficient for phytoplankton decomposition
Θ_{12}	-	Temperature coefficient for nitrification
Θ_{1R}	-	Temperature coefficient for endogenous respiration
Θ_{2D}	-	Temperature coefficient for denitrification
Θ_{71}	-	Temperature coefficient for organic nitrogen mineralization
Θ_{83}	-	Temperature coefficient for dissolved organic phosphorus mineralization

Θ_C	-	Carbon-Chlorophyll ratio
Θ_D	-	Temperature coefficient for organic carbon oxidation in the water column
Θ_{DS}	-	Temperature coefficient for organic carbon oxidation in the sediment layer
Θ_S	-	Temperature coefficient DO diffusive exchange
VR3	-	Organic matter resuspension velocity (m/day)
VS3	-	Organic matter settling velocity (m/day)
VS4	-	Phytoplankton settling velocity (m/day)

TABLE XII. Coefficients of Water Quality Model Used by WASP and This Study

COEFFICIENT	WASP	ZONE 1	ZONE 2	ZONE 3	ZONE 4	ZONE 5
AHJ	10--30 (cm)	33.0	19.0	16.0	15.0	19.0
ANC	0.25 (mg N/mg C)	0.17	0.17	0.17	0.17	0.17
AOC	32/12 (mg O_2/mg C)	2.667	2.667	2.667	2.667	2.667
APC	0.025 (mg P/mg C)	0.025	0.025	0.025	0.025	0.025
C3JCS		0.005	0.005	0.005	0.005	0.005
C7JCS		1.0	1.0	1.0	1.0	1.0
C8JCS		0.005	0.005	0.005	0.005	0.005
DP1	0.09--0.1 (day^{-1})	0.09	0.09	0.09	0.09	0.09
EDIF	2--2.5 E-4 (m^2/day)	2.0E-4	2.0E-4	2.0E-4	2.0E-4	2.0E-4
F1		1.0	1.0	1.0	1.0	1.0
F1J		0.9	0.4	0.3	0.25	0.35
F2		1.0	1.0	1.0	1.0	1.0
F2J		1.0	1.0	1.0	1.0	1.0
FD5	0.5	0.9	0.9	0.9	0.9	0.9
FD5J		0.02	0.05	0.05	0.05	0.05
FD7	1.0	1.0	1.0	1.0	1.0	1.0
FD7J	1.0	1.0	1.0	1.0	1.0	1.0
FD8		0.2	0.2	0.2	0.2	0.2

FD8J		0.01	0.01	0.01	0.01	0.01
FDAY	0.3--0.7	0.5	0.5	0.5	0.5	0.5
FDIN		0.4	0.4	0.4	0.4	0.4
FDIP		0.4	0.4	0.4	0.4	0.4
FIMAX	720.0 (mg C/μE)	720	720	720	720	720
FON	0.5	0.05	0.2	0.2	0.2	0.2
FOP	0.5	0.5	0.5	0.5	0.5	0.5
K12	0.09--0.13 (day^{-1})	0.3	0.6	0.5	0.4	0.4
K12j		0.0008	0.0001	0.0001	0.0001	0.0001
K1C	2.0 (day^{-1})	0.55	0.85	0.85	0.90	0.60
K1D	0.02 (day^{-1})	0.02	0.02	0.02	0.02	0.02
K1R	0.125 (day^{-1})	0.13	0.13	0.13	0.13	0.13
K2	0.4848	0.4848	0.4848	0.4848	0.4848	0.4848
K2D	(day^{-1})	0.2	0.2	0.3	0.3	0.3
K71	0.075 (day^{-1})	0.075	0.075	0.075	0.075	0.075
K83	0.22 (day^{-1})	0.22	0.22	0.22	0.22	0.22
KBOD	0.5 (mg O_2 / L)	0.5	0.5	0.5	0.5	0.5
KC	0.017 (m^2/mg Chl-a)	0.017	0.017	0.017	0.017	0.017
KD	0.21--0.16 (day^{-1})	0.18	0.18	0.18	0.18	0.18
KDS	0.0004 (day^{-1})	0.015	0.015	0.017	0.017	0.015

KDS	0.0004 (day^{-1})	0.015	0.015	0.017	0.017	0.015
KE	0.1--5.0 (m^{-1})	1.5	1.5	1.5	1.5	1.5
KMN	25.0 (μg-N/L)	25.0	25.0	25.0	25.0	25.0
KMP	1.0 (μg-P/L)	1.0	1.0	1.0	1.0	1.0
KMPC	1.0 (mg C/L)	1.0	1.0	1.0	1.0	1.0
KNIT	2.0 (mg O_2/L)	2.0	2.0	2.0	2.0	2.0
KNO3	0.1 (mg N/L)	0.1	0.1	0.1	0.1	0.1
KOND	0.0004 (day^{-1})	0.0004	0.0004	0.0004	0.0004	0.0004
KOPD	0.0004 (day^{-1})	0.0004	0.0004	0.0004	0.0004	0.0004
KPZD	0.02 (day^{-1})	0.2	0.2	0.2	0.2	0.2
S1C	1.068	1.068	1.068	1.068	1.068	1.068
SOLARI	200--500 (lg/day)	500	500	500	500	500
SOND	1.08	1.08	1.08	1.08	1.08	1.08
SOPD	1.08	1.08	1.08	1.08	1.08	1.08
SPZD	1.08	1.08	1.08	1.08	1.08	1.08
Θ_{12}	1.08	1.08	1.08	1.08	1.08	1.08
Θ_{1R}	1.045	1.045	1.045	1.045	1.045	1.045
Θ_{2D}	1.08	1.08	1.08	1.08	1.08	1.08
Θ_{71}	1.08	1.08	1.08	1.08	1.08	1.08
Θ_{83}	1.08	1.08	1.08	1.08	1.08	1.08

Θ_C	20--50	30	30	30	30	30
Θ_D	1.047	1.047	1.047	1.047	1.047	1.047
Θ_{DS}	1.08	1.08	1.08	1.08	1.08	1.08
Θ_S	1.08	1.08	1.08	1.08	1.08	1.08
VR3	(m/day)	0.10	0.10	0.10	0.10	0.10
VS3	(m/day)	1.0	1.0	1.0	1.0	1.0
VS4	0.1 (m/day)	0.008	0.001	0.001	0.001	0.001

3.3. THE SEAGRASS MODEL

3.3.1.Background

Seagrasses play important roles in the ecology of estuarine systems (e.g. Culter, 1992; Tomasko, 1995; Phillips and Menez, 1988; Short, 1980) since they serve as habitat for fish and benthic invertebrates. Seagrass leaves provide substrate for many epiphytic organisms. Herbivores such as manatees, fishes, sea turtles, and sea urchins graze directly on seagrass blades. Dead leaves constitute the majority of the detritus pool. Seagrass also interact with the physical components of the estuary by slowing down the currents and reinforcing the deposition of organic and inorganic material from the water column. Their presence also inhibits the resuspension of sediments, which also affects the nutrient cycles. Since each species of seagrass has its own particular response to physical and oceanographic factors, one species is usually dominant in any given area (Dawes *et al.*, 1985; Williams, 1990; Short *et al.*, 1989). Some studies even suggested that succession or replacement can be attributed to the water quality and eutrophic state of the system (Tomasko *et al.*, 1995). According to these authors, Thalassia can be characterized as a truly oligotrophic species, which cannot prevail in areas of elevated nutrient loading. Therefore, seagrass is a crucial indicator of the state of the estuarine system, and restoration goals to seagrass can be linked exclusively to environmental quality, providing a more direct assessment of the restoration processes (Dennison *et al.*, 1993).

Seagrasses are unique for the marine environment as they are the only land plant that has totally returned to the sea (Zieman, 1982). Florida enjoys one the largest seagrass resources on earth. Of the 10,000 km^2 of seagrass bed in the Gulf of Mexico, over 8,500 km^2 are in Florida waters, primarily in the southern end of the peninsula. Physical and oceanographic factors drastically reduce the amount of seagrass bed north of Florida Bay, on both coasts. Along the Atlantic coast, which is a wave dominated environment, a relatively unstable substrate confine seagrass beds to inlets and lagoons. Along the Gulf coast, seagrass beds diminish due to the high-turbidity waters coming from the Everglades drainage and reduced salinity. North of this area, several bays, including Tampa Bay and Boca Ciega Bay, formerly possessed extensive seagrass coverage, but anthropogenic perturbations have greatly reduced the extent of these beds (Zieman, 1982). Culter (1992) described the seagrass distribution and evolution in Sarasota Bay. Figure 14 shows the distribution of seagrass in Sarasota Bay during 1986.

According to den Hartog (1977), seagrasses comprise approximately 49 species in 12 genera of this marine aquatic angiosperm. The three dominant species of the west coast of Florida are Thalassia testudinum, Halodule wrightii, and Syringodium filiforme (Zieman and Zieman, 1989). A detailed description of physiology and production ecology of seagrasses can be found in McRoy and Helfferich (1977), Phillips and McRoy (1980), Zieman (1982), and Phillips and Menez (1987). The following is a brief description of each species reproduced from Zieman (1982). Figure 15 shows the three species. Thalassia testudinum (turtle grass) is the largest and most robust of the southwest Florida seagrasses. Leaves are ribbon-like, typically 4 to 12 mm wide with rounded tips and are 10 to 35 cm in length. There are commonly two to five leaves per short shoot. Rhizomes are typically 3 to 5 mm wide and may be found as deep as 25 cm in the sediment. Turtle grass forms extensive meadows throughout most of its range. Halodule wrightii (shoal grass) is extremely important as an early colonizer of disturbed areas. It is found primarily in disturbed areas where Thalassia or Syringodium are excluded because of prevailing conditions. Shoal grass grows commonly in water too shallow for the other two species of seagrasses. Leaves are flat, typically 1 to 3 mm wide and 10 to 20 cm long, and arise from erect shoots. The tips of the leaves are not rounded, but have two or three points, an important recognition character. Shoal grass is the most tolerant of all seagrasses to variations in temperature, salinity, and exposure. Syringodium filiforme (manatee grass) is distinctive in having cylindrical leaves which are quite fragile and buoyant,

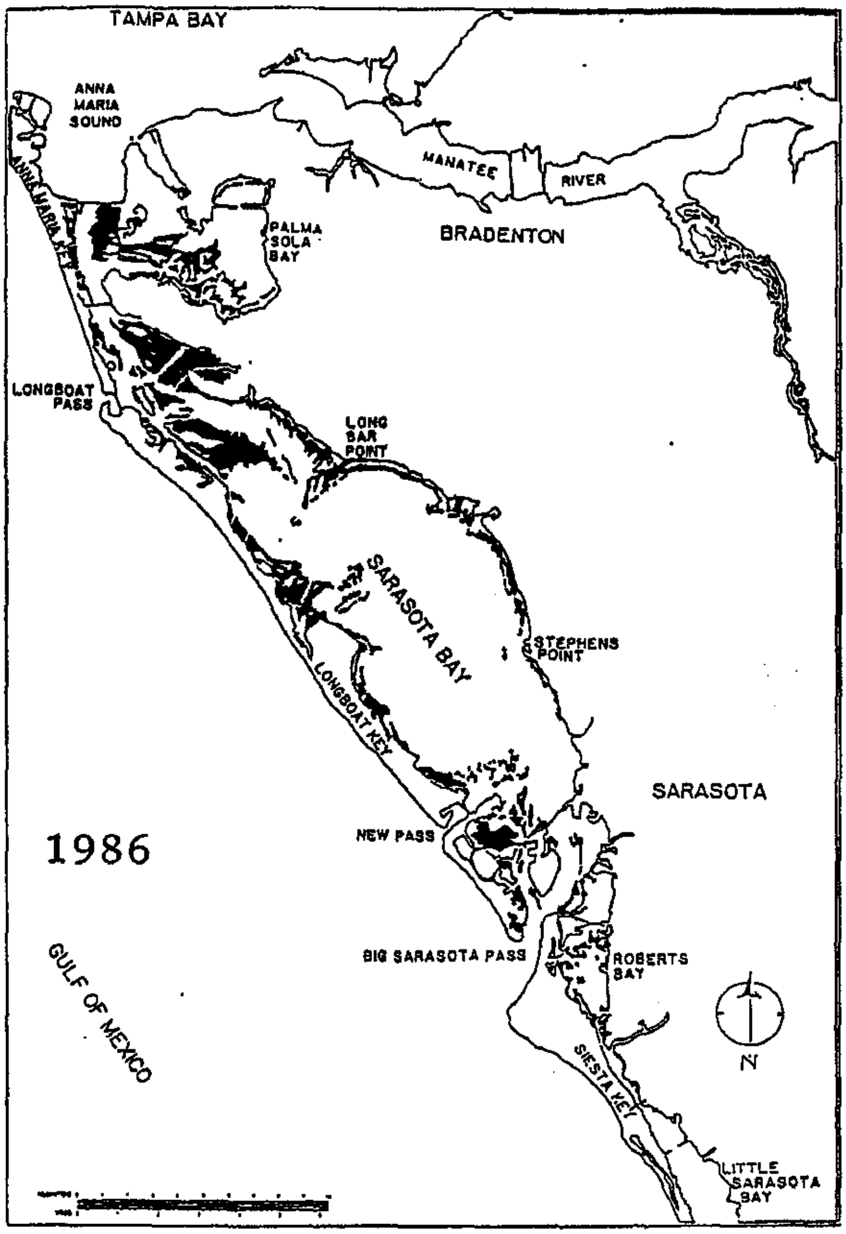

Figure 14. Seagrass bed in Sarasota Bay during 1986.

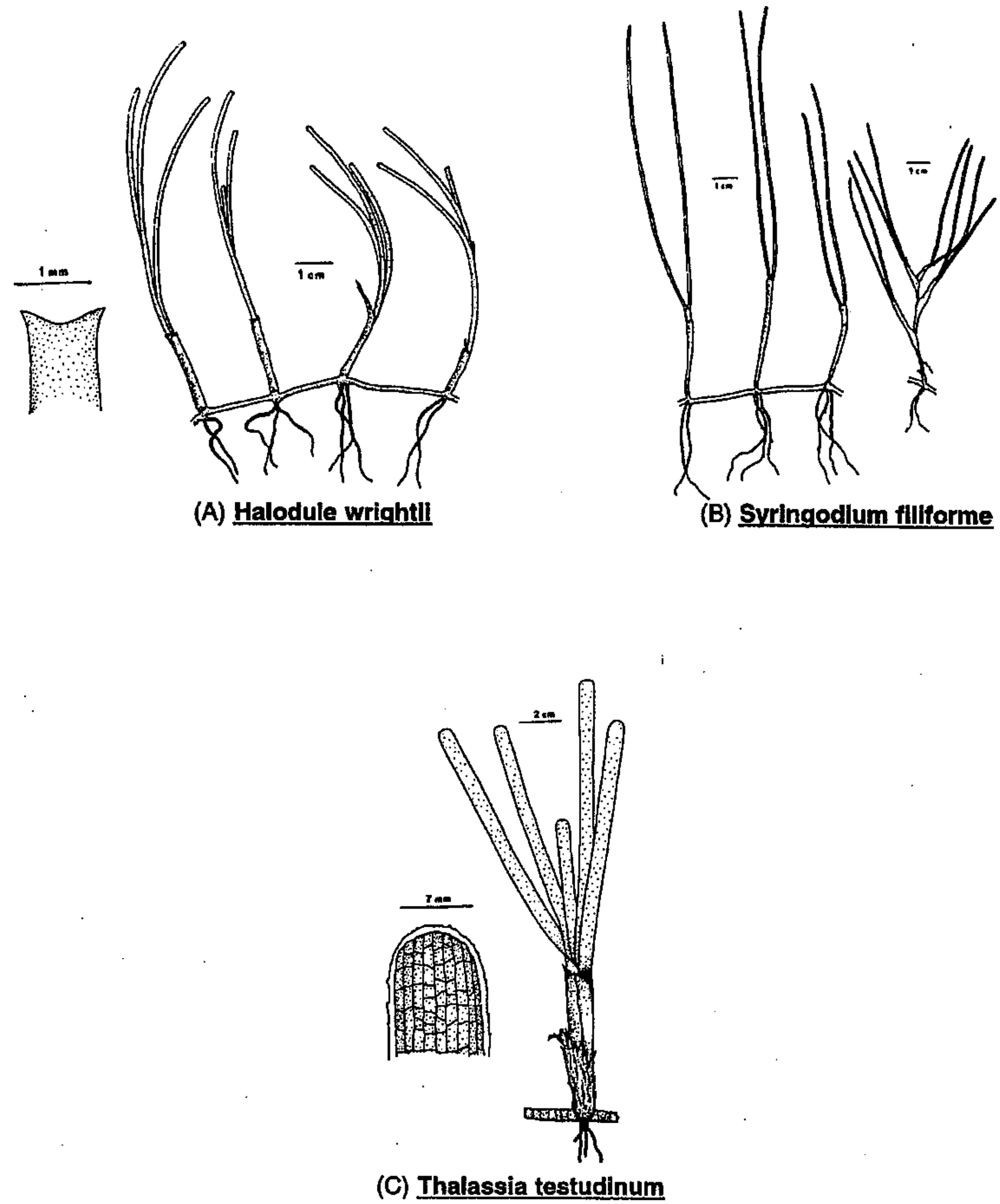

Figure 15. Three different types of seagrasses found in Florida estuaries.

and thus are readily broken off and exported from the immediate area by winds and currents. There are commonly two to four leaves per shoot, and these are 1.0 to 1.5 mm in diameter. Length is highly variable, but can exceed 50 cm. The rhizome is less robust than that of Thalassia and more surficially rooted. Manatee grass is commonly mixed with the other seagrasses, or in small, dense, monospecific patches. It rarely forms the extensive meadows like Thalassia.

3.3.2. Development of the Numerical Model

The development of a numerical model of the seagrass community may provide a mechanism for synthesizing all the dynamic functions of an estuarine ecosystems. The conceptual model used in this study was developed by Fong and Harwell (1994), which was able to describe the major dynamic interactions that drive the seagrass community structure in the Florida Keys. However, the model developed by Fong and Harwell is a simple box model which does not have any spatial dynamics. Their model was applied to Florida Keys area and may not work in Roberts Bay. In order to develop a seagrass model which include the spatial dynamics and is applicable to Roberts Bay, we made the following enhancements:

- We adapted the model to conditions of Roberts Bay;
- We added horizontal advection and diffusion processes to the model;
- We improved the model by adding a more realistic mathematical description of the available light to the seagrass bed; and
- We incorporated the seagrass and light model into the multi-dimensional framework of the coupled hydrodynamics-sediment-water quality model.
- The seagrass model consists of four biotic variables, including three species of seagrass

found in Roberts Bay, Thalassia testudinum, Halodule wrightii, and Syringodium filiforme, and a functional form of epiphytic algae on seagrass (Figure 16). In the model the epiphytic algae is controlled by light, temperature, water-column nutrient concentration, and available substrate (seagrass density) (Figure 17).

The abundance of each species of seagrass is controlled by available light, temperature, salinity, sediment nutrient concentration, and physical disturbance through bottom shear stress (Figure 18). An important characteristic of this model is the feedback loop between the abundance of epiphytes and the amount of light reaching the seagrass blades, leading to a predator-prey type of relationship.

3.3.3. Mathematical Equations of the Seagrass and Light Model

Light

Light regime is the primary environmental factor influencing photosynthesis, growth and depth distribution of seagrasses (Dennison, 1987). Light availability is often the primary limiting factor for seagrass growth (e.g. Wetzel and Penhale, 1983; Dennison and Alberte, 1985). Studies showing the decline of seagrass due to increases in water turbidity demonstrate the crucial role of light in determining seagrass distribution (Orth and Moore, 1983; Cambridge and McComb, 1984). Therefore, determination of the relationship between light regime, available light and seagrass growth and distribution is of extreme importance in a modeling effort. The seasonal variation of surface irradiance is represented in the model by a sine curve:

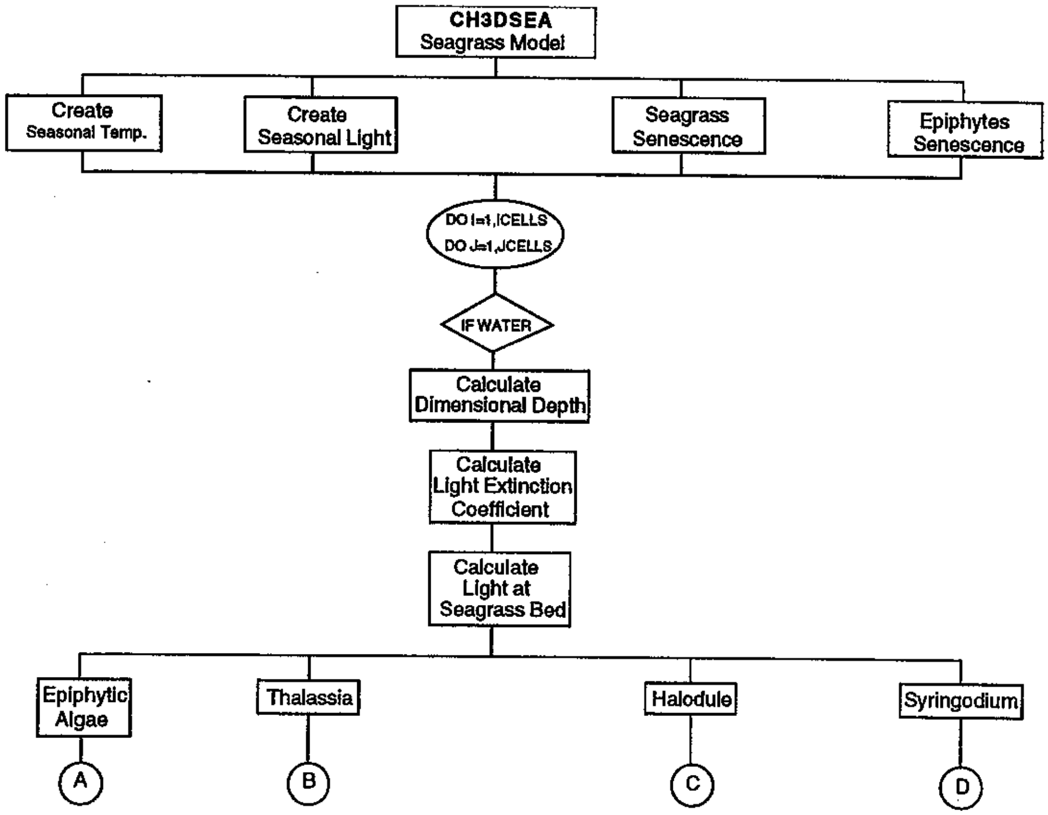

Figure 16. Structure and components of the numerical seagrass model used for this study.

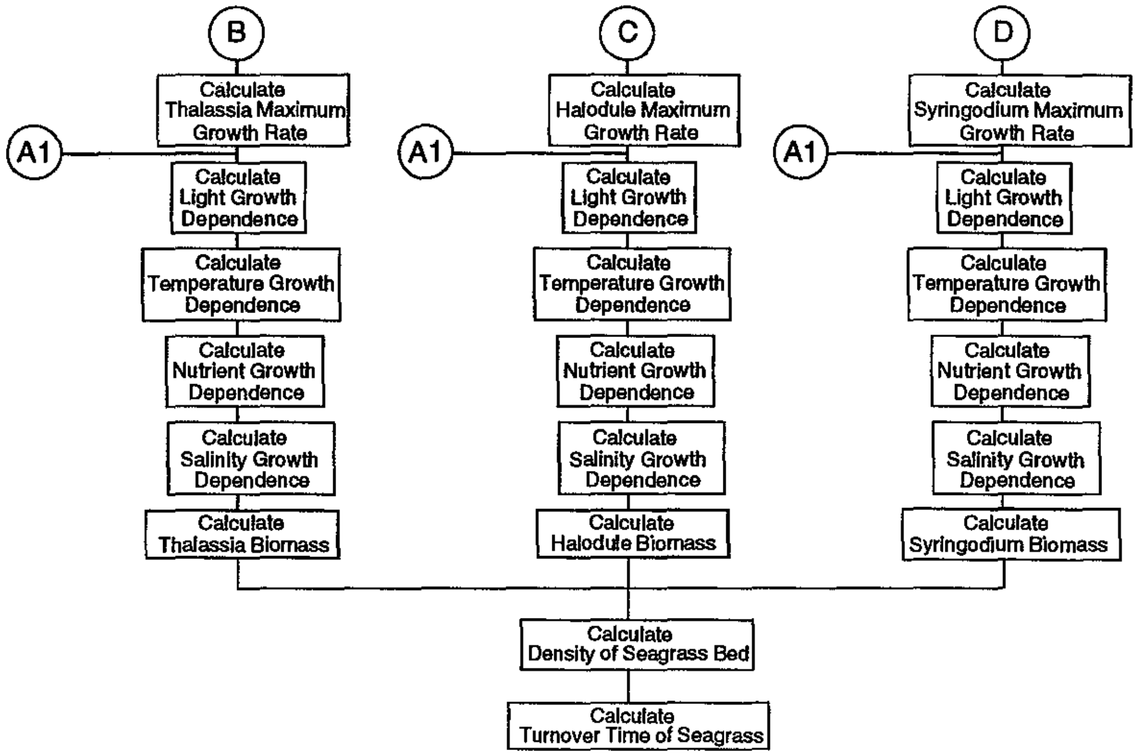

Figure 17. Flow charts of the seagrass model used for this study.

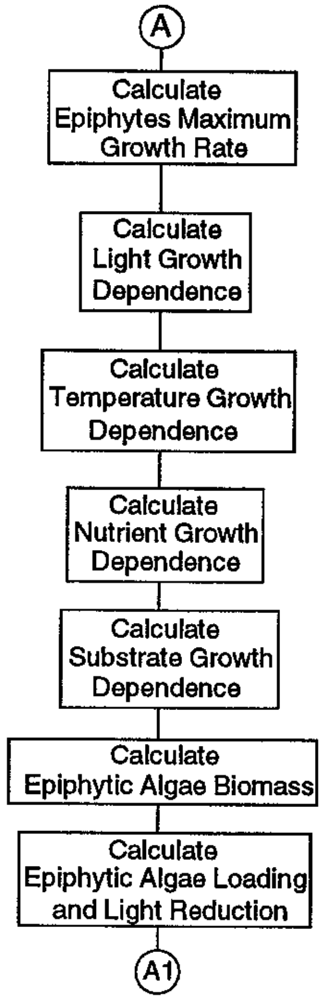

Figure 18. Flow chart of the epiphyte algae model.

$$I_o = 1800 + \left(400 \cdot \sin\left(\frac{3\pi}{2} + 2\pi \cdot \left(\frac{day}{365}\right)\right)\right) \tag{68}$$

corresponding to high levels of insulation during summer and the lowest levels during winter.The Beer-Lambert law was used to describe the loss of light with depth, as shown in Equation (69):

$$I_z = I_o e^{-kz} \tag{69}$$

where I_o is light intensity at the water surface given by Equation (68), I_z is light intensity at depth z, z is the depth in meters, and k is the vertical light attenuation coefficient in m^{-1}. A simple formula developed by McPherson and Miller (1994) was used to represent vertical attenuation of photosynthetically active radiance (PAR). Originally, the attenuation coefficient was partitioned into a set of partial attenuation coefficients:

$$k_o = k_w + E_2 \cdot C_2 + E_3 \cdot C_3 + E_4 \cdot C_4 \tag{70}$$

where k_w is the PAR-waveband average attenuation coefficient of seawater, 0.0384 m^{-1} (Lorenzen, 1972); E_2 is the attenuation coefficient of dissolved matter, in (m Pt-Co units)$^{-1}$; C_2 is the water color, in Pt-Co units; E_3 is the attenuation coefficient of chlorophyll and other matter associated with chlorophyll a, in m^2 mg^{-1}; C_3 is the concentration of chlorophyll a, in mg m^{-3}; E_4 is the attenuation coefficient of nonchlorophyll suspended matter (NSM), which includes inorganic and organic particulate not directly associated with color or chlorophyll a, in m^2 mg^{-1}; and C_4 is the concentration of NSM, in mg m^{-3}. The lack of good measurements of NSM (in terms of total suspended solids and turbidity) constrained the determination of the $E_4 \cdot C_4$ term, and the equation was modified to (McPherson and Miller, 1994):

$$k_o = 0.014 \cdot C_2 + 0.062 \cdot (turbidity) + 0.049 \cdot C_3 + 0.30 \tag{71}$$

with the coefficients E_2 and E_3 determined from Tampa Bay and Charlotte Harbor data. Equation (70) will be used in this study, with C_2 representing the average water color, in Pt-Co units; C_3 is the chlorophyll a concentration in mg m^{-3}; and turbidity is given in NTU. Data of water color and turbidity for each segment of the bay was obtained through a monitoring program conducted by Tomasko (1995). Chlorophyll-a concentration is determined from the water quality portion of the model.

Temperature

The seasonal variation of water temperature is represented in the model by a sine curve:

$$Temp = 23 + \left(7 \cdot \sin\left(\frac{3\pi}{2} + 2\pi \cdot \left(\frac{day}{365}\right)\right)\right) \tag{72}$$

corresponding to an annual average of 23 °C, higher temperature levels during summer (maximum of 30 °C) and the lowest levels during winter (minimum of 16 °C) (Zieman and Zieman, 1989).

Relationships Controlling Seagrasses

For each species of seagrass, literature values of maximum growth rates and biomass were obtained, and incorporated to a density-dependent growth function. Subsequently, environmental variability in light, temperature, salinity, and sediment nutrient concentration would result in stresses to the growth rate, reducing the maximum growth rate according to species-specific sensitivity. Death rates is accelerated when extreme values of salinity and temperature endure for extended period of time. *Density-dependent Growth Rate.* For Thalassia, Williams (1988) found maximum growth rates up to 27,000 mg dry wt m^{-2} day^{-1} in pristine areas of the Virgin Islands, and Fourqurean and Zieman (1991) found maximum biomass to be 470,000 mg dry wt m^{-2} in Florida Bay. Powell *et al.* (1989) found that Halodule in Florida Bay can growth as fast as 16,320mg dry wt m^{-2} day^{-1}, and a maximum biomass of 150,000 mg dry wt m^{-2}. For Syringodium, Short *et al.* (1985) reported a maximum growth rate of 6,300 mg dry wt m^{-2} day^{-1}, in the Bahamas, and a maximum biomass of 190,000 mg dry wt m^{-2}. Thus, the hierarchy for growth rates is Thalassia > Halodule > Syringodium and for maximum biomass is Thalassia > Halodule ≈ Syringodium, resulting in a density-dependent growth curve that favors Thalassia throughout the range of densities. This curve is for "normal" environmental conditions, however, each growth rate is further modified by light, temperature, salinity, and sediment nutrient concentration,. resulting in a possible alteration in the growth-rate hierarchy.

Light: Most studies on seagrass distribution and growth reveal the light is an important factor controlling seagrass distribution (e.g. Williams, 1987; Dawes and Tomasko, 1988; Dunton, 1990). Fourqurean and Zieman (1991) established the relationship between light and photosynthesis for Thalassia, specifying P_{max} of 200 $\mu g{\cdot}O_2{\cdot}g^{-1}{\cdot}min^{-1}$. In this model, we assumed saturation occurring at 425 $\mu E{\cdot}m^{-2}{\cdot}sec^{-1}$, and no photoinhibtion at high light levels; the compensation point is approximately 15.1-15.7 $\mu E{\cdot}m^{-2}{\cdot}sec^{-1}$. Williams (1987) found that light saturation levels for Halodule and Syringodium were similar. Fong and Harwell (1994) assumed that Halodule may require less light than the other species for maximum productivity, so in the model the saturation point for Halodule is 300 $\mu E{\cdot}m^{-2}{\cdot}sec^{-1}$. Based on these data, Fong and Harwell (1994) postulates that growth of Thalassia and Syringodium is reduced when available light is less than 425 $\mu E{\cdot}m^{-2}{\cdot}sec^{-1}$, while growth remains maximum for Halodule until light is below 300 $\mu E{\cdot}m^{-2}{\cdot}sec^{-1}$. The mathematical formulation of the growth rate dependence on light is given by:

$$
\begin{aligned}
T_{light} &= 1. - e^{-0.013 \cdot xavl(i,j)} \\
H_{light} &= 1. - e^{-0.016 \cdot xavl(i,j)} \\
S_{light} &= 1. - e^{-0.013 \cdot xavl(i,j)}
\end{aligned}
\tag{73}
$$

where *xavl(i,j)* represents the available light at the seagrass bed.

Salinity: There are few studies that directly test the effect of altered salinity on seagrasses. We performed a laboratory experiment to study the response of three species of tropical seagrasses to salinity fluctuations (Yassuda, 1995), and preliminary results demonstrate that tolerance are species-specific, with Halodule being the most tolerant to salinity variations, and Syringodium being the least tolerant. This results agree with literature and the hypothesis of the original model (Fong, 1994). The seagrass growth-salinity relationship specific for each species shows that Thalassia has the widest salinity optimum, with growth being reduced for salinity below 30 and above 45 ppt. The mathematical formulation of the growth rate dependence on salinity is given by:

For Thalassia:

$$
\begin{aligned}
\text{salinity} &< 31.67 \\
T_{sal} &= 3.5E-4 \cdot e^{0.25 \cdot sal} \\
31.67 < \text{sal.} &< 35.0 \\
T_{sal} &= 0.009 \cdot sal + 0.685 \\
35.0 < \text{sal.} &< 41.67 \\
T_{sal} &= 1.0 \\
41.67 < \text{sal.} &< 45.0 \\
T_{sal} &= -0.003 \cdot sal + 1.125
\end{aligned}
\tag{74}
$$

For Halodule:

$$
\begin{aligned}
\text{salinity} &< 18.33 \\
H_{sal} &= 0.006 \cdot sal - 0.0751 \\
18.33 < \text{sal.} &< 28.33 \\
H_{sal} &= -0.0109 \cdot sal^2 + 0.5963 \cdot sal - 7.20 \\
28.33 < \text{sal.} &< 31.60 \\
H_{sal} &= 1.0 \\
35.0 < \text{sal.} &< 38.33 \\
H_{sal} &= -0.3003 \cdot sal + 11.5105
\end{aligned}
\tag{75}
$$

Temperature: Tomasko and Dawes (1990) reported some seasonal trends in the growth rate of Sarasota Bay seagrasses. To be consistent with the hypothesis that Halodule is an opportunistic species that often dominates in transition areas, the model specifies a broader range of optimum temperature for Halodule, followed by Thalassia, and assigns to Syringodium the least temperature variation tolerance. Optimum growth of Thalassia occurs at 25 °C, and growth rates decreases at higher or lower temperatures. The mathematical formulation of the growth rate dependence on temperature is given by:

For Thalassia:

$$T_{temp} = -0.0059 \cdot temp^2 + 0.329 \cdot temp - 3.5862 \tag{76}$$

For Halodule:

$$H_{temp} = -0.0124 \cdot temp^2 + 0.6094 \cdot temp - 6.485 \tag{77}$$

For Syringodium:

$$S_{temp} = -0.0059 \cdot temp^2 + 0.329 \cdot temp - 3.5862 \quad (78)$$

Sediment Nutrients: Roberts Bay has been reported to be nitrogen limited (Tomasko *et al.*, 1995). Likewise other parameters, Halodule would be favored in more extreme conditions of an eutrophic organic-rich sediment. Syringodium is favored in low sediment concentration, since its distribution is restricted to more oceanic environments. Thalassia has a wide range of sediment nutrient concentration tolerance, but cannot survive in anaerobic conditions that commonly occur in nutrient-rich sediments. by

4. RESULTS OF MODEL SIMULATIONS

4.1. Simulations of Circulation

In order to assess the impact of reduced nutrient loading on the water quality and seagrass dynamics in the study area, long-term (longer than one month) simulations must be performed. In this study, we simulate the circulation and water quality dynamics in the study area for 90-180 days. Due to the extreme shallow depths and the long-term simulations, we decided to use the vertically-integrated version , instead of the fully 3-D version, of the 3-D model of the Sarasota Bay system. In the following, we describe the computational grid, the ocean and river boundary conditions, and the model results.

4.1.1. Computational Grid

Figure 5 shows the curvilinear grid designed for the limited area of this study, while Figure 6 shows the numerical grid for the entire Sarasota Bay system used by Sheng et al. (1995). The limited area grid shown in Figure 5 is more refined than the baywide grid in the study area, since smaller scale processes need to be considered.

The limited area numerical grid shown in Figure 5 extends from its northern boundary near the null-zone in Big Sarasota Bay to its southern boundary at Venice Inlet, and covers the entire Roberts Bay, Little Sarasota Bay, and Blackburn Bay. In the offshore region, the grid extends about 5 km into the Gulf of Mexico. The grid contains 144 cells in the longitudinal direction (approximately north-south) and 34 cells in the transverse direction. The maximum grid spacing is on the order of 1 km, whereas the minimum spacing is on the order of 30 meters. The advantage of a curvilinear boundary-fitted grid is evident in its ability to represent the complex geometry associated with the Intracoastal Waterway (ICW), the multiple islands, rivers and creeks, and tidal inlets.

The depth contours of the study area are also presented in Figure 5. The data used to generate the depths were taken from existing NOAA charts along with a bathymetric survey conducted by the University of Florida in September of 1990.

4.1.2. Boundary Conditions

Tidal Forcing

In the hydrodynamic simulations, the tidal forcing can be prescribed either through the realtime water level data or the harmonic constituents. The three-month simulations were performed using realtime tidal data. The test runs and longer simulations were performed using the five major tidal components determined from the harmonic analysis of the tidal data. The measured tide data at the ocean boundary during 1991 (Sheng et al. 1995) are compared with the re-constructed tide using the five major tidal constituents in Figure 19. Table XII presents the amplitude and phases for the five major components.

TABLE XII. Amplitudes and phases of five major tidal constituents determined from 1991 tide data.

Constituent	Amplitude	Phase
M2	16.6	166.12
S2	3.9	337.09
O1	19.0	288.94
K1	24.4	124.66
P1	8.1	-149.35

Freshwater Inflow

Freshwater inflows to the system are incorporated into the model through river discharge via Phillippi Creek. Based on USGS data obtained in 1991 and 1992, the wet-season can be characterized by an average discharge of 1 m^3/s, and the dry-season by an average discharge of 0.5 m^3/s.

4.1.3. Results of the Hydrodynamic Model

The CH3D model was sufficiently calibrated and validated with data from Tampa Bay and Sarasota Bay (Sheng and Peene 1991, Peene et al. 1991, Sheng and Peene 1992, Sheng and Peene 1993, Sheng *et al.*, 1995). For this study, the 2-D version of CH3D was calibrated using the surface elevation and velocity field obtained by the three-dimensional simulations.

Two-dimensional, depth integrated models are very sensitive to the parameterization of bottom friction. The utilization of Chezy-Manning formulation requires a large amount of data for calibration. Although the 3-D version of CH3D also contains some model coefficients, these coefficients are much less empirical, and the bottom friction formulation is more robust (Yassuda and Sheng, 1994). During the calibration of the 2-D model, bottom stress and horizontal diffusion coefficients were adjusted until a good agreement between the depth averaged velocity field of the 3-D simulation and the 2-D results was obtained. Figure 20 shows the water level at an offshore station during the last 30 days of a 3-month simulation in 1991. Figures 21, 22, and 23 show the water level during the same period at stations in Sarasota Bay, Roberts Bay, and Little Sarasota Bay, respectively.

Figure 24 presents the residual (time-averaged) velocity field (vectors) and surface elevation (contours) in Sarasota Bay during the last 30 days of a 3-month simulation. Figure 25 shows the residual circulation in Roberts Bay during the last month of the 3-month simulation. Figure 26 shows the residual flow field in Little Sarasota Bay. The residual flow fields indicate that flow and material from Phillippi Creek will primarily enter into Sarasota Bay, although some will enter into Little Sarasota Bay where there is a large null zone. There is also a large null zone near the northern boundary of the model domain.

TIDAL FORCING

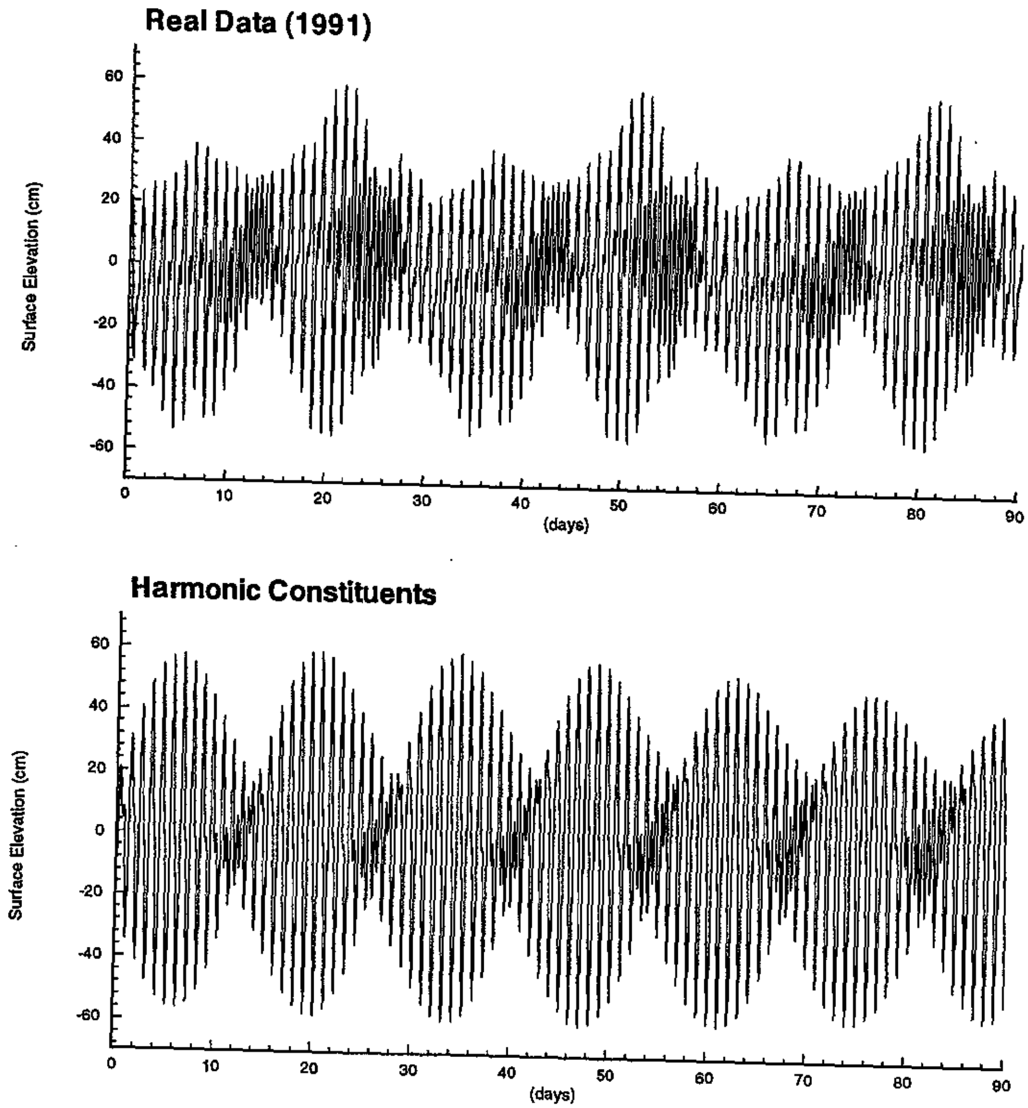

Figure 19. Measured and reconstructed water level at the ocean boundary during a 3-month period in 1991.

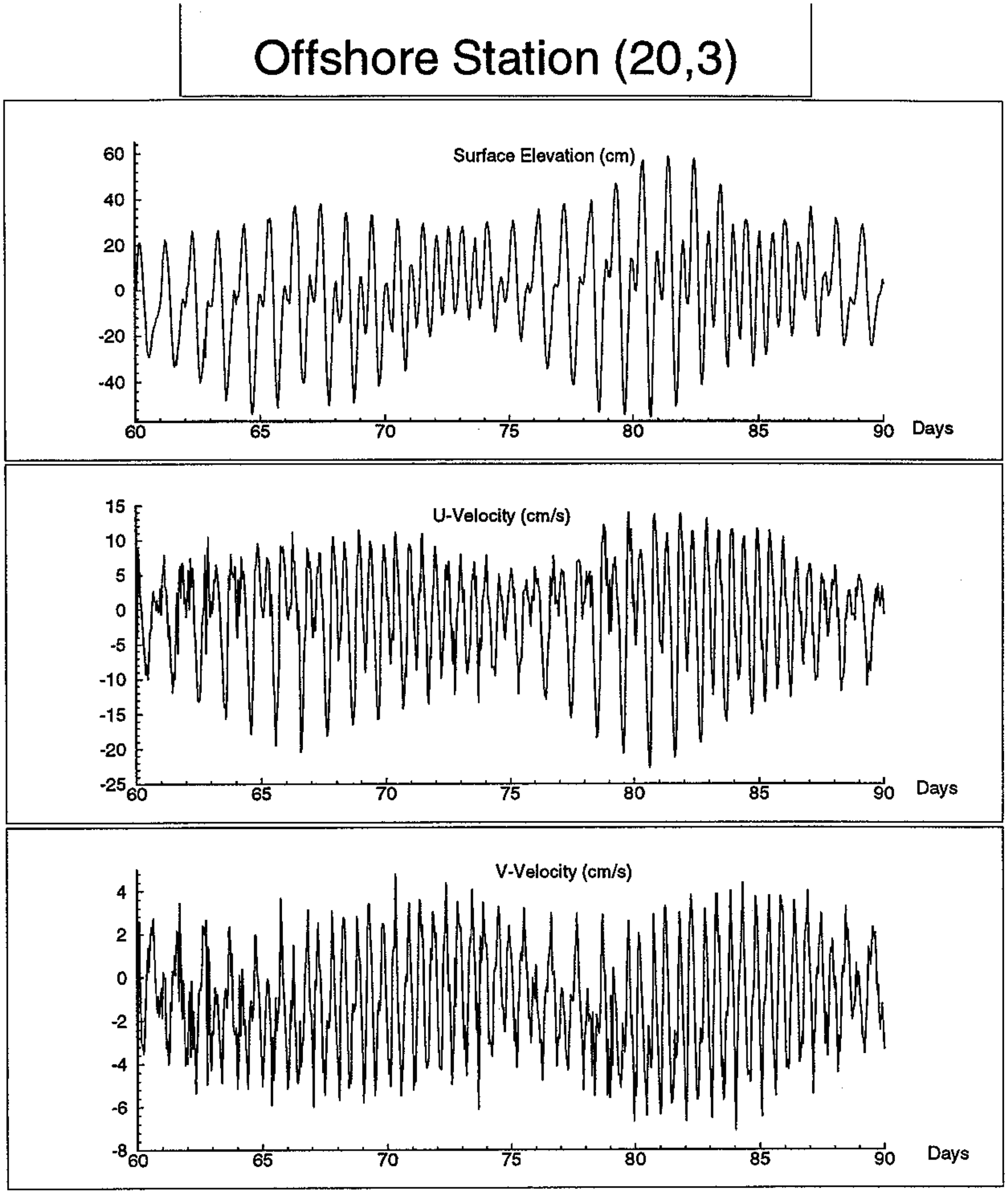

Figure 20. Water level at an offshore station during the last 30 days of a 3-month period in 1991.

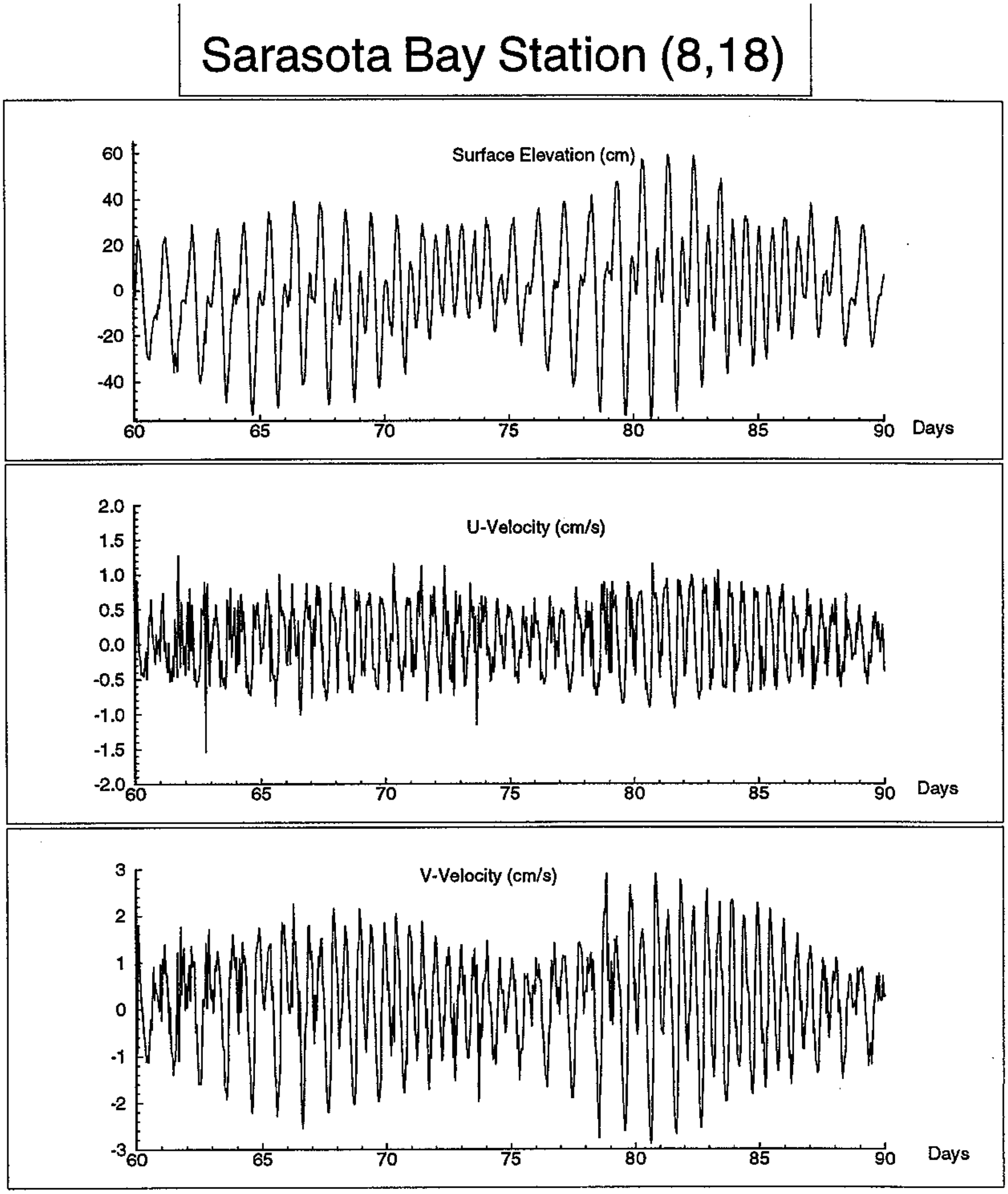

Figure 21. Simulated water level at a station in Sarasota Bay during the last 30 days of a 3-month period in 1991.

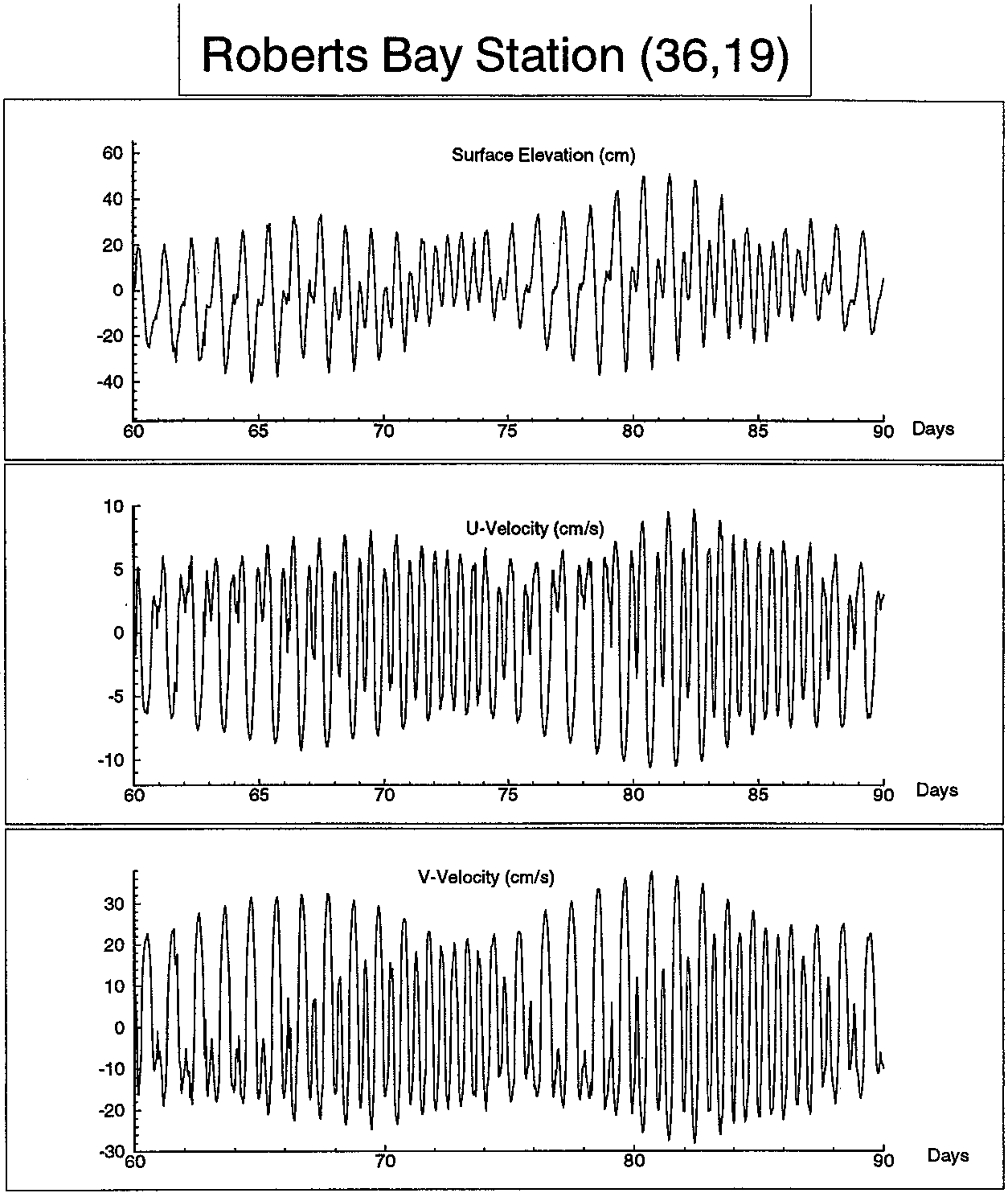

Figure 22. Simulated water level at a station in Roberts Bay during the last 30 days of a 3-month period in 1991.

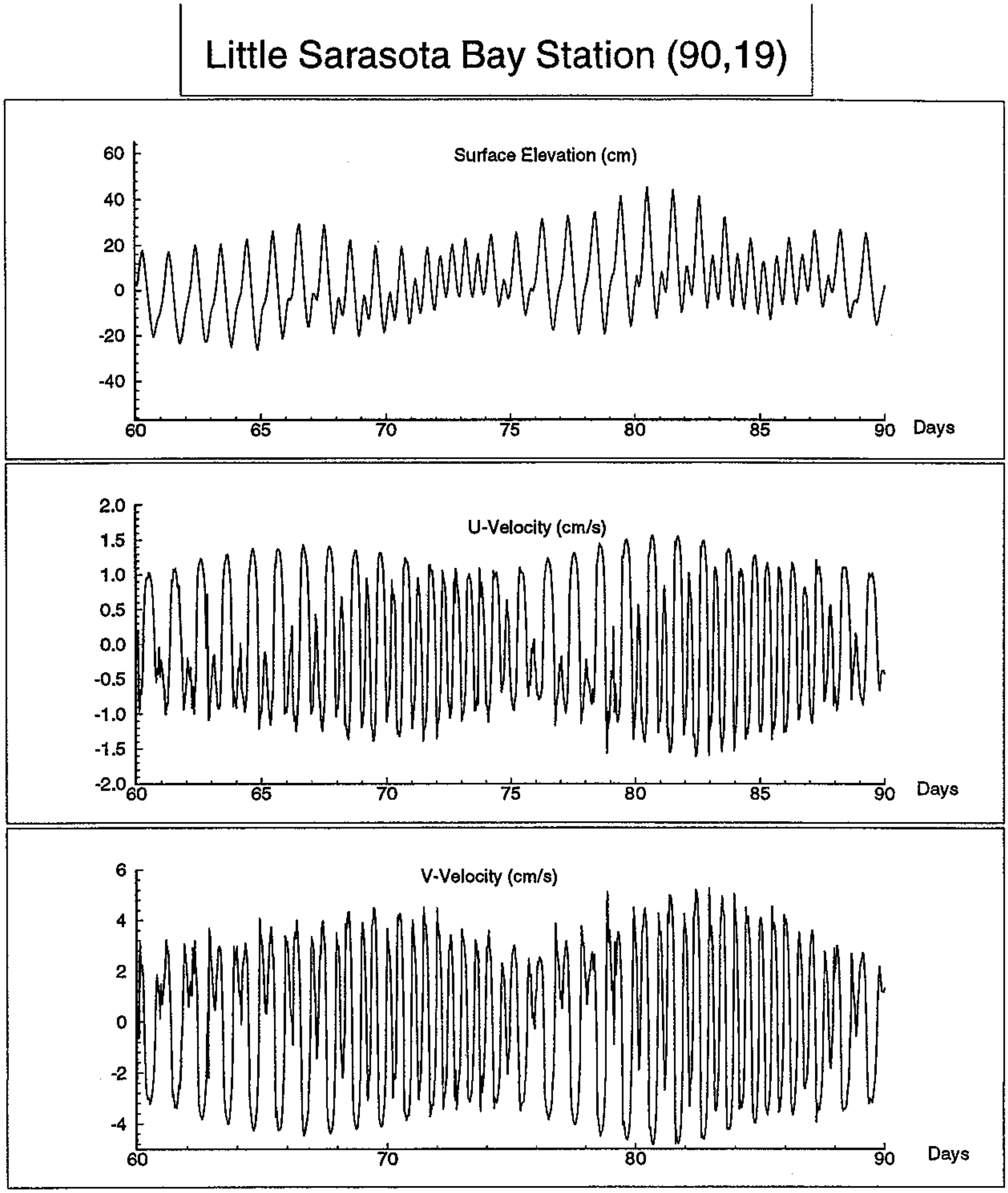

Figure 23. Simulated water level at a station in Little Sarasota Bay during the last 30 days of a 3-month period in 1991.

SARASOTA BAY

Residual Circulation for the last 30 days

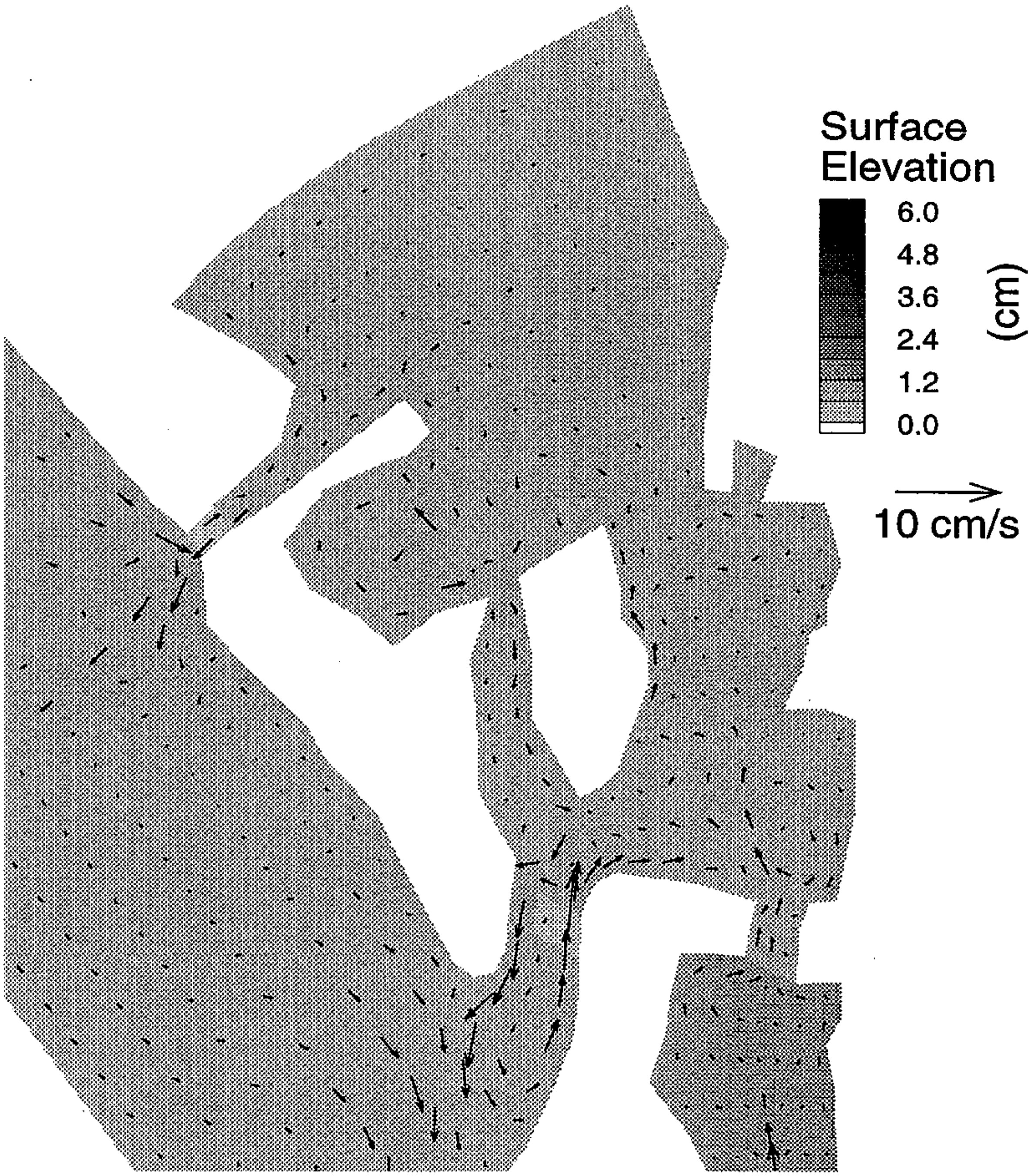

Figure 24. Residual flow field and water level in Sarasota Bay during the last 30 days of a 3-month period in 1991.

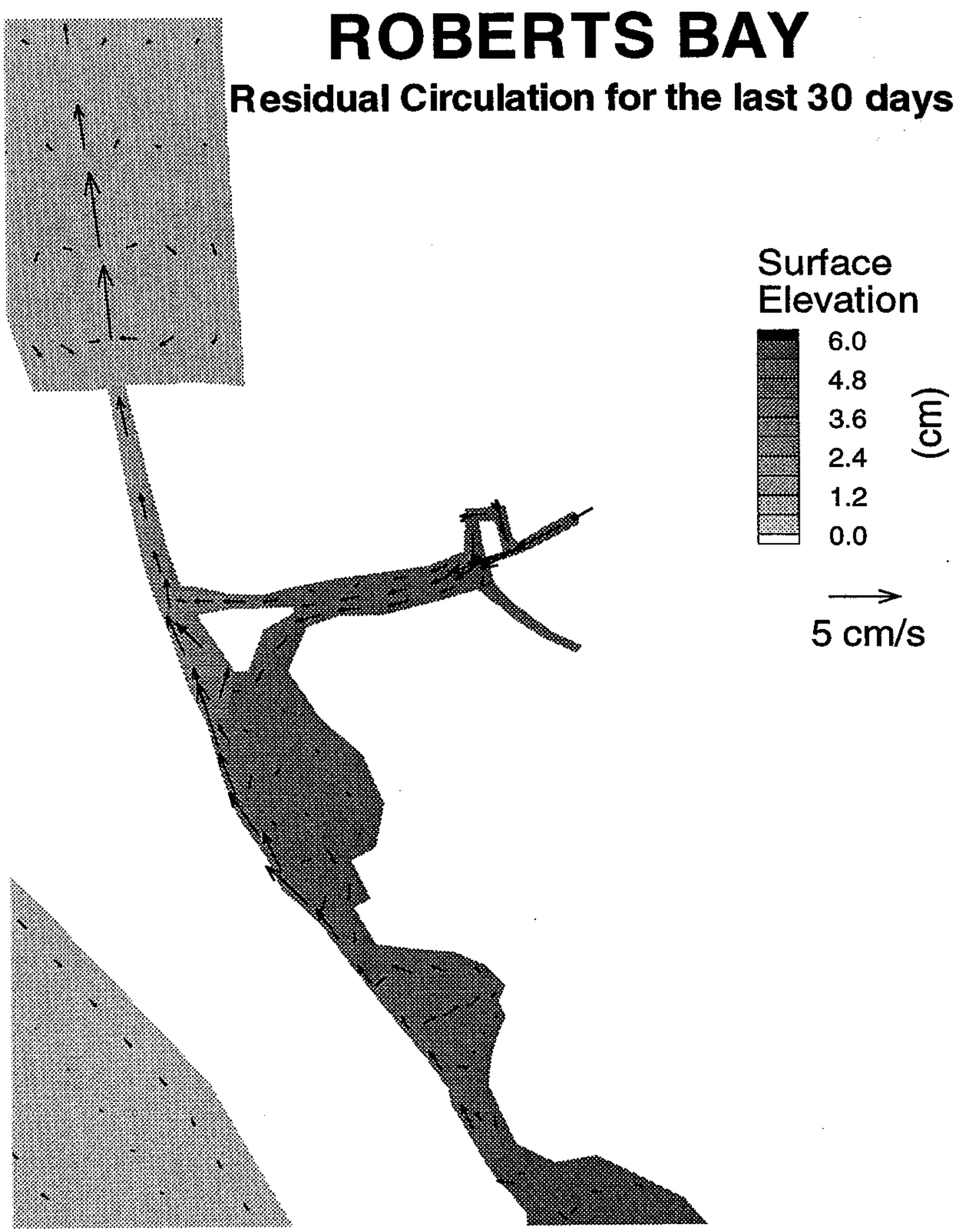

Figure 25. Residual flow field and water level in Roberts Bay during the last 30 days of a 3-month period in 1991.

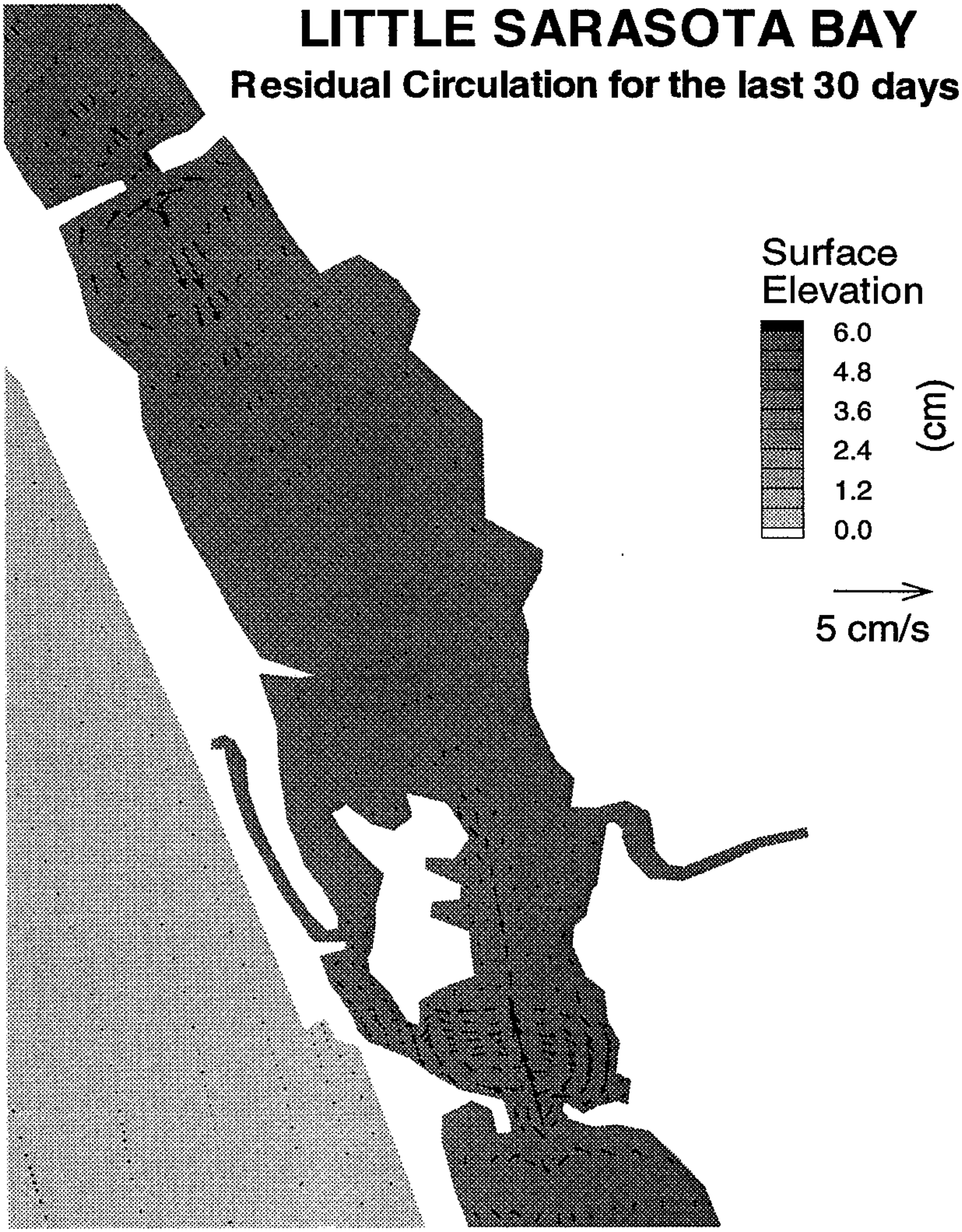

Figure 26. Residual flow field and water level in Little Sarasota Bay during the last 30 days of a 3-month period in 1991.

4.2. Simulations of Water Quality Dynamics

For water quality simulations, the hydrodynamics model and water quality model are run simultaneously with the same time step and spatial grid. We first conducted simulations of the present condition using the quarterly synoptic water quality data presented previously in this report. After the model has been calibrated with the limited water quality data, we then conducted simulations of the water quality with reduced nutrient loading from Phillippi Creek. In both cases, model simulations are longer than 90 days. Since the impact of reduced loading is expected to be greater during wet season/year than in dry season/year, we focus our model simulations with the wet season/year data.

In order to determine the proper initial conditions for the water quality model, the computational grid is divided into 5 zones as shown in Figure 27, according to physical location and sediment type. Water quality data within each zone were determined by spatial averaging of the measured water quality data. The zone-averaged water quality data are shown in Chapter 3. The zone-averaged water quality data are used as initial condition of model run, since the data are too sparse to allow specification of initial concentrations at all of the fine grid points. The zone-averaged mean concentrations and variances are used to calibrate the water quality model. The water quality simulations, however, are always conducted using the fine numerical grid, primarily to minimize uncertainty/error associated with the coupling between two types of models and to reduce the excessive "tuning" of "advective fluxes" and "dispersion coefficients", which is the major component in traditional water quality modeling. The four sets of synoptic data do not allow us to calibrate the temporal dynamics of water quality parameters. If sufficient water quality data were available at many locations over various time scales, it would then be possible to compare the model results with data at some particular locations.

Since the water quality data were obtained in the water column only, it was necessary to carefully choose the initial conditions of nutrient concentrations in the sediment column. The water quality model was run for at least 90 days to allow an equilibrium established between the water column and the sediment column.

4.2.1. Existing Condition

The water quality simulations with present land use condition are conducted with the zone-averaged water quality data on August 8, 1990 described in Chapter 2 as the initial condition, and with the model coefficients described in Table XII. The zone-averaged concentrations of six water quality variables (DO, CBOD, Ammonia-N, Nitrate+Nitrite-N, phytoplankton, and DON) in three zones (Sarasota Bay, Roberts Bay, and Little Sarasota Bay) are plotted and compared with data whenever possible. Model results in Sarasota Bay are shown in Figures 28, 29, and 30. Model results for Roberts Bay are shown in Figures 31, 32, and 33, while those in Little Sarasota Bay are shown in Figures 34, 35, and 36. All the results showed that the water quality parameters have reached equilibrium conditions in all the zones within 90 days of model simulation. Model simulated DO compared very well with data. Model simulated phytoplankton and Ammonia Nitrogen are generally within the measured variability of data. Model simulated Nitrate+Nitrite appear to be lower than the measured data. The model results showed tidal (semi-diurnal, diurnal and longer period) influence on the water quality parameter concentrations.

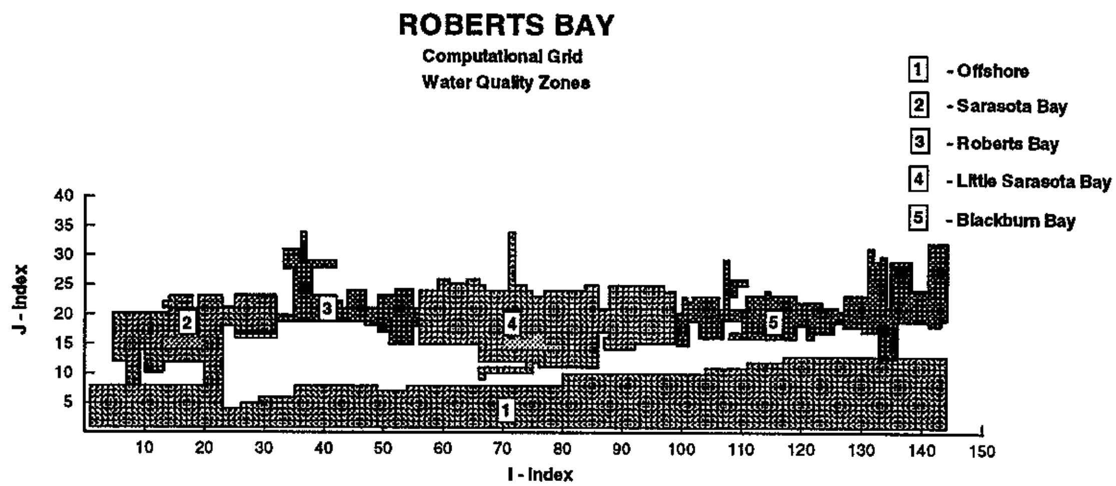

Figure 27. Five zones in the computational grid of the study area used for water quality model simulations.

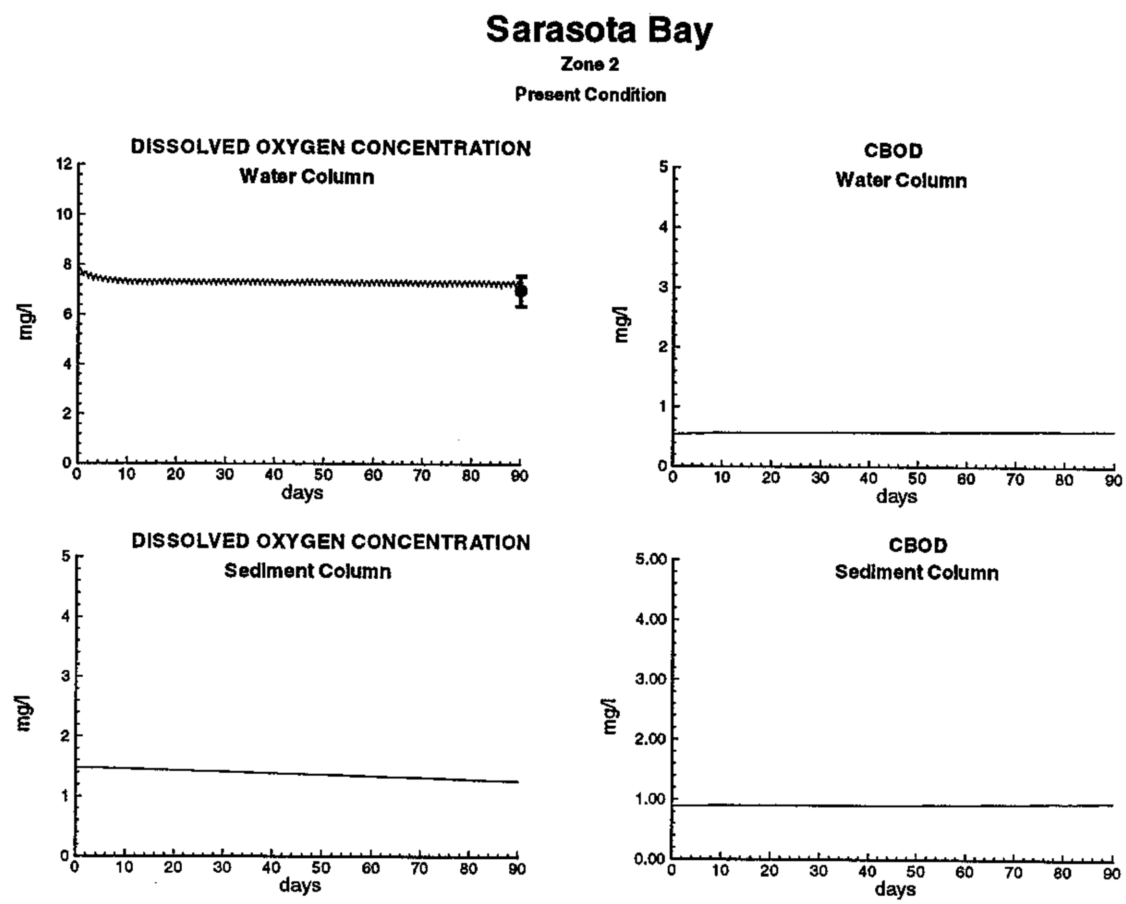

Figure 28. Simulated zone-averaged DO and CBOD concentrations in water and sediment columns in Sarasota Bay during the 90 day simulation with present land use condition.

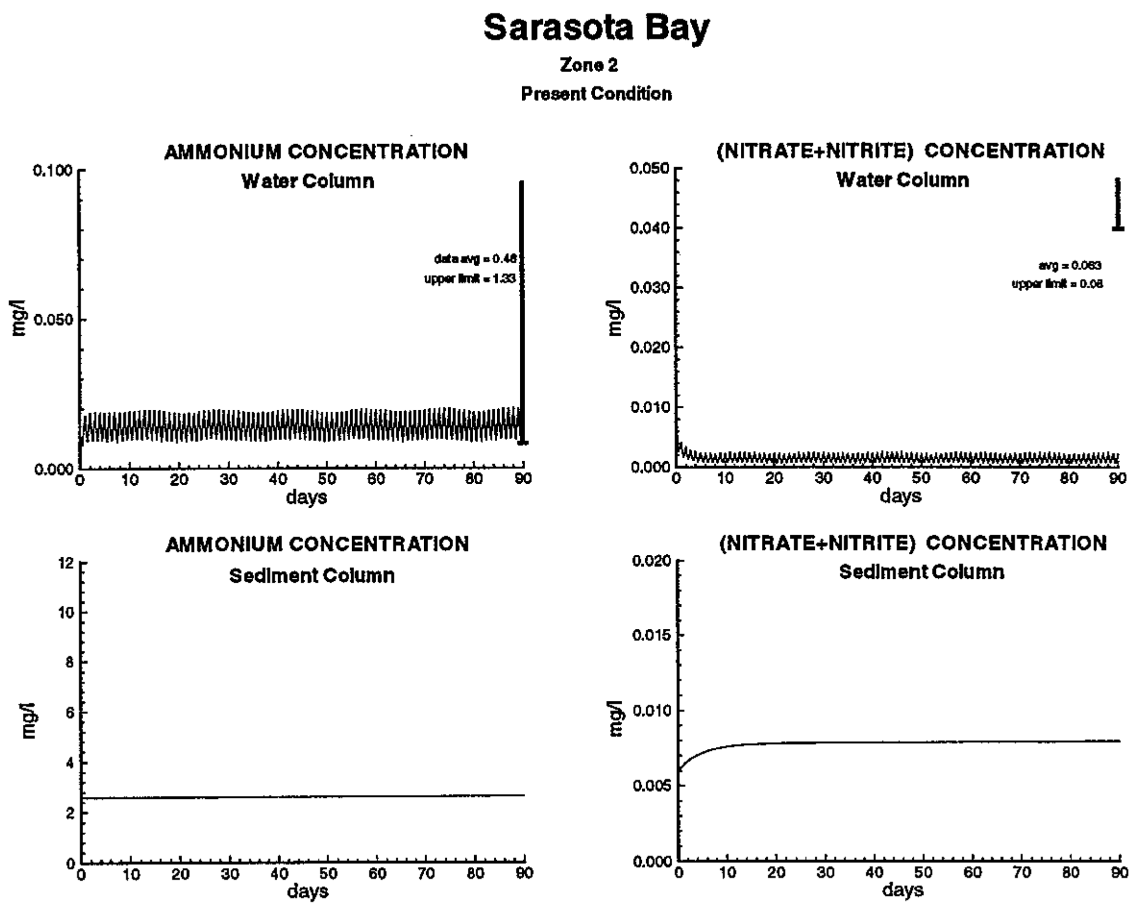

Figure 29. Simulated zone-averaged Ammonia-N and (Nitrate+Nitrite)-N in water and sediment columns in Sarasota Bay during the 90 day simulation with present land use condition.

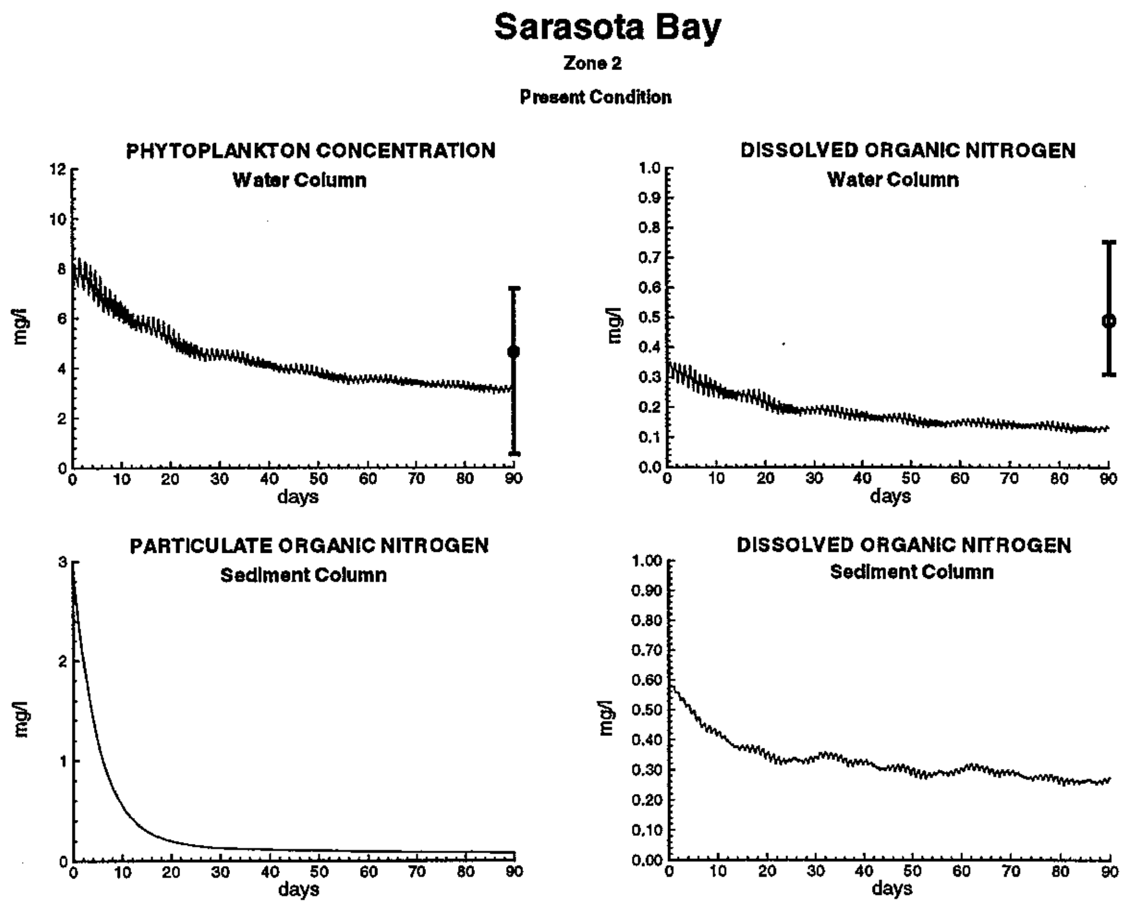

Figure 30. Simulated zone-averaged phytoplankton and DON concentrations in water and sediment columns in Sarasota Bay during the 90 day simulation with present land use condition.

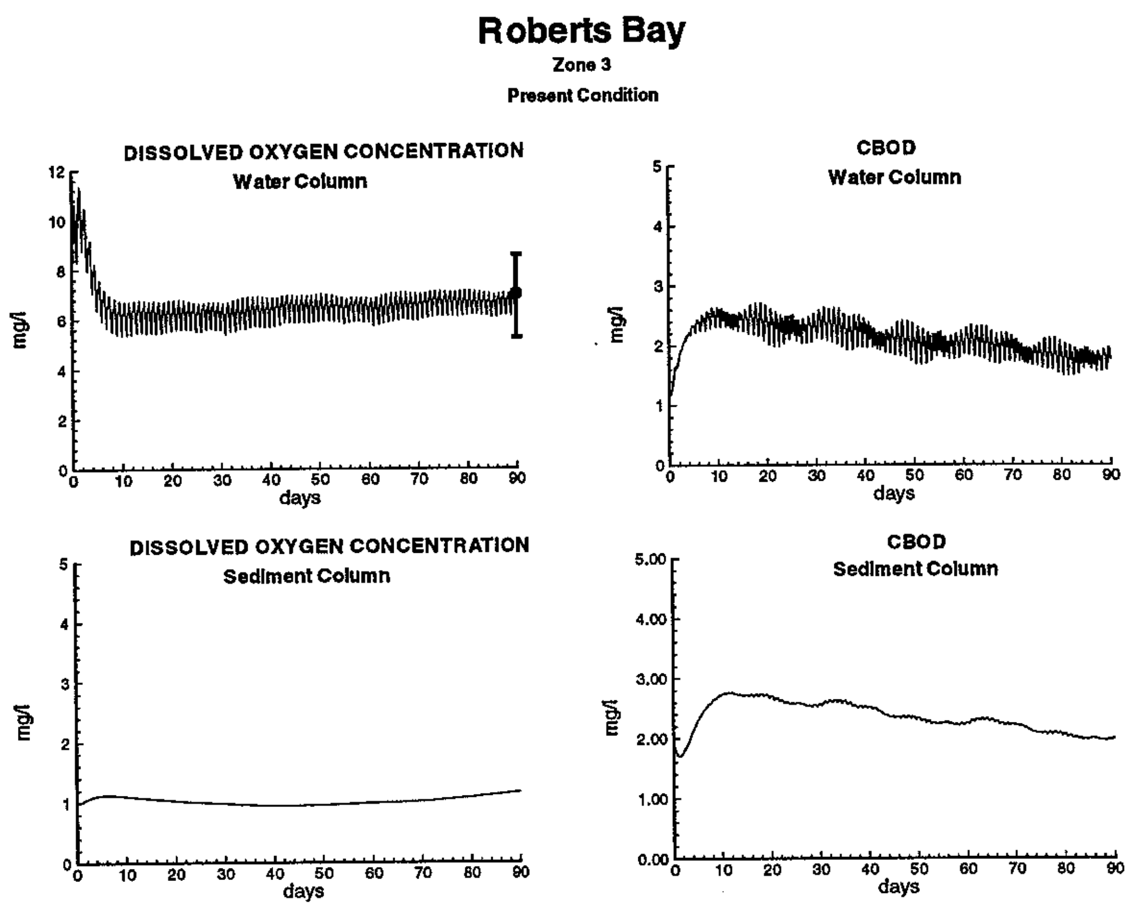

Figure 31. Simulated zone-averaged DO and CBOD concentrations in water and sediment columns in Roberts Bay during the 90 day simulation with present land use condition.

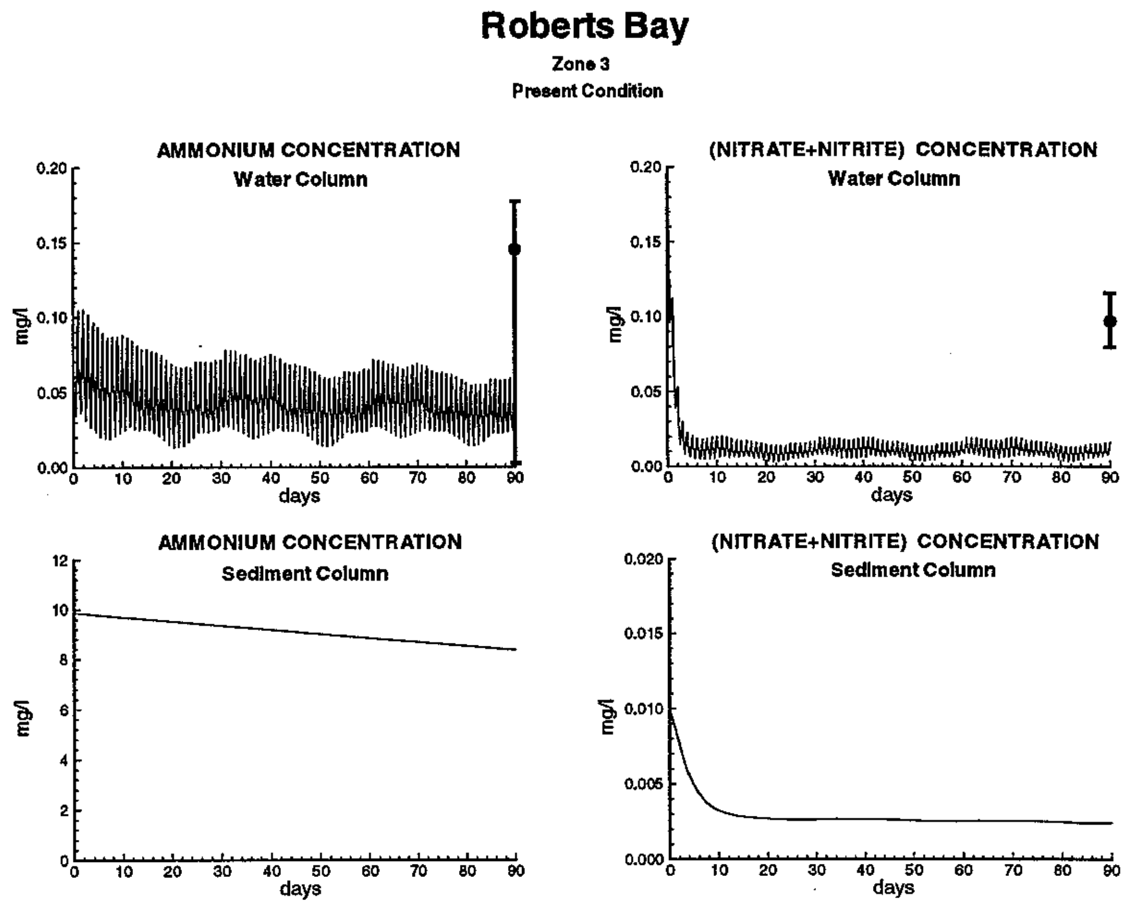

Figure 32. Simulated zone-averaged Ammonia-N and (Nitrate+Nitrite)-N concentrations in water and sediment columns in Roberts Bay during the 90 day simulation with present land use condition.

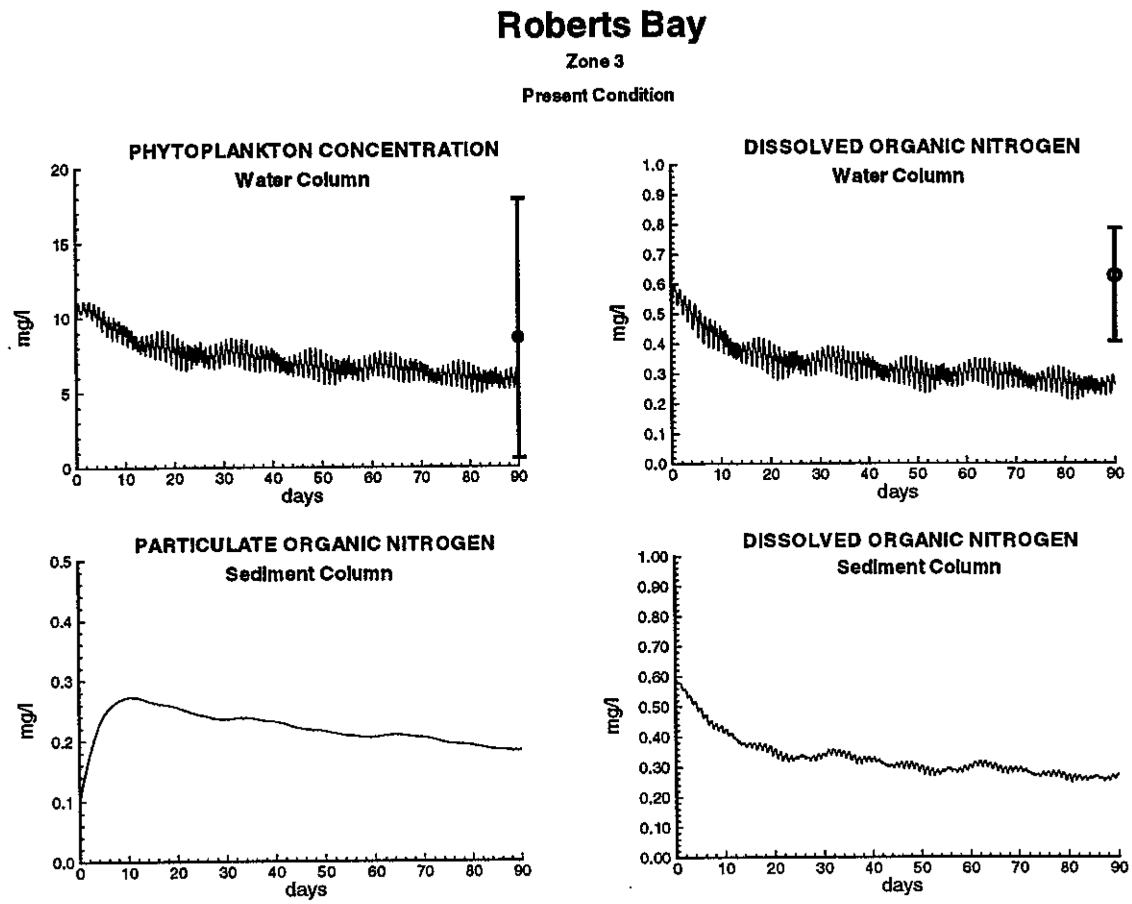

Figure 33. Simulated zone-averaged phytoplankton and DON concentrations in water and sediment columns in Roberts Bay during the 90 day simulation with present land use condition.

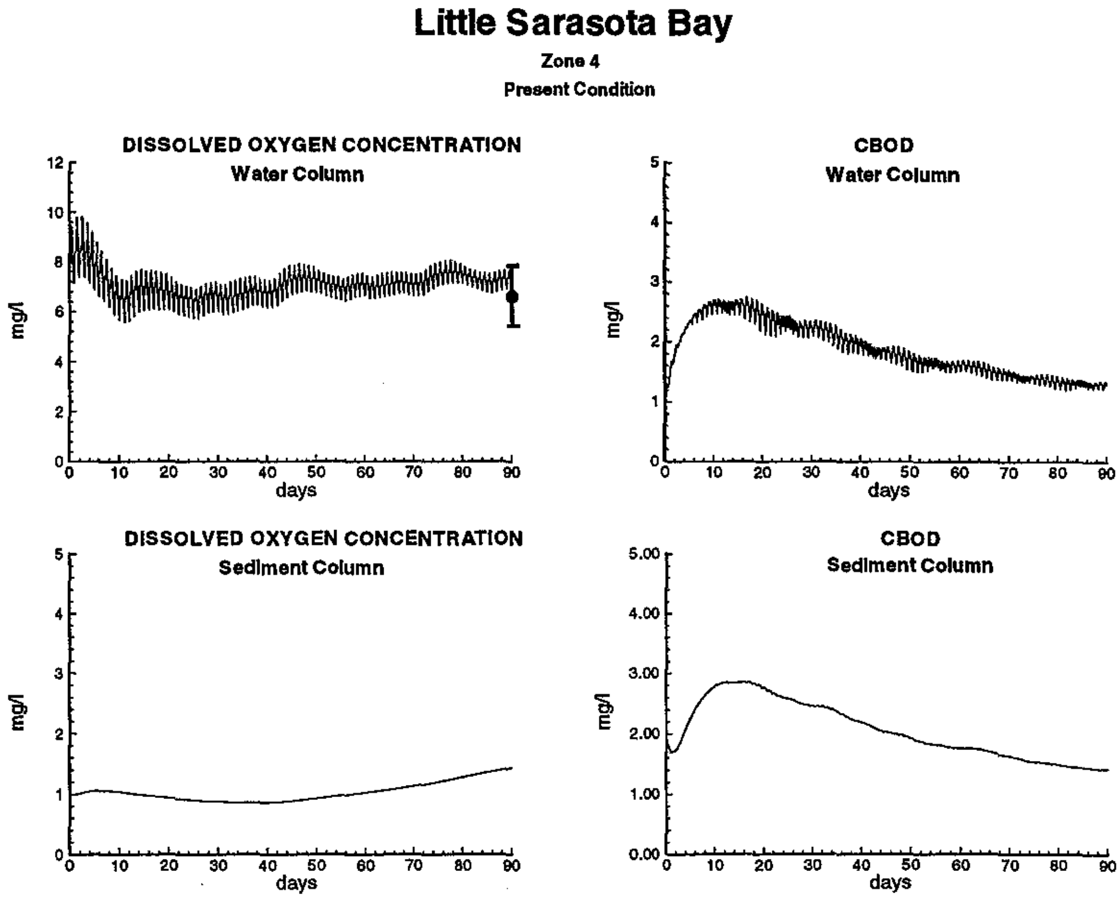

Figure 34. Simulated zone-averaged DO and CBOD concentrations in water and sediment columns in Little Sarasota Bay during the 90 day simulation with present land use condition.

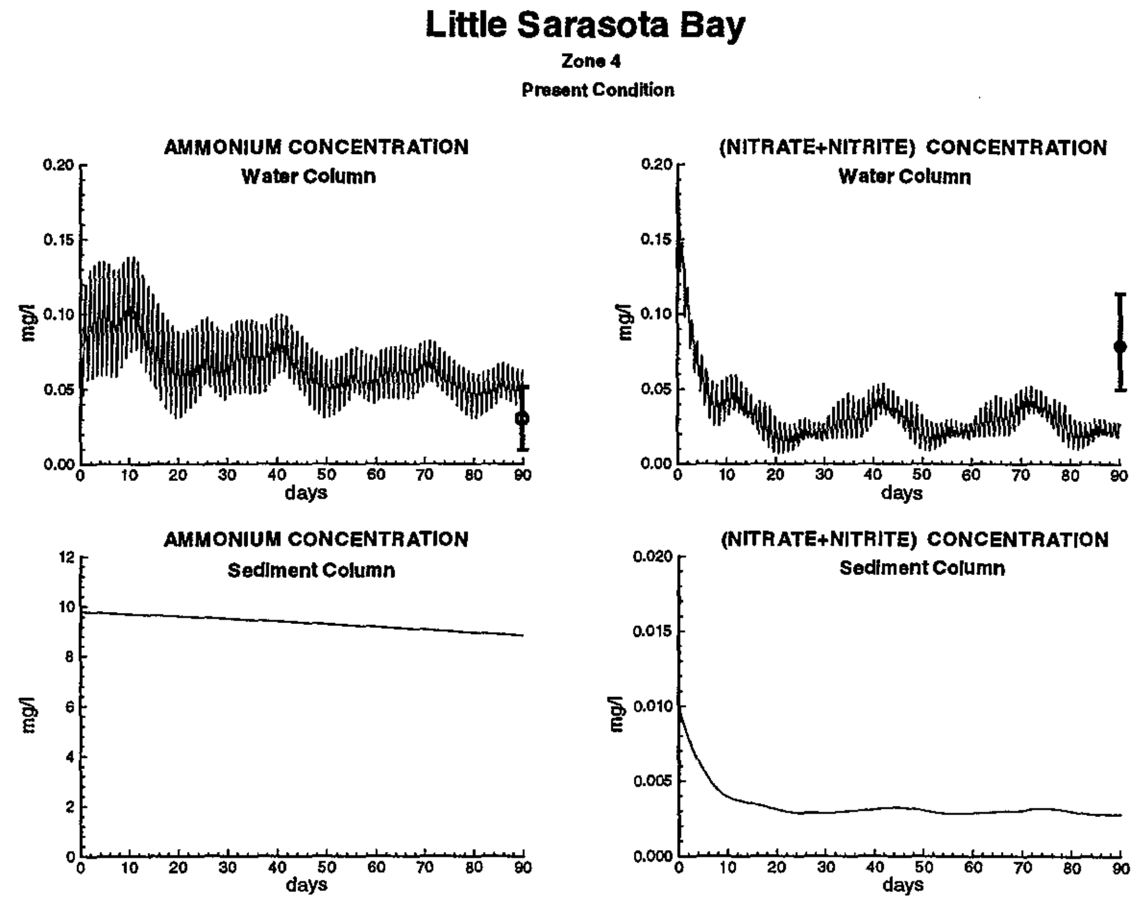

Figure 35. Simulated zone-averaged Ammonia-N and (Nitrate+Nitrite)-N concentrations in water and sediment columns in Little Sarasota Bay during the 90 day simulation with present land use condition.

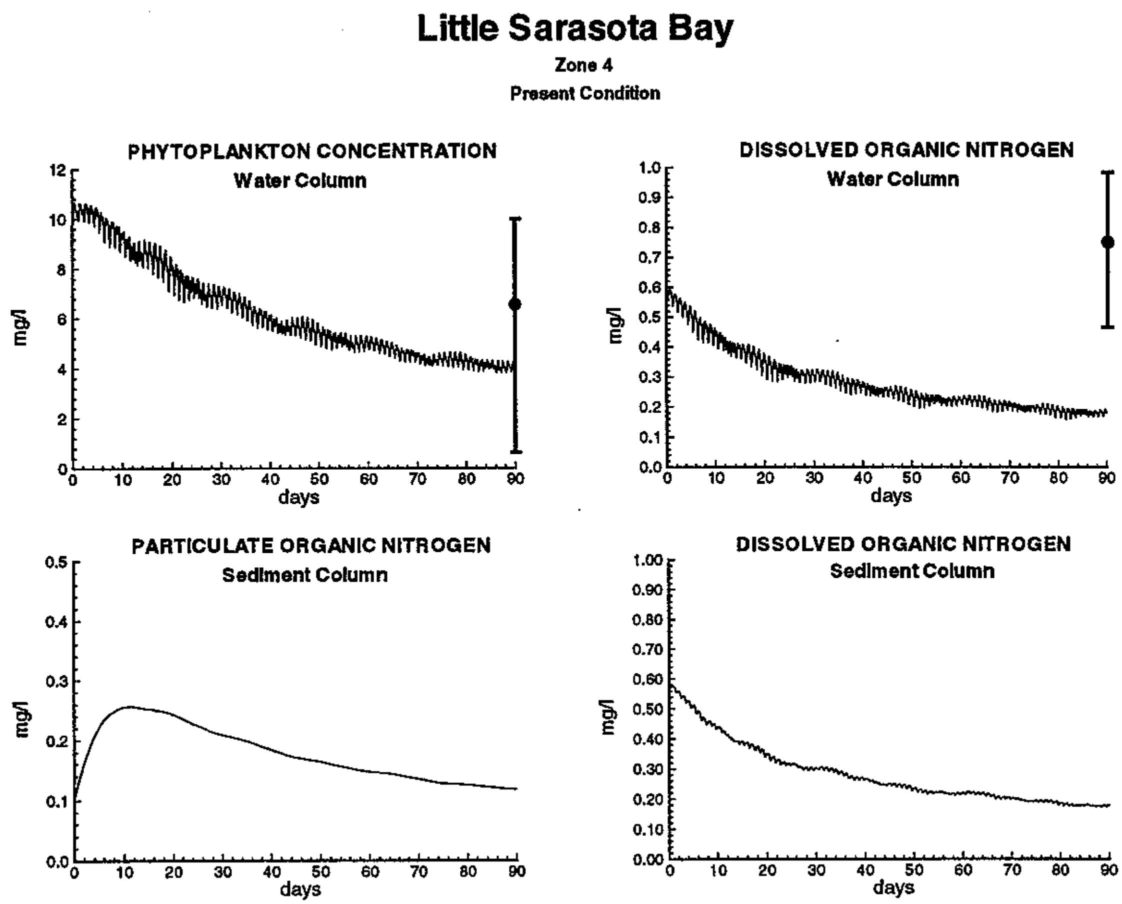

Figure 36. Simulated zone-averaged phytoplankton and DON concentrations in water and sediment columns in Little Sarasota Bay during the 90 day simulation with present land use condition.

4.2.2. Future Condition

We considered the following two scenarios of load reduction: i)a 31% reduction in the nutrient loading from Phillippi Creek, and ii)a 100% reduction in nutrient loading from Phillippi Creek. Boundary conditions for the case of 31% load reduction are shown in Chapter 2. Initial conditions for the water quality model simulation with future land use condition are given by the zone-averaged water quality concentrations obtained by the 90 day simulation with present land use condition.

Results for the case with 31% reduction in nutrient loading are shown in Figures 37, 38, and 39 for Sarasota Bay, Figures 40, 41, and 42 for Roberts Bay, Figures 43, 44, and 45 for Little Sarasota Bay. Most of the water quality parameters have reached a new equilibrium at the end of the 90 day simulation. As can be seen from these figures, load reduction has led to some noticeable improvements in Roberts Bay area: a slight increase in water column DO, a noticeable reduction in water column CBOD, a slight reduction in water column Ammonia-N, a slight increase in water column Nitrate+Nitrite, a slight decrease in sediment column Ammonia, a slight decrease in water column phytoplankton and dissolved organic nitrogen. The effects of load reduction are less discernable in Little Sarasota Bay and Big Sarasota Bay. The simulated impact of reduced loading appears to be reasonable: the slight increase in DO concentration leads to enhanced nitrification and increased nitrate and nitrite but decreased ammonia, the decrease in phytoplankton should lead to increase in available light and slightly increased seagrass.

To further examine the extent of the region being influenced by nutrient load reduction, we compare the model results at various stations in Sarasota Bay, Roberts Bay, Little Sarasota Bay and Roberts Bay obtained with load reduction of 31% and 100%. The locations of these stations are shown in Figure 46.

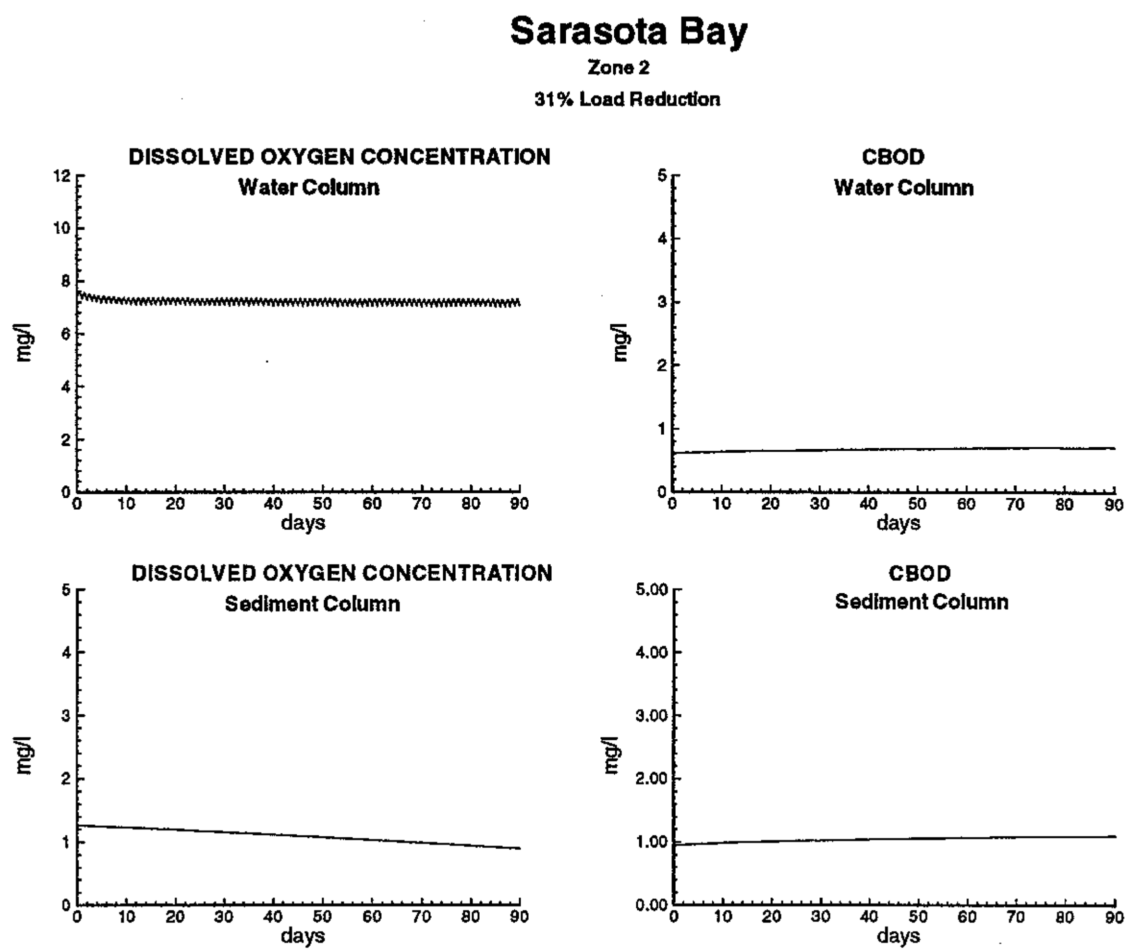

Figure 37. Simulated zone-averaged CBOD and DO concentrations in Sarasota Bay during the 90 day simulation with 31% reduction in nutrient loading.

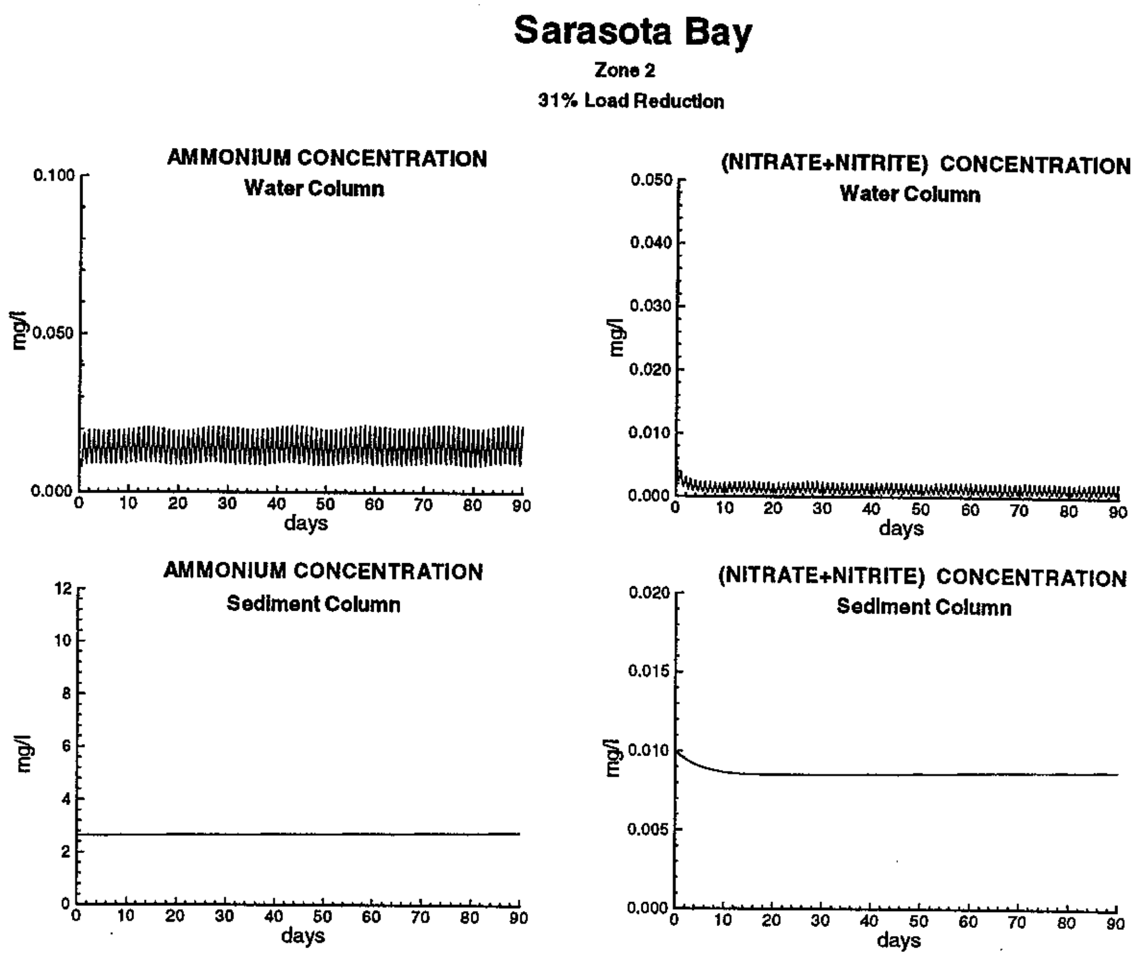

Figure 38. Simulated zone-averaged Ammonia-N and (Nitrate+Nitrite)-N concentrations in Sarasota Bay during the 90 day simulation with future land use condition.

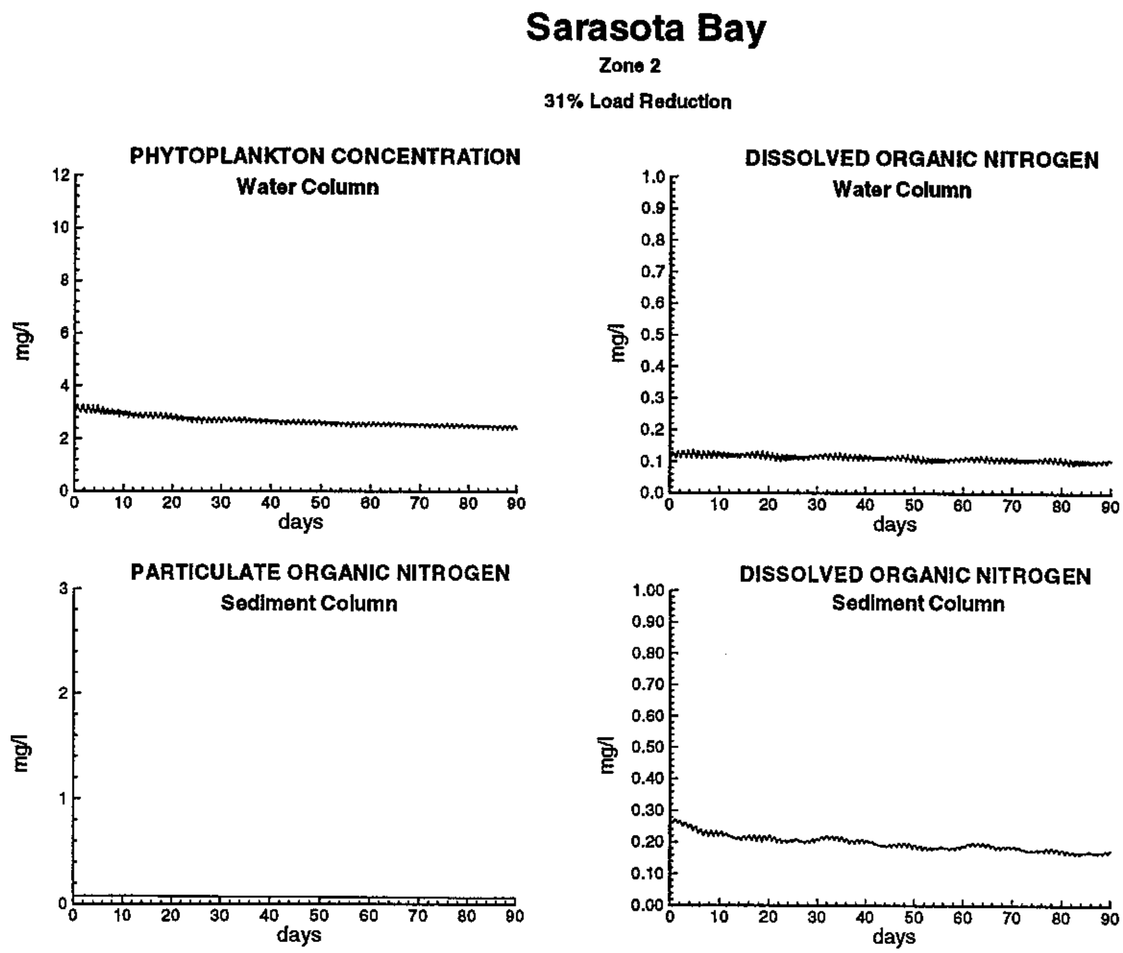

Figure 39. Simulated zone-averaged phytoplankton and DON concentrations in Sarasota Bay during the 90 day simulation with future land use condition.

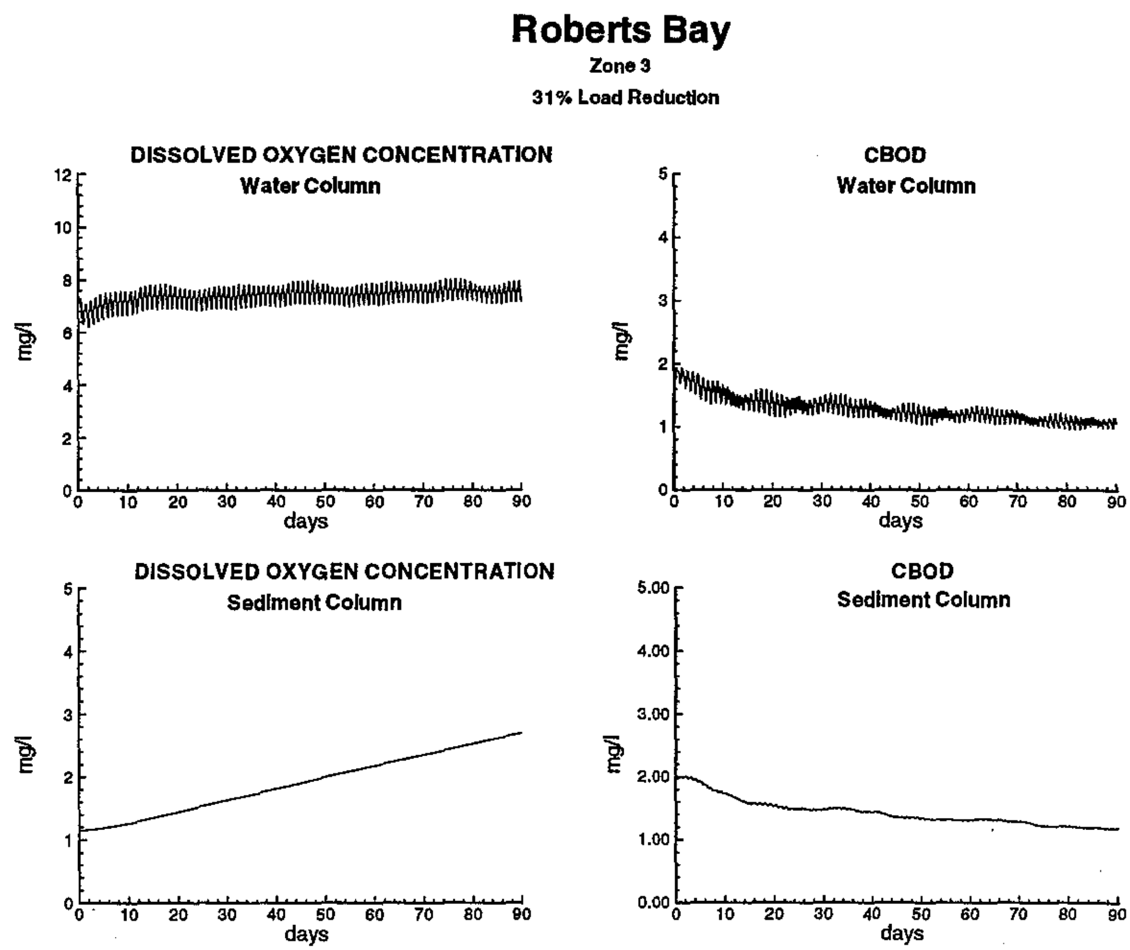

Figure 40. Simulated zone-averaged CBOD and DO concentrations in Roberts Bay during the 90 simulation with future land use condition.

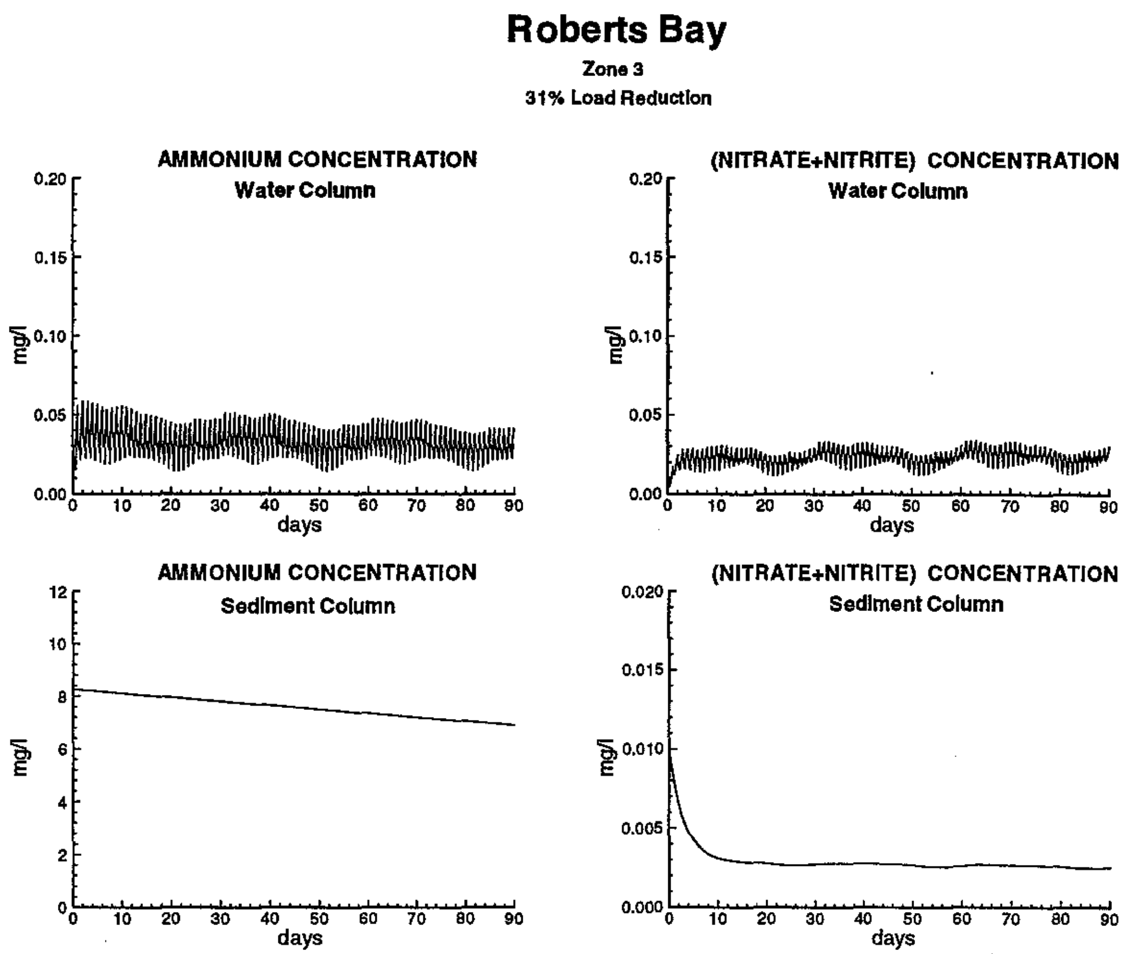

Figure 41. Simulated zone-averaged Ammonia-N and (Nitrate+Nitrite)-N concentrations in Roberts Bay during the 90 simulation with future load condition.

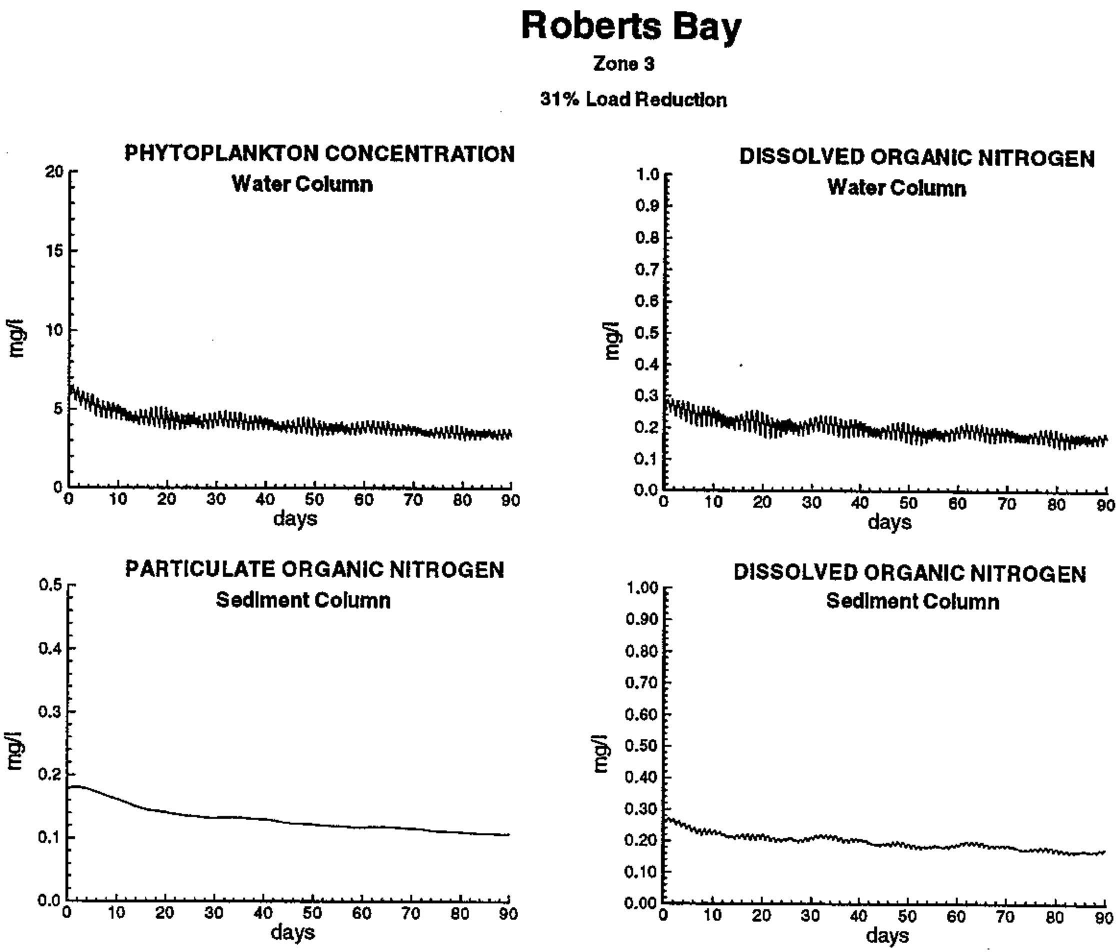

Figure 42. Simulated zone-averaged phytoplankton and DON concentrations in Roberts Bay during the 90 simulation with future land use condition.

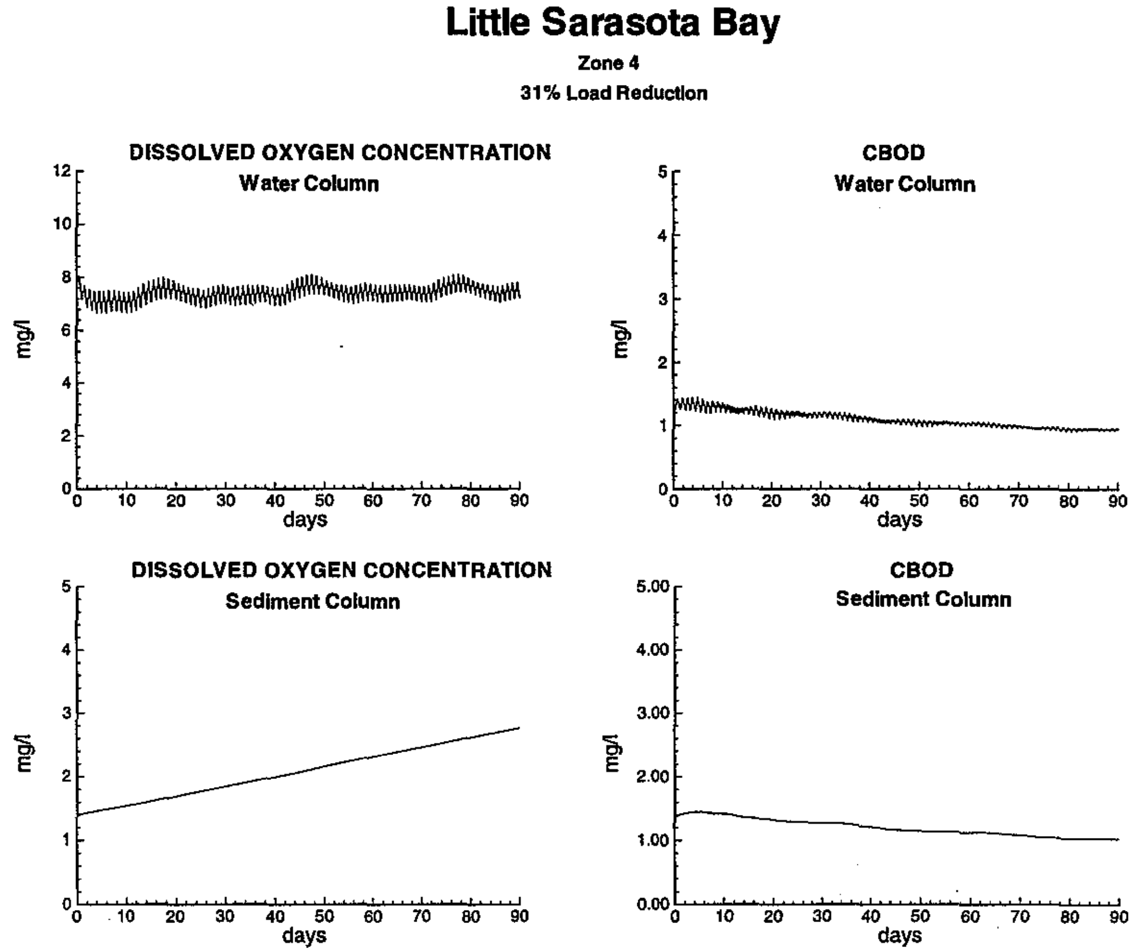

Figure 43. Simulated zone-averaged CBOD and DO concentrations in Little Sarasota Bay during the 90 day simulation with future land use condition.

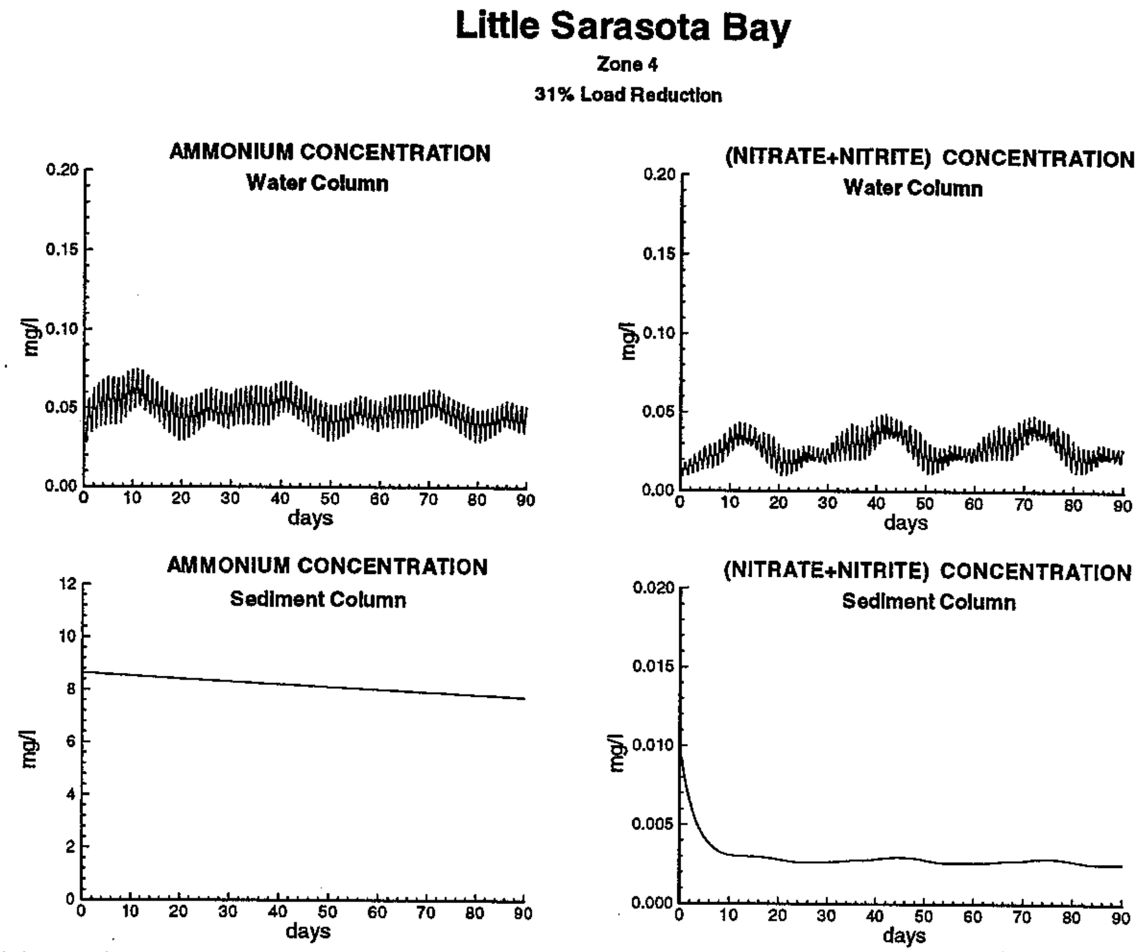

Figure 44. Simulated zone-averaged Ammonia-N and (Nitrate+Nitrite)-N concentrations in Little Sarasota Bay during the 90 simulation with future land use condition.

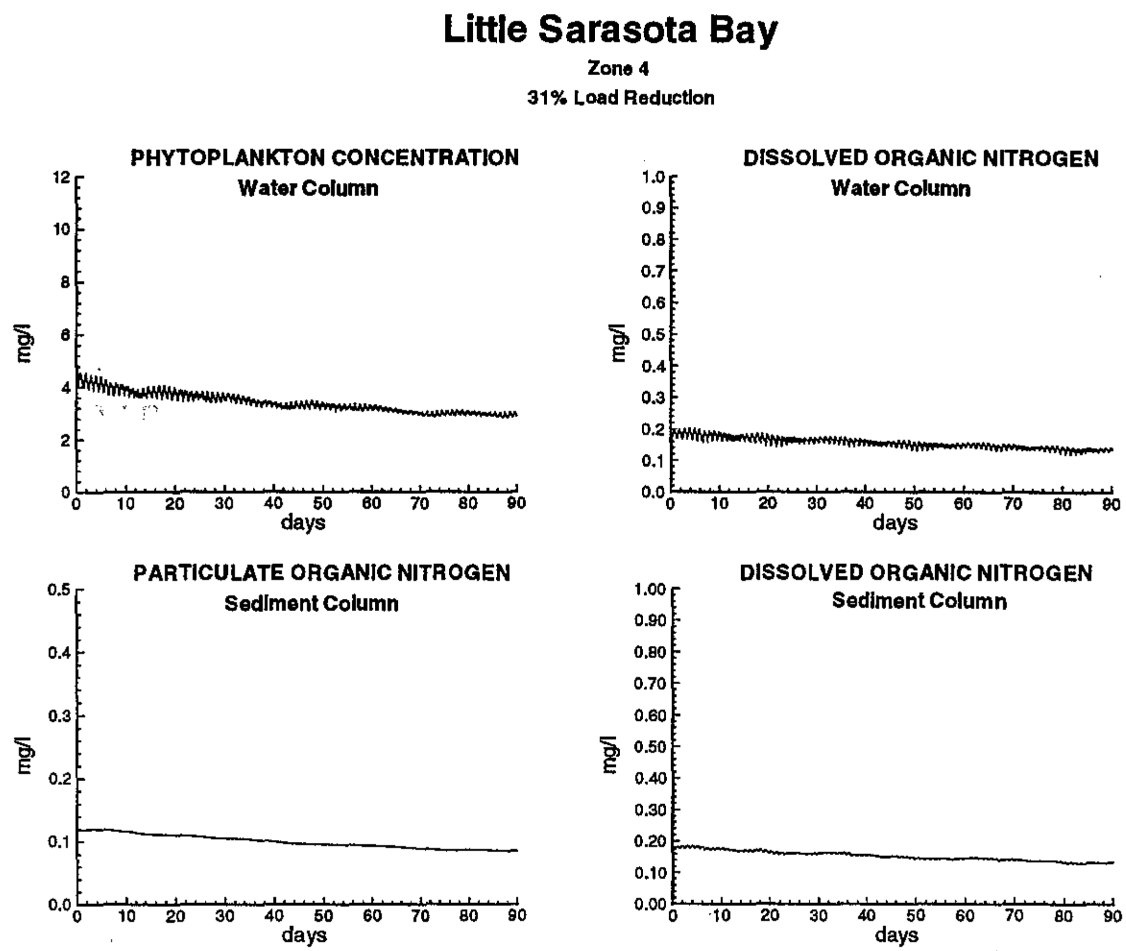

Figure 45. Simulated zone-averaged phytoplankton and DON concentrations in Little Sarasota Bay during the 90 day simulation with future land use condition.

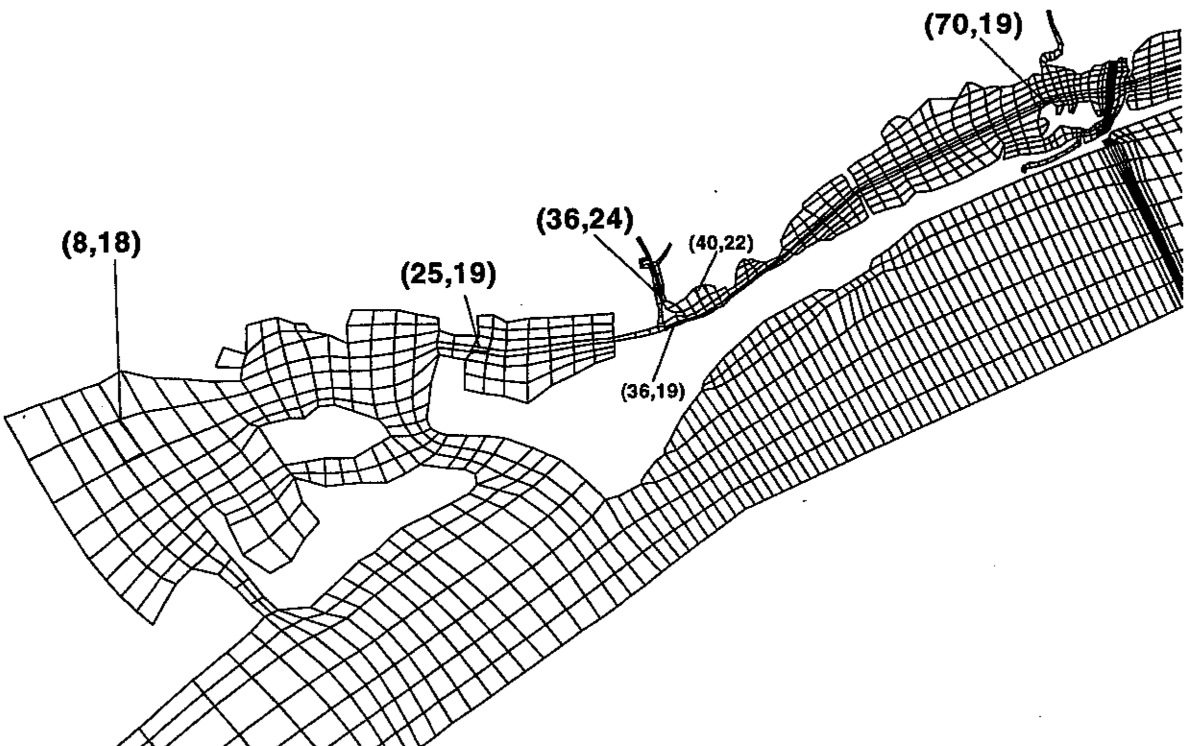

Figure 46. Locations of stations in the study area for examination of region of influence due to nutrient load reduction.

At each of the stations, for comparison purposes, we will compare the model results of phytoplankton, DO, daily maximum ammonia, and nitrate+nitrite due to 31% and 100% load reductions. At the Sarasota Bay station where the grid indices (I,J)=(8,18), as shown in Figure 47, model results for 31% and 100% load reductions are nearly identical, suggesting that load reduction has practically no influence there. As shown in Figure 48, at the Roberts Bay station where (I,J) = (25,19), phytoplankton and daily maximum ammonia clearly reduced as the nutrient loading reduction went from 31% to 100%, while DO and nitrate+nitrite changed slightly. This same trend is more apparent in Figures 49 and 50 for two other Roberts Bay stations near Phillippi Creek where (I,J) = (36,19) and (I,J) = (36,24) when load reduction increased from 31% to 100%. At the southern Roberts Bay station where (I,J) = (40,22), the effect of load reduction is also quite apparent as shown in Figure 51. In the Little Sarasota Bay station near the Midnight Pass where (I,J) = (70,19), as shown in Figure 52, the effect of load reduction is negligible. It is interesting to note, however, as nutrient load reduction is increased from 31% to 100%, DO concentration actually decreases slightly. The model results show that, as the nutrient load reduction increases from 31% to 100%, phytoplankton which is the source for DO decreases appreciably, while CBOD which is the sink for DO decreases very slightly. This result, howver, could change if the model runs were carried out much longer as CBOD depends on such process as decomposition of organic nitrogen which takes place very slowly.

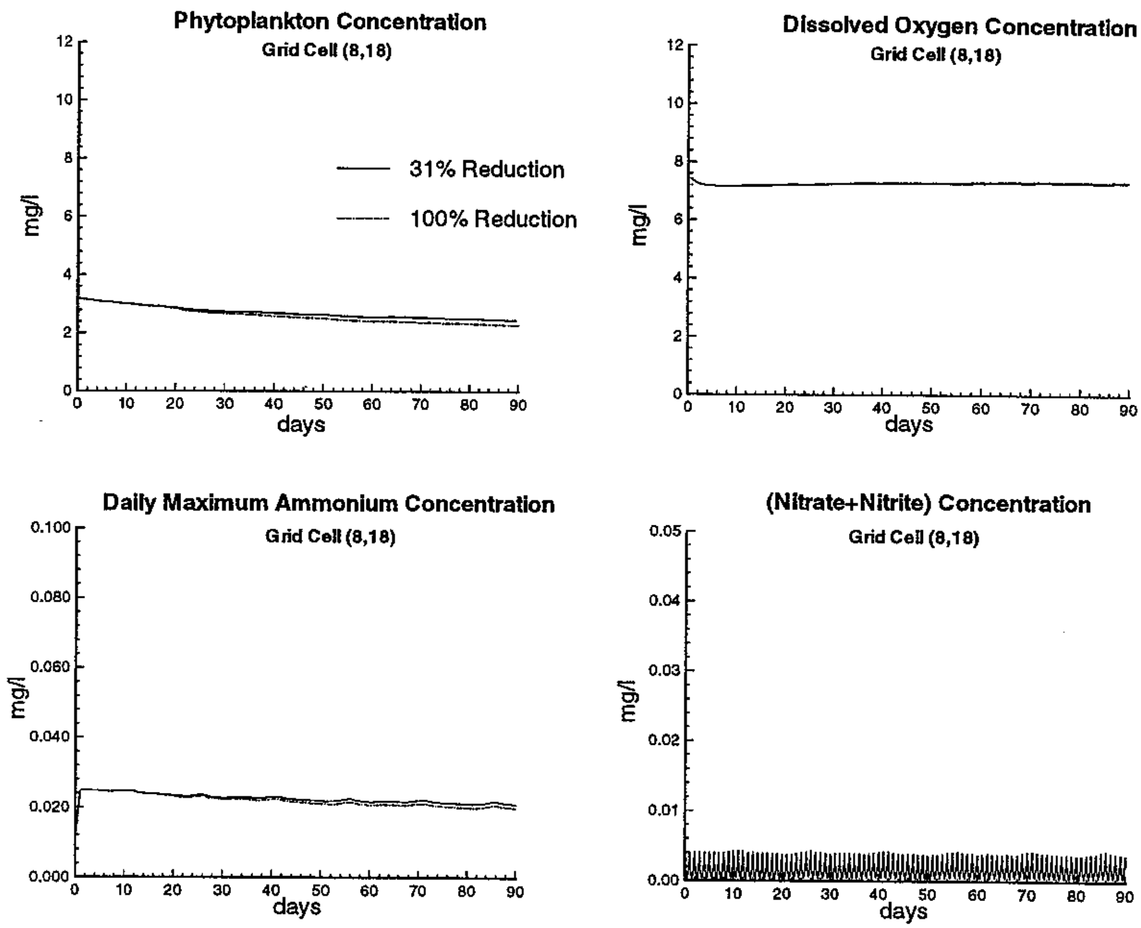

Figure 47. Simulated concentrations of phytoplankton, DO, daily maximum ammonia, and nitrate+nitrite at a Sarasota Bay station due to 31% and 100% nutrient load reduction.

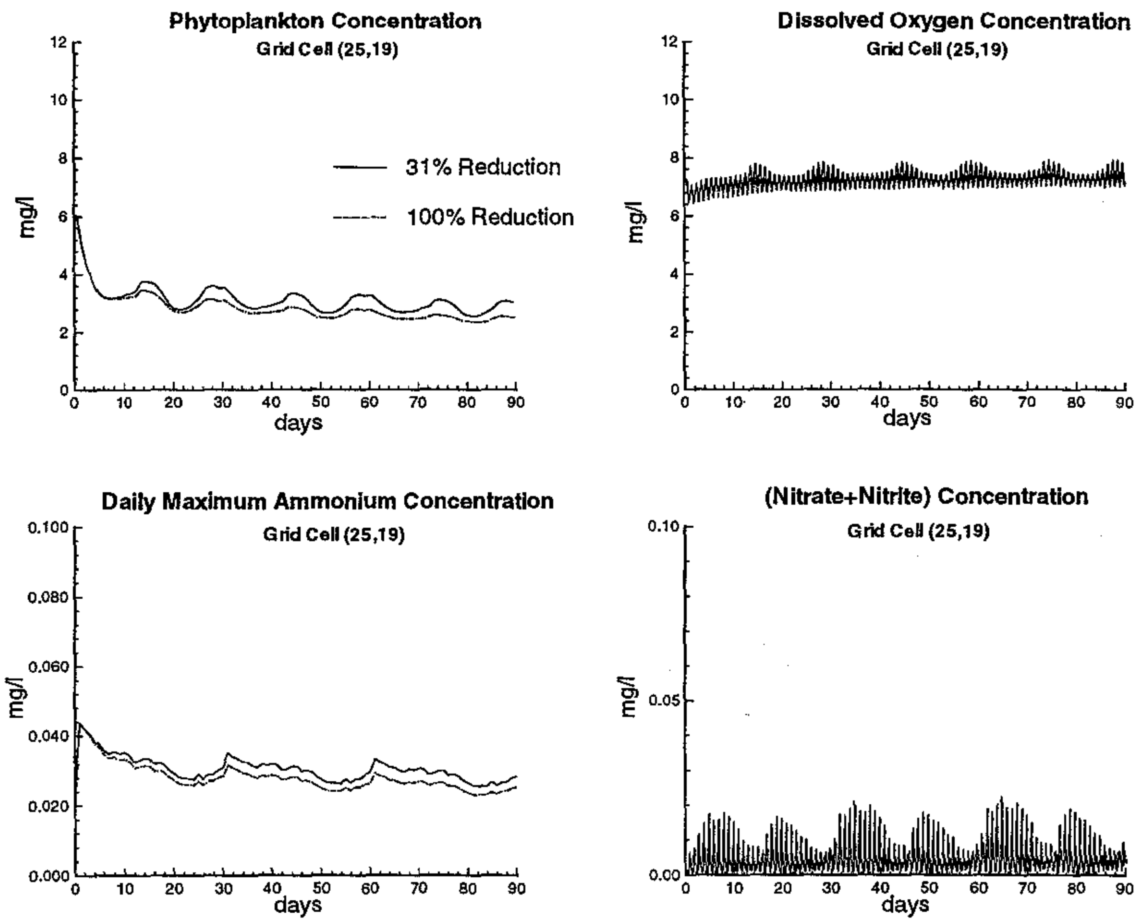

Figure 48. Simulated concentrations of phytoplankton, DO, daily maximum ammonia, and nitrate+nitrite at a Roberts Bay station (I,J)=(25,19) due to 31% and 100% nutrient load reductions.

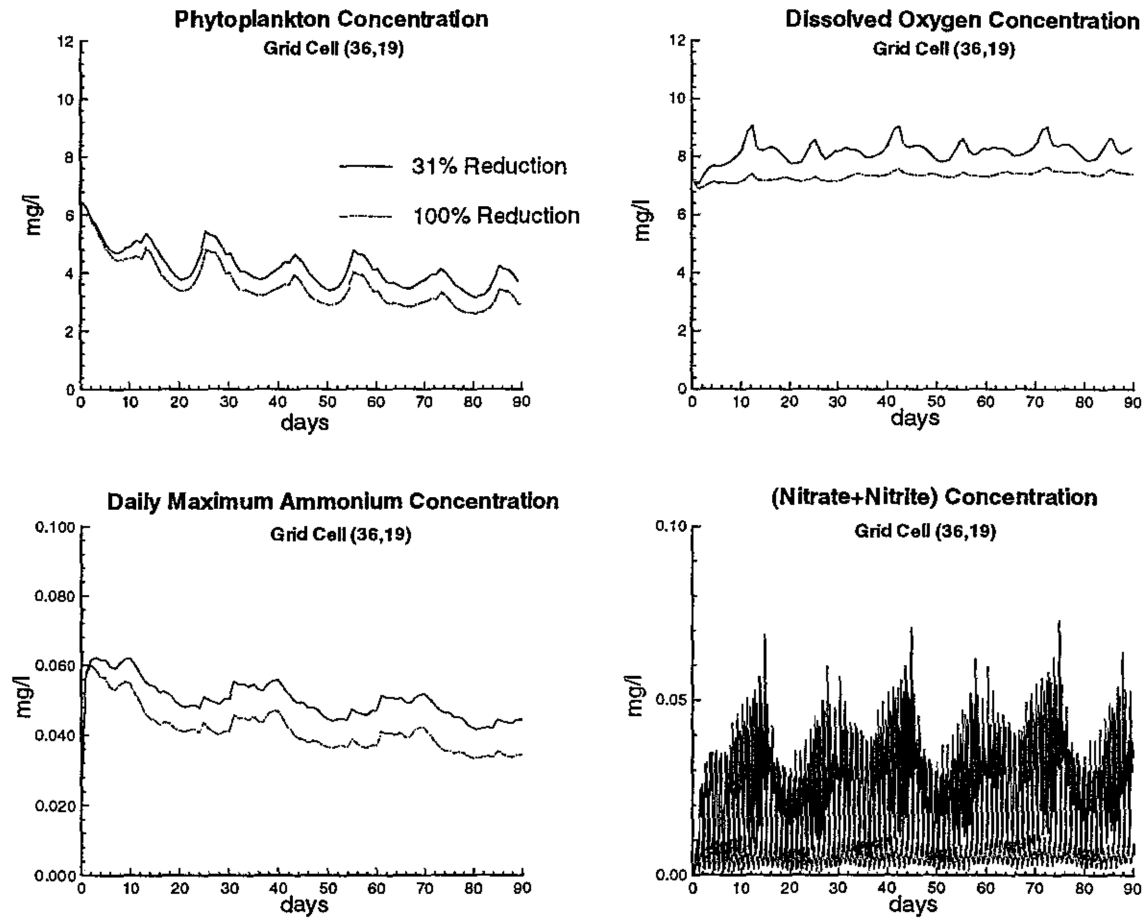

Figure 49. Simulated concentrations of phytoplankton, DO, daily maximum ammonia and mitrate+nitrite at a Roberts Bay station (I,J)=(36,19) due to 31% and 100% load reductions.

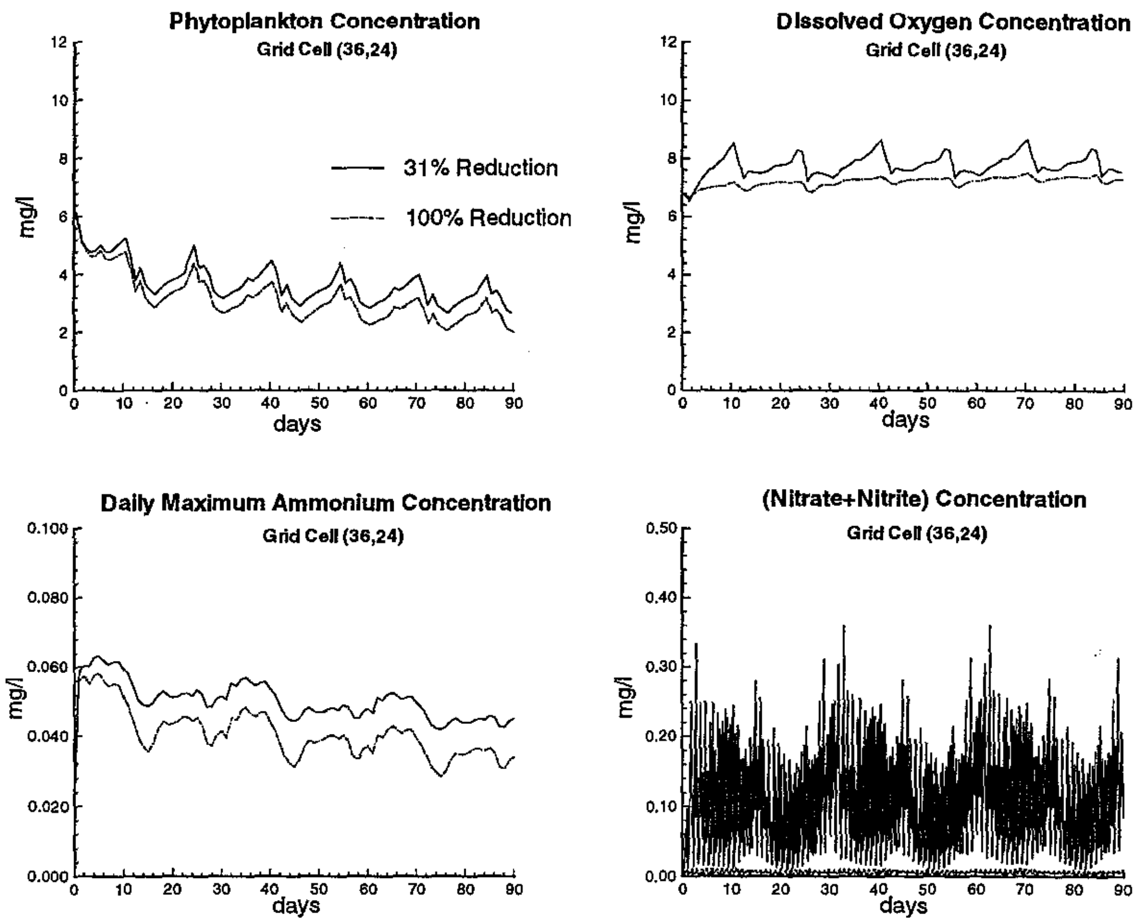

Figure 50. Simulated concentrations of phytoplankton, DO, daily maximum ammonia, and nitrate+nitrite at a Roberts Bay station where (I,J)=(36,24) due to 31% and 100% nutrient load reductions.

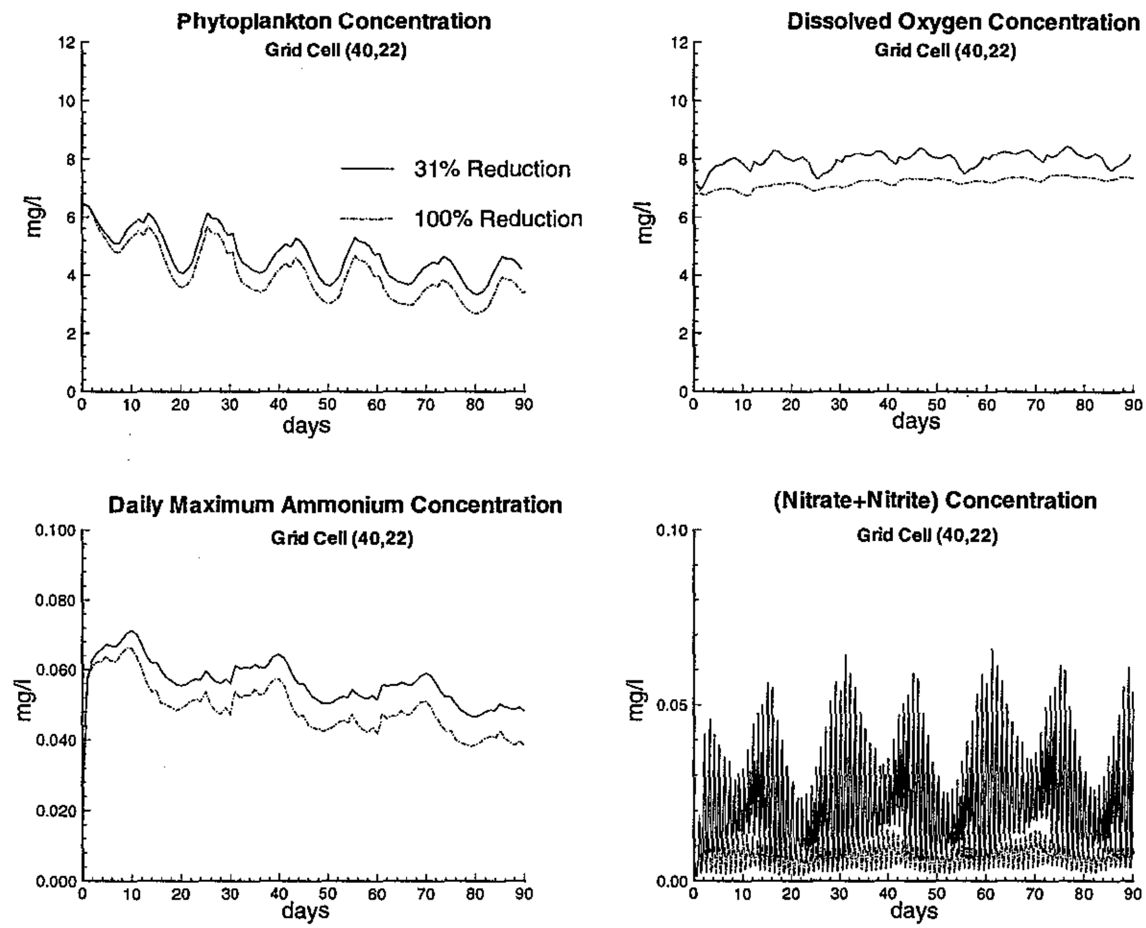

Figure 51. Simulated concentrations of phytoplankton, DO, daily maximum ammonia, and nitrate+nitrite at a Roberts Bay station where (I,J)=(40,22) due to 31% and 100% nutrient load reductions.

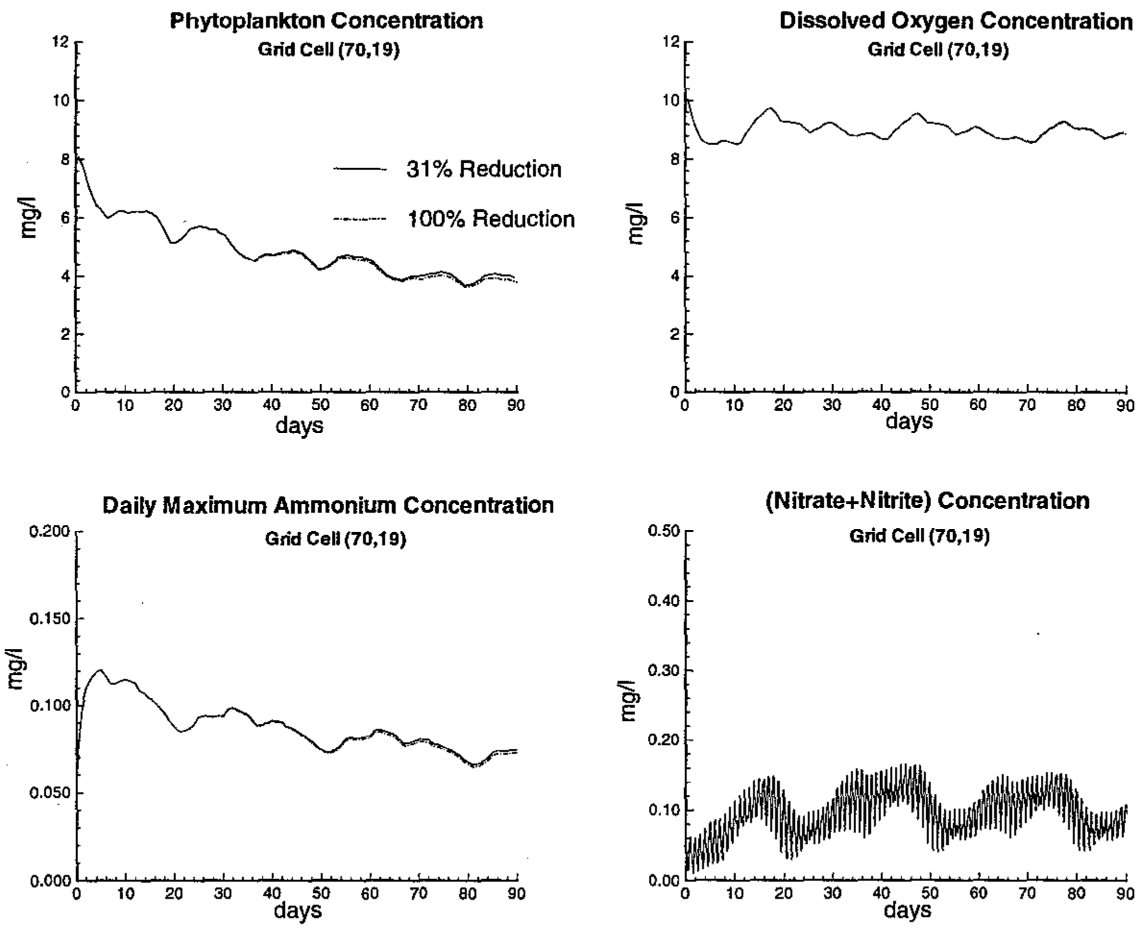

Figure 52. Simulated concentrations of phytoplankton, DO, daily maximum ammonia, and nitrate+nitrite at a Little Sarasota Bay station where (I,J)=(70,19) due to 31% and 100% nutrient load reductions.

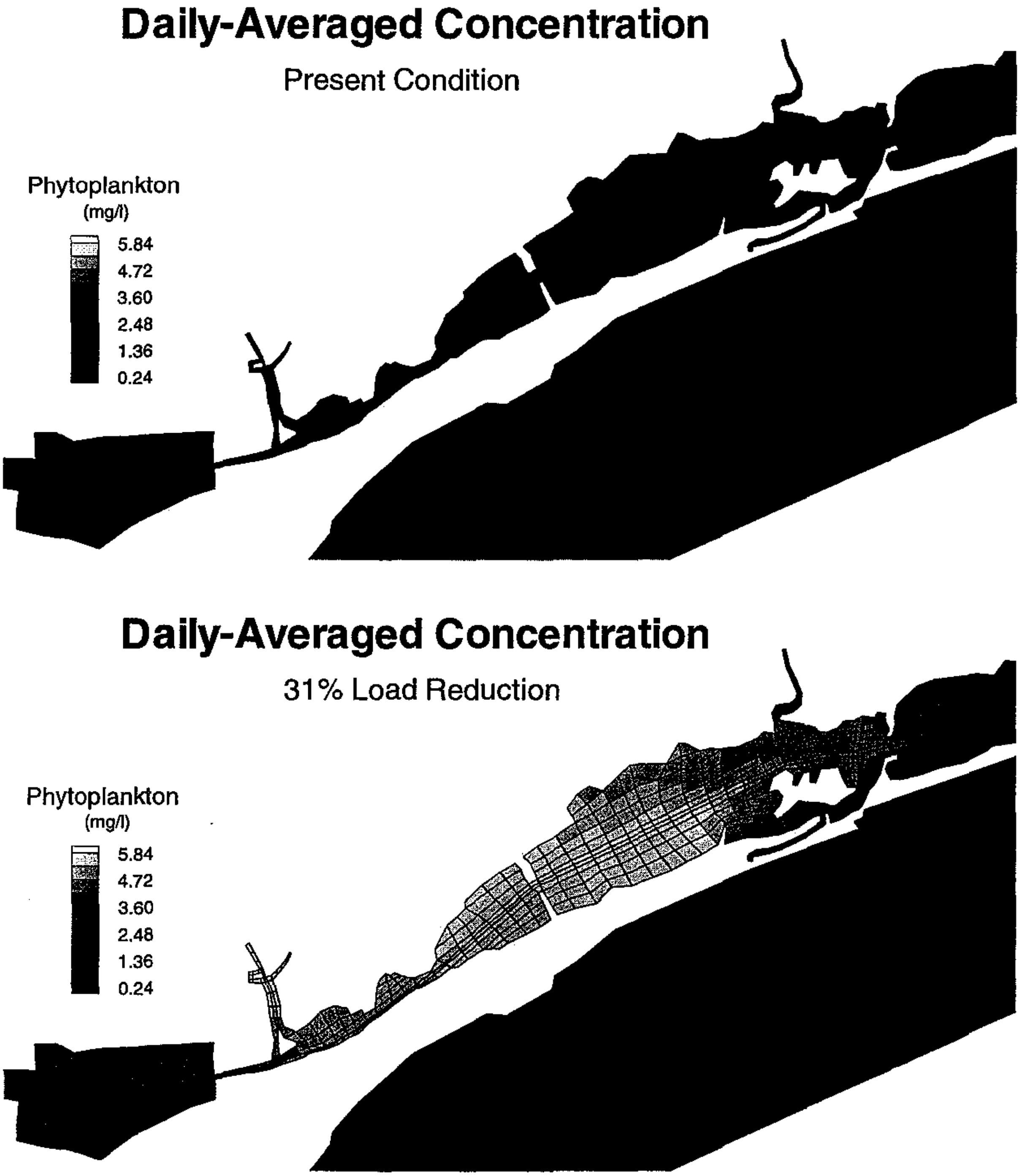

Figure 53. Simulated basin-wide phytoplankton concentrations on the last day of 90-day simulations with present and future land use conditions.

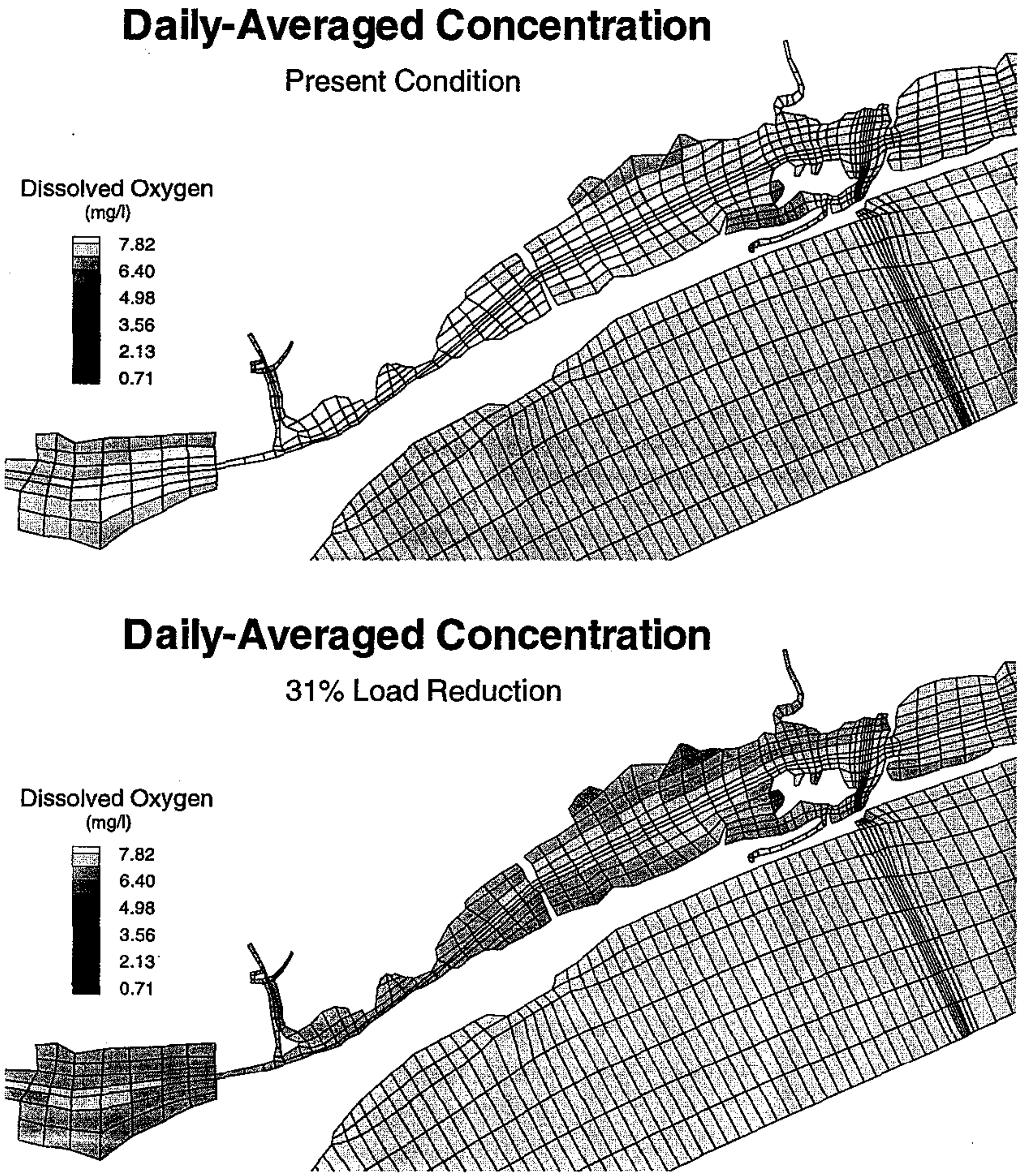

Figure 54. Simulated basin-wide DO concentrations in the study area at the end of 90 day simulations with present and future land use conditions.

4.3. Simulation of Seagrass and Light

As the results suggest in the previous section, nutrient load reduction is expected to lower the concentrations of water column phytoplankton, ammonia, and dissolved organic nitrogen, but increase the water column concentrations of DO, primarily in Roberts Bay. These changes are expected to increase the available light for seagrass and hence increase the seagrass biomass. As a first step, we run the coupled hydrodynamics-water quality-seagrass-light model for 90 days with the present land use condition. We then repeat the simulation with reduced nutrient loading corresponding to future land use condition.

4.3.1. Present Condition

To generate the seagrass distribution in the study area for the present land use condition, we started the seagrass model simulation with initial distributions of Thalassia and Halodule based on limited information from the *Framework for Action* report (SBNEP 1992) and from Tomasko (Private Communication 1995). Model results during a 90-day simulation showed that conditions of the study area are not favorable for Thalassia but more favorable for Halodule. As shown in Figure 55 for a Roberts Bay station where (I,J) = (36,24), the available light gradually increased while Thalassia continued to decrease. Halodule initially declined but continued to increase after the first 20 days. The temporal fluctuation in available light appears to be related to the spring-to-neap tidal fluctuations which affect the water depths that the light must penetrate before reaching the seagrass. The seagrass biomasses in the study area at the end of the 90 day simulation are shown in Figure 56. Significant spatial variation in Halodule biomass is found while Thalassia is mostly less than 2 gdw/m^2 over the entire area.

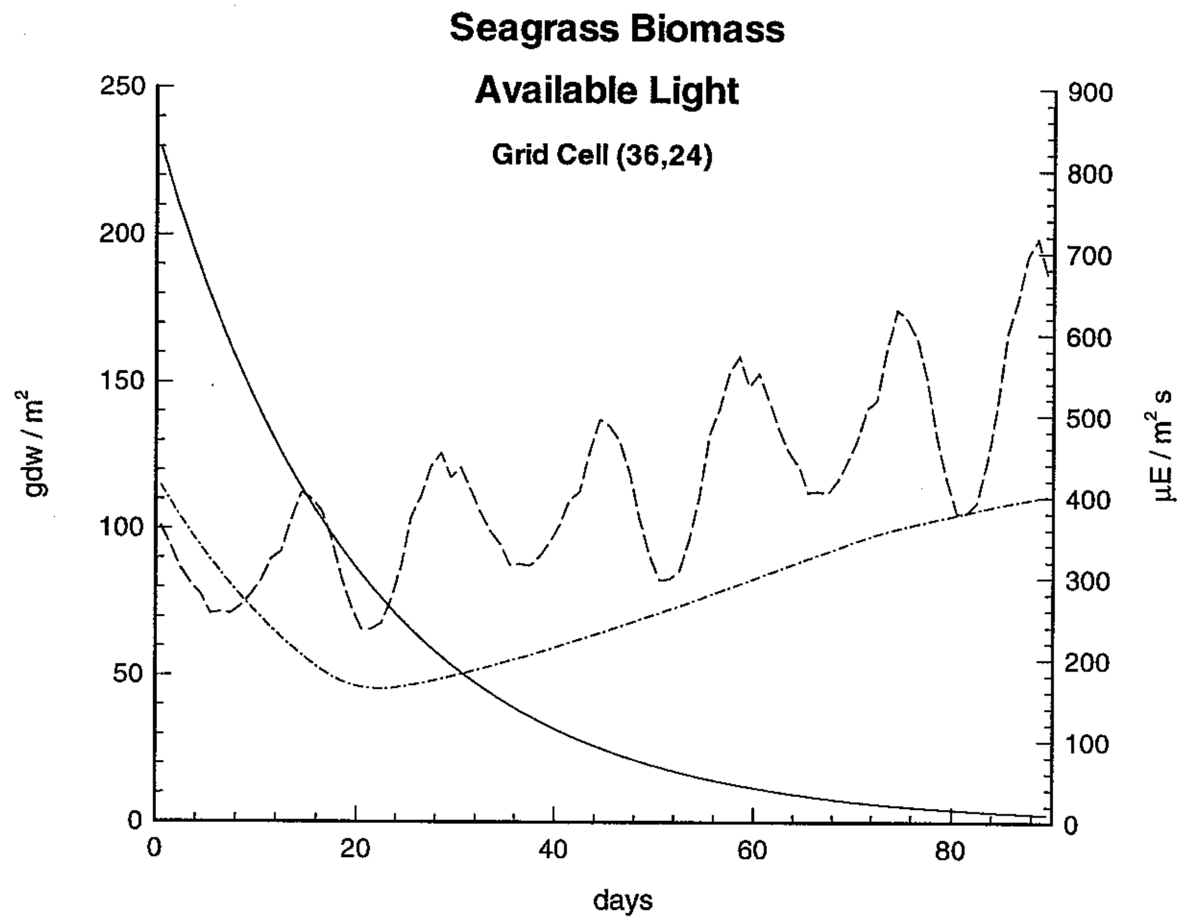

Figure 55. Simulated available light (dashed line) and seagrass biomass (solid line for Thalassia and broken line for Halodule) at a ROberts Bay station during the 90 day simulation with present land use condition.

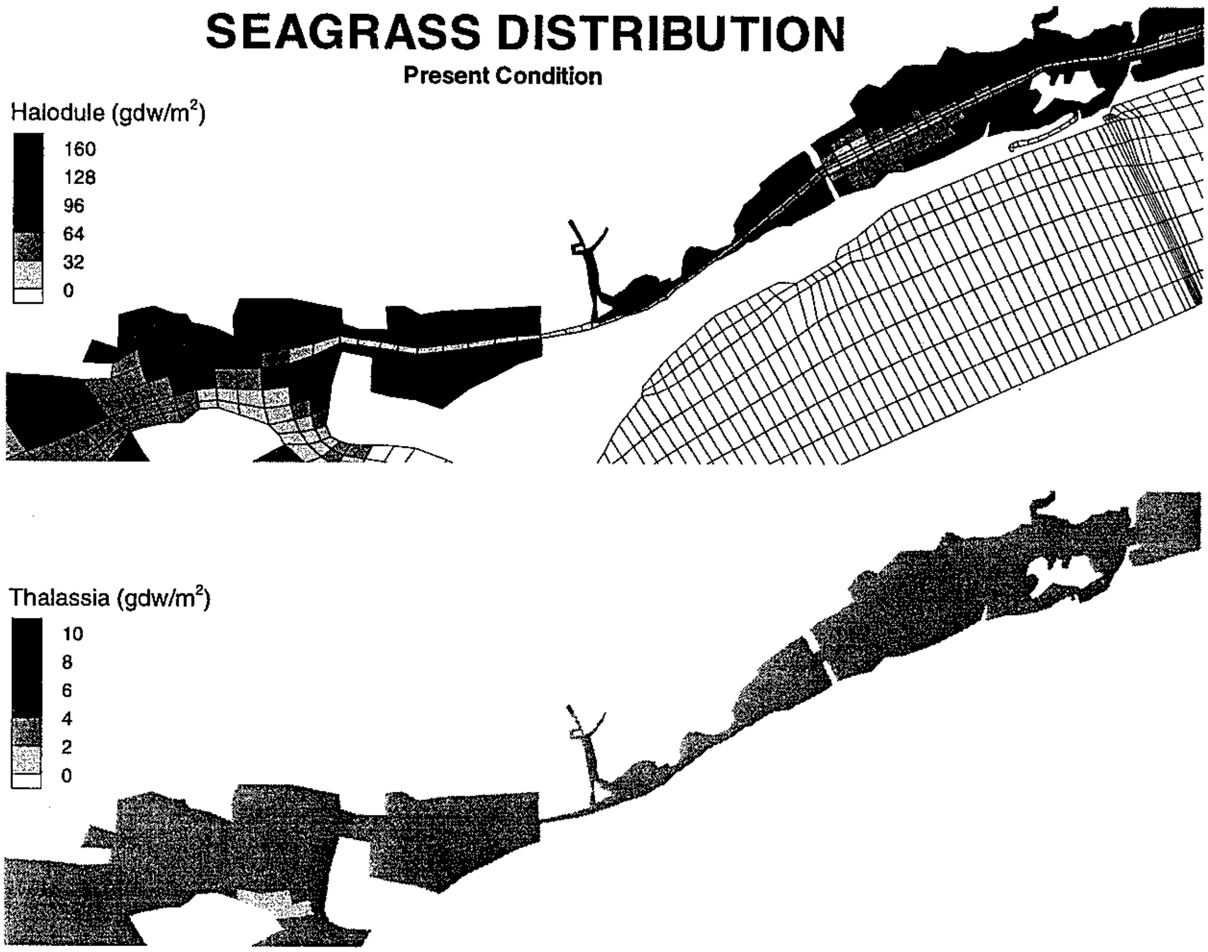

Figure 56. Simulated Halodule and Thalassia distribution in the study area at the end of a 90 day simulation with present land use condition.

4.3.2. Future Condition

As shown in the results for water quality parameters in the previous section, a 31% reduction in nitrogen loading does appear to lead to appreciable reduction in concentrations of CBOD, ammonia, DON, and phytoplankton, but increases in DO, in Roberts Bay. However, the effect of nutrient load reduction on available light is less significant since available light depends on phytoplankton, water color, turbidity and total suspended solids (TSS), which are mostly un-affected by the nutrient load reduction. Consequently the effect of nutrient load reduction on seagrass is not significant. Examination of the time-dependent model results at a Roberts Bay station near Phillippi Creek showed about 5% reduction in available light. As shown in Figure 57, the effect of 31% load reduction does produce some reduction in light attenuation coefficient. However, as shown in Figure 58, Halodule distributions in the study area showed little difference between the present condition and the future condition. The seagrass distribution, however, does appear to be well correlated with the available light distribution.

Of course, the model results presented here depend on the model formulation which presently cannot be sufficiently calibrated and validated due to the lack of field data. The precise manner in which light attenuation is affected by phytoplankton, water color, turbidity and TSS is site-specific and largely unknown for Roberts Bay and Sarasota Bay.

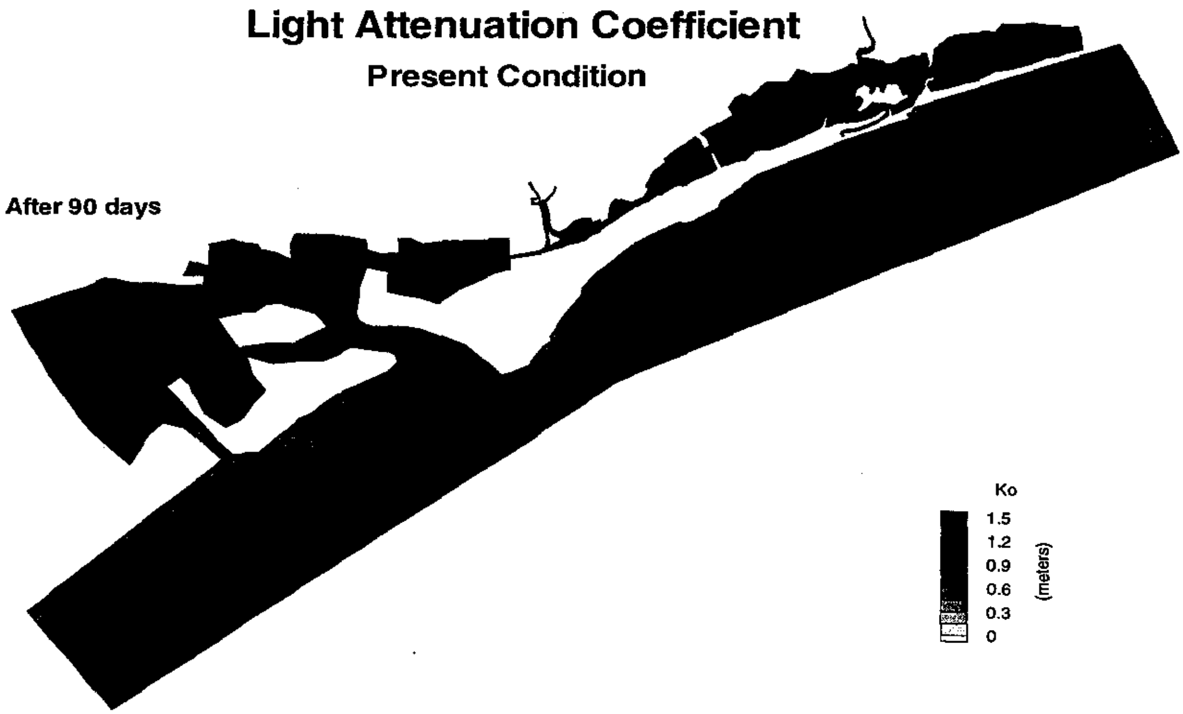

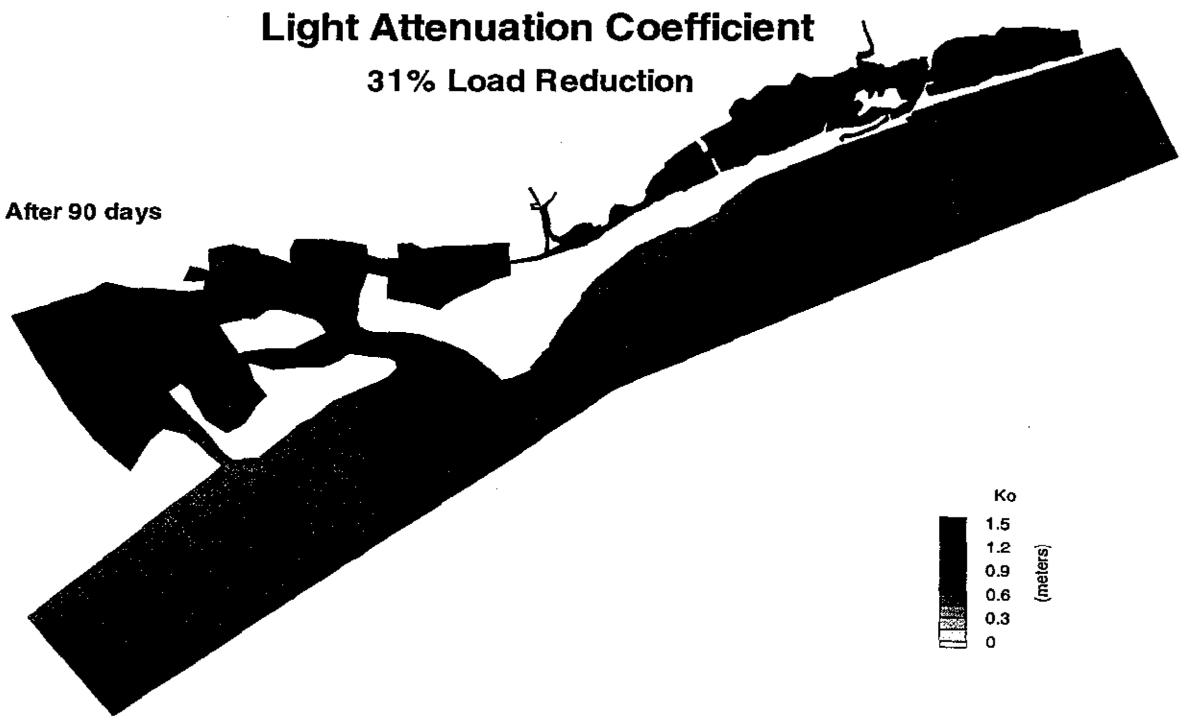

Figure 57. Simulated light attenuation coefficients in the study area for the present and future land use conditions.

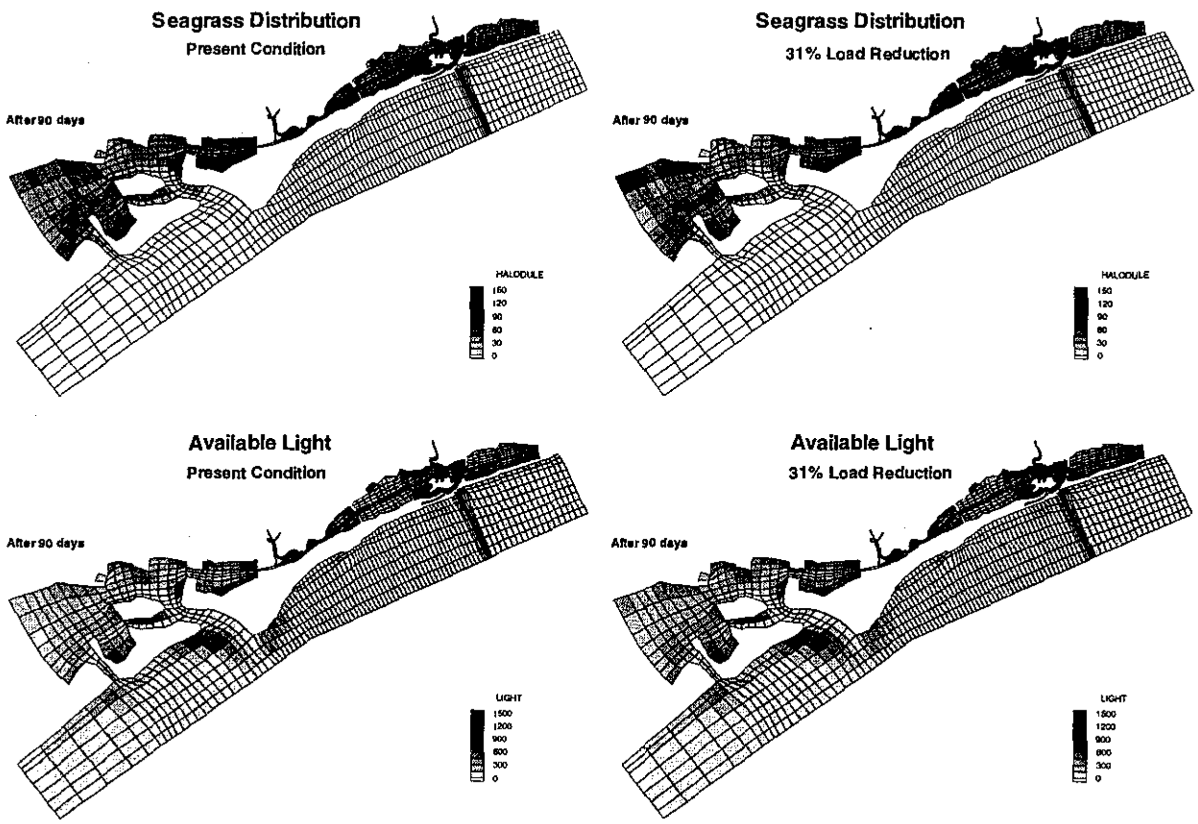

Figure 58. Simulated seagrass (Halodule) biomass and available light over the study area for present and future land use conditions.

5. CONCLUSIONS AND RECOMMENDATIONS

A coupled hydrodynamics-water quality-seagrass-light model has been developed for Roberts Bay. After calibration with limited water quality data provided by the SBNEP, we used the coupled model to assess the impact of reduced nutrient loading to the water quality and seagrass/light in Roberts Bay and surrounding waters. Major conclusions and recommendations of the study are summarized in the following:

- The coupled model allows dynamic coupling between all the component models (hydrodynamics, water quality parameters, light, and seagrass. The same time step and spatial grid are used by all the component models. The effect of hydrodynamics have been incorporated into the water quality model without any ad-hoc tuning of advective fluxes and dispersion coefficient.

- The simulated residual flow patterns in the study area show that flow and materials entering Roberts from Phillippi Creek flow primarily into Big Sarasota Bay and partially into Little Sarasota Bay. There is a large null zone inside Little Sarasota Bay.

- The coupled model produced reasonable water quality results which compare well with the limited water quality data. Most of the water quality parameters reached a dynamic equilibrium at the end of 90 day simulation. The sediment nutrient concentration appears to be reasonable, although no sediment column data was available. The lack of dynamic data and the paucity of synoptic data prevented us from developing site-specific model coefficients/processes.

- With 31% reduction in nutrient loading into Roberts Bay, the coupled model showed that noticeable impact is generally found in Roberts Bay, but not in Little Sarasota Bay and Big Sarasota Bay.

- Within Roberts Bay, a 31% reduction in loading is expected to lead to slight increase in DO, CBOD, and nitrate and nitrite, but reduced ammonia, dissolved organic nitrogen, and phytoplankton. These changes in turn lead to slight increase in available light and seagrass biomass.

- The lack of comprehensive water quality and seagrass/light data necessarily means that there may be considerable uncertainty in the model coefficients and results. The model results presented in this report should be used cautiously.

- Based on comparison between the model results produced with 31% load reduction vs. 100% load reduction, further information is obtained as to the region and parameters influenced by the load reduction. As shown in the model results for the two cases, some of the water quality parameters show no discernable differences, while other parameters exhibit significant differences.

- It is clear that there is a severe lack of data for developing reliablt water quality models for Roberts Bay and Sarasota Bay. Since models are necessary for developing quantitative pollutant load reduction goals, it is essential to design a monitoring study aimed to collect for a water quality model such as the one developed here.

- Based on increased understanding of the complex relationships among light-seagrass-nutrient-sediment-hydrodynamics, we have developed a process-based model which, pending further calibration and validation with comprehensive field data, could be used for managing seagrass and other resources in shallow Florida estuaries.

- Data collection programs in Florida estuaries in the past have generally focused on only limited number of parameters. In view of the complex relationships among the various components of the ecosystem and the site-specific nature of estuaries, it is prudent to design monitoring program which will collect all essential parameters at the same locations over long time periods to augment the typical monthly or quarterly synoptic surveys. It is also recommened that such monitoring program be designed with participations of modelers, to ensure that the data could be used for trend analysis and model development.

REFERENCES

Culter, J., 1992: ''Estuarine Bottom Habitat Assessment,'' *Framework for Action*, Sarasota Bay National Estuary Program, pp. 8.2-8.18.

Dendrou, S.A., C.I. Moore, and R. Walton, 1983: "Final Report, Little Sarasota Bay Circulation Study", Technical Report, Camp, Dresser and McKee, 250 p.

Fischer, H.B., E.J. List, R.C. Koh, Y. Imberger and N.H. Brooks, 1979, Mixing in Inland and Coastal Waters, Academic Press, Inc., Florida.

Heyl, M.G., 1992: ''Point- and Nonpoint-Source Pollutant Loading Assessment,'' *Framework for Action*, Sarasota Bay National Estuary Program, pp. 12.2-12.19.

Marshall, M. and J. Leverone, 1994: ''The Distribution and Effects of Hypoxia on Marine Organisms in Sarasota Bay, '' Final Report to SBNEP, Mote Marine Laboratory, Sarasota, FL, 34236.

Mote Marine Laboratory, 1993: ''Water and Sediment Quality: Trends and Status for sarasota Bay,'' Final Report Submitted to Sarasota Bay National Estuary Program, Mote Marine Laboratory Technical Report No. 254.

Peene, S.J., Y.P. Sheng, and S.H. Houston, 1992: "Modeling Tidal and Wind Driven Circulation in Sarasota and Tampa Bay", Estuarine and Coastal Modeling, American Society of Civil Engineers, pp. 112-113.

SBNEP (Sarasota Bay National Estuary Program), 1992, *Framework for Action of Sarasota Bay*, Report by Sarasota Bay National Estuary Program.

Sheng, Y.P., 1986: "CH3D: A Three-Dimensional Numerical Model of Coastal and Estuarine Circulation and Transport in Generalized Curvilinear Grids", Technical Report No. 587, Aeronautical Research Associates of Princeton, Inc., Princeton, New Jersey.

Sheng, Y.P., 1987: "On Modeling Three-Dimensional Estuarine and Marine Hydrodynamics", In Three-Dimensional Models of Marine and Estuarine Dynamics, Elsevier Oceanographic Series, Elsevier, pp. 35-54.

Sheng, Y.P., 1989: "Evolution of a 3-D Curvilinear-Grid Hydrodynamic Model: CH3D", Estuarine and Coastal Modeling (M.L. Spaulding, Ed.), ASCE, pp. 40-49.

Sheng, Y.P., 1994: ''Modeling Hydrodynamics and Water Quality Dynamics in Shallow Waters,'' *Keynote Paper*, International Symposium on Ecology and Engineering, Taman Negara, Malaysia, November 1994.

Sheng, Y.P. and S.J. Peene, 1991: "A Modeling and Field Study of Circulation and Transport in Sarasota Bay", Proceedings of the 1991 EPA/NOAA National Estuary Scientific Symposium, USEPA.

Sheng, Y.P. and S.J. Peene, 1992: "Circulation and Its Effect on Water Quality in Sarasota Bay", In

Framework for Action, Sarasota Bay, Sarasota Bay National Estuary Program, pp V.2-V.18.

Sheng, Y.P. and S.J. Peene, 1993: "A Field and Modeling Study of Residual Circulation in Sarasota Bay and Tampa Bay, Florida", Estuarine and Coastal Modeling, III, ASCE.

Sheng, Y.P. and E.A. Yassuda, 1995: ''Application of Three-Dimensional Circulation Model to WASP Modeling of Tampa Bay Water Quality,'' Final Report to Tampa Regional Planning Council.

Thompson, J.E., 1983: "General Curvilinear Coordinate Systems", in Numerical Grid Generation (J.E. Thompson, Ed., Elsevier Science Publishing Company, Inc., pp. 1-30.

Tomasko, D.A., C.J. Dawes and M.O. Hall, 1995: ''The Effects of Anthropogenic Nutrient Enrichment on Trutle Grass (Thalassia Testudinum) in Sarasota Bay, Florida (USA), *Estuaries*, In Press.

van de Kreeke, J., 1971: "Tide-Induced Mass Transport in Shallow Lagoons", Technical Report No. TR-008, University of Florida, Gainesville, FL.

van de Kreeke, J. and Dean, R.G., 1975: "Tide-Induced Mass Transport in Lagoons", Journal of the Waterways Harbors and Coastal Engineering Division, 101(4, pp. 393-403.

van de Kreeke, J. and Zimmerman, J. T. F., 1990: "Gravitational Circulation in Well- and Partially-mixed Estuaries", pp. 495-521.

Yassuda, E.A. and Y.P. Sheng, 1994: ''Application of Three-Dimensional Hydrodynamics Model to Studies of Inlet Dynamics,'' Proceedings of International Conference on Coastal Engineering, Kobe, Japan, ASCE.

APPENDIX A

THE ORIGINAL WASP EQUATIONS FOR TRANSFORMATION PROCESSES

The following equations (Ambrose et al. 1994) describe the transformation processes for DO, CBOD, Nitrogen, and Phosphorus in the water column and sediment column. In this study, we use these basic equations, with some modifications, to describe the transformation processes of DO, CBOD, P, and N at each numerical grid point in a curvilinear grid system. Advection and diffusion terms are added to the equations, as shown in the water quality equations in Chapter 2.

5. CARBONBACEOUS BIOCHEMICAL OXYGEN DEMAND

$$\frac{\partial C_5}{\partial t} = \underbrace{a_{oc} K_{1D} C_4}_{\textit{death}} - \underbrace{k_D \Theta_D^{(T-20)} \left(\frac{C_6}{K_{BOD} + C_6} \right) C_5}_{\textit{oxidation}} - \underbrace{\frac{v_{s3} (1 - f_{D5})}{D} C_5}_{\textit{settling}}$$

$$- \underbrace{\frac{5}{4} \frac{32}{14} k_{2D} \Theta_{2D}^{(T-20)} \left(\frac{K_{NO3}}{K_{NO3} + C_6} \right) C_2}_{\textit{denitrification}}$$

6. DISSOLVED OXYGEN

$$\frac{\partial C_6}{\partial t} = \underbrace{k_2 (C_s - C_6)}_{\textit{reaeration}} - \underbrace{k_d \Theta_d^{T-20} \left(\frac{C_6}{K_{BOD} + C_6} \right) C_5}_{\textit{oxidation}} - \underbrace{\frac{64}{14} k_{12} \Theta_{12}^{T-20} \left(\frac{C_6}{K_{NIT} + C_6} \right) C_1}_{\textit{nitrification}}$$

$$- \underbrace{\frac{SOD}{D} \Theta_s^{T-20}}_{\textit{sediment demand}} + \underbrace{G_{P1} \left(\frac{32}{12} + \frac{48}{14} \frac{14}{12} (1 - P_{NH3}) \right) C_4}_{\textit{phytoplankton growth}} - \underbrace{\frac{32}{12} k_{1R} \Theta_{1R}^{T-20} C_4}_{\textit{respiration}}$$

Figure 4.2 Oxygen balance equations.

Reaeration

4. PHYTOPLANKTON NITROGEN

$$\frac{\partial (C_4 a_{nc})}{\partial t} = \underbrace{G_{P1} a_{nc} C_4}_{\text{growth}} - \underbrace{D_{P1} a_{nc} C_4}_{\text{death}} - \underbrace{\frac{v_{s4}}{D} a_{nc} C_4}_{\text{settling}}$$

8. ORGANIC NITROGEN

$$\frac{\partial C_7}{\partial t} = \underbrace{D_{P1} a_{nc} f_{on} C_4}_{\text{death}} - \underbrace{k_{71} \theta_{71}^{T-20} \left(\frac{C_4}{K_{mPc} + C_4} \right) C_7}_{\text{mineralization}} - \underbrace{\frac{v_{s3} (1 - f_{D7})}{D} C_7}_{\text{settling}}$$

1. AMMONIA NITROGEN

$$\frac{\partial C_1}{\partial t} = \underbrace{D_{P1} a_{nc} (1 - f_{on}) C_4}_{\text{death}} + \underbrace{k_{71} \theta_{71}^{T-20} \left(\frac{C_4}{K_{mPc} + C_4} \right) C_7}_{\text{mineralization}} - \underbrace{G_{P1} a_{nc} P_{NH3} C_4}_{\text{growth}} - \underbrace{k_{12} \theta_{12}^{T-20} \left(\frac{C_6}{K_{NIT} + C_6} \right) C_1}_{\text{nitrification}}$$

2. NITRATE NITROGEN

$$\frac{\partial C_2}{\partial t} = \underbrace{k_{12} \theta_{12}^{T-20} \left(\frac{C_6}{K_{NIT} + C_6} \right) C_1}_{\text{nitrification}} - \underbrace{G_{P1} a_{nc} (1 - P_{NH3}) C_4}_{\text{growth}} - \underbrace{k_{2D} \theta_{2D}^{T-20} \left(\frac{K_{NO3}}{K_{NO3} + C_6} \right) C_2}_{\text{denitrification}}$$

where

$$P_{NH3} = \underbrace{C_1 \left(\frac{C_2}{(K_{mN} + C_1)(K_{mN} + C_2)} \right) + C_1 \left(\frac{K_{mN}}{(C_1 + C_2)(K_{mN} + C_2)} \right)}_{\text{ammonia preference factor}}$$

Figure 5.5 Nitrogen cycle equations.

4. PHYTOPLANKTON PHOSPHORUS

$$\frac{\partial (C_4 a_{pc})}{\partial t} = \underbrace{G_{P1} a_{pc} C_4}_{growth} - \underbrace{D_{P1} a_{pc} C_4}_{death} - \underbrace{\frac{v_{s4}}{D} a_{pc} C_4}_{settling}$$

8. ORGANIC PHOSPHORUS

$$\frac{\partial C_8}{\partial t} = \underbrace{D_{P1} a_{pc} f_{op} C_4}_{death} - \underbrace{k_{83} \theta_{83}^{T-20} \left(\frac{C_4}{K_{mPc} + C_4} \right) C_8}_{mineralization} - \underbrace{\frac{v_{s3} (1 - f_{D8})}{D} C_8}_{settling}$$

3. INORGANIC PHOSPHORUS

$$\frac{\partial C_3}{\partial t} = \underbrace{D_{P1} a_{pc} (1 - f_{op}) C_4}_{death} + \underbrace{k_{83} \theta_{83}^{T-20} \left(\frac{C_4}{K_{mPc} + C_4} \right) C_8}_{mineralization} - \underbrace{G_{P1} a_{pc} C_4}_{growth}$$

Figure 5.4 Phosphorus cycle equations.

5. CARBONACEOUS BIOCHEMICAL OXYGEN DEMAND

$$\frac{\partial C_{5j}}{\partial t} = \underbrace{a_{OC} k_{PZD} \Theta_{PZD}^{T-20} C_{4j}}_{\text{decomposition}} - \underbrace{k_{DS} \Theta_{DS}^{T-20} C_{5j}}_{\text{oxidation}} - \underbrace{\frac{5}{4}\frac{32}{14} k_{2D} \Theta_{2D}^{T-20} C_{2j}}_{\text{denitrification}}$$

$$+ \underbrace{\frac{v_{s3}}{D_j}(1 - f_{D5i})\, C_{5i}}_{\text{settling}} - \underbrace{\frac{v_{R3}}{D_j}(1 - f_{D5j})\, C_{5j}}_{\text{resuspension}} + \underbrace{\frac{E_{DIF}}{D_j^2}(C_{5i} f_{D5i} - C_{5j} f_{D5j})}_{\text{diffusion}}$$

6. DISSOLVED OXYGEN

$$\frac{\partial C_6 j}{\partial t} = - \underbrace{k_{DS} \Theta_{DS}^{T-20}}_{\text{oxidation}} + \underbrace{\frac{E_{DIF}}{D_j^2}(C_6 i - C_6 j)}_{\text{diffusion}}$$

SEDIMENT OXYGEN DEMAND (g/m²-day)

$$SOD = \frac{E_{DIF}}{D_j}(C_6 i - C_6 j)$$

(for benthic segment j, water segment i)

Figure 4.3 Benthic layer oxygen balance equations.

7. ORGANIC NITROGEN

$$\frac{\partial C_7}{\partial t} = k_{PZD}\theta_{PZD}^{T-20} a_{nc} f_{on} C_4 - k_{OND}\theta_{OND}^{T-20} C_7$$

algal decomposition mineralization

1. AMMONIA NITROGEN

$$\frac{\partial C_1}{\partial t} = k_{PZD}\theta_{PZD}^{T-20} a_{nc} (1 - f_{on}) C_4 + k_{OND}\theta_{OND}^{T-20} C_7$$

algal decomposition mineralization

2. NITRATE NITROGEN

$$\frac{\partial C_2}{\partial t} = - k_{2D}\theta_{2D}^{T-20} C_2$$

denitrification

8. ORGANIC PHOSPHORUS

$$\frac{\partial C_8}{\partial t} = k_{PZD}\theta_{PZD}^{T-20} a_{PC} f_{op} C_4 - k_{OPD}\theta_{OPD}^{T-20} f_{D8} C_8$$

algal decomposition mineralization

3. INORGANIC PHOSPHORUS

$$\frac{\partial C_3}{\partial t} = k_{PZD}\theta_{PZD}^{T-20} a_{PC} (1 - f_{op}) C_4 + k_{OPD}\theta_{OPD}^{T-20} f_{D8} C_8$$

algal decomposition mineralization

Sediment Flux for Chemical k (g/m²-day)

$$FLUX_k = \frac{E_{DIF}}{D_j} (C_{kj} f_{kj} - C_{ki} f_{ki})$$

(for benthic segment j, water segment i)

Figure 5.8 Benthic nutrient equations.